

Alma Mater Studiorum - Università di Bologna

DOTTORATO DI RICERCA IN
SCIENZE E TECNOLOGIE AGRARIE, AMBIENTALI E ALIMENTARI

Ciclo 35

Settore Concorsuale: 07/E1 - CHIMICA AGRARIA, GENETICA AGRARIA E PEDOLOGIA

Settore Scientifico Disciplinare: AGR/07 - GENETICA AGRARIA

CHARACTERIZATION AND CLONING OF CHEMICALLY-INDUCED MUTANTS
IN BARLEY (HORDEUM VULGARE L.)

Presentata da: Serena Rosignoli

Coordinatore Dottorato

Massimiliano Petracchi

Supervisore

Silvio Salvi

Esame finale anno 2023

ABSTRACT	3
CHAPTER 1. CLONING THE BARLEY <i>NEC3</i> DISEASE LESION MIMIC MUTANT	4
1 INTRODUCTION	4
2 OBJECTIVES	6
3 MATERIALS AND METHODS	6
3.1 <i>Plant material and growth conditions</i>	6
3.2 <i>Phenotyping of the F₂ populations</i>	7
3.3 <i>Whole genome shotgun (WGS) sequencing and variant calling</i>	7
3.4 <i>Bulked segregant analysis (BSA) and fine mapping</i>	8
3.5 <i>PCR amplification and Sanger sequencing</i>	8
3.6 <i>Homology modelling calculations</i>	9
3.7 <i>Phylogenetic analysis of CYP71P1 gene family</i>	9
4 RESULTS	10
4.1 <i>Collection of leaf disease lesion mimic (DLM) mutants in barley</i>	10
4.2 <i>Mendelian inheritance and impact on plant vigour of the necrotic trait</i>	14
4.3 <i>BSA-based mapping of necrotic mutants</i>	16
4.4 <i>TM4118 has the same causal gene as the previously described <i>nec1</i> mutant</i>	17
4.5 <i>Cloning orange blotch mutations by complementation by sequencing (CBS)</i>	18
4.6 <i>Functional validation of cytochrome P450 as causal gene for the orange blotch and the historical <i>nec3</i> barley mutations</i>	26
4.7 <i>Homology modelling of <i>NEC3</i></i>	28
4.8 <i>P450 and its evolution in plants</i>	31
5 DISCUSSION	36
6 REFERENCES	40
7 SUPPLEMENTARY MATERIAL	45
CHAPTER 2. MAPPING AND CLONING THE TILLMORE BROAD LEAF BARLEY MUTANT TM2544	52
1 INTRODUCTION	52
2 OBJECTIVES	53
3 MATERIALS AND METHODS	53
3.1 <i>Plant material and growth conditions</i>	54
3.2 <i>Phenotyping</i>	54
3.3 <i>BSA-Seq and Whole Genome Sequencing (WGS)</i>	54
4 RESULTS	55
4.1 <i>Phenotyping TM2544 and of F₁ and F₂ populations</i>	55
4.2 <i>Whole genome sequencing</i>	62
4.3 <i>BSA-Seq</i>	62
5 DISCUSSION	64
6 REFERENCES	65
INTRODUCTION TO CHAPTERS 3 AND 4: ROOTS AND ROOT SYSTEM ARCHITECTURE AND ANATOMY IN BARLEY	68
1. <i>Anatomy and structure of barley roots and their potential for plant breeding</i>	68
2. <i>Molecular genetics of root development and architecture</i>	73
CHAPTER 3. MAPPING AND CLONING THE SHORT AND RIGID ROOT MUTANT TM390	78
1. OBJECTIVES	78
2. MATERIALS AND METHODS	78
2.1 <i>Plant material and growth conditions</i>	78
2.2 <i>Phenotyping</i>	78
2.3 <i>Mapping TM390 with MutMap+</i>	78
2.4 <i>Whole Genome Sequencing (WGS)</i>	79
2.5 <i>Functional validation of candidate genes</i>	80
3. RESULTS	80

3.1	<i>Barley mutant TM390 has short and semi-rigid roots</i>	80
3.2	<i>TM390 maps on chromosome 2H</i>	84
3.3	<i>WGS of the two bulks compared to TM390 finds 8 candidate genes</i>	85
3.4	<i>Functional validation of candidate genes</i>	86
4.	DISCUSSION AND CONCLUSIONS	89
5.	REFERENCES	91

CHAPTER 4. CLONING THE BARLEY HYPERGRAVITROPIC ROOT MUTANTS *EGT1* AND *EGT2*
.....**92**

1.	OBJECTIVES	92
2.	MATERIALS AND METHODS	92
2.1	<i>Plant material, growth conditions, and phenotyping</i>	92
2.2	<i>Bulked Segregant Analysis (BSA)</i>	95
2.3	<i>Whole Genome Sequencing</i>	95
2.4	<i>CRISPR/CAS9 generation of a second allele of <i>egt2</i></i>	96
2.5	<i>Haplotype Analysis of <i>HvEGT1</i> in the WHEALBI Barley Collection</i>	96
2.6	<i><i>egt1</i> and <i>egt2</i> durum wheat mutants</i>	97
3.	RESULTS	97
3.1	<i>TM194 and TM3580 are allelic and distinct from TM2835</i>	97
3.2	<i><i>egt1</i> and <i>egt2</i> have hypergravitropic roots of all classes</i>	98
3.3	<i><i>egt1</i> and <i>egt2</i> have a root-specific angle defect</i>	102
3.4	<i>Root growth angle of <i>egt1</i> and <i>egt2</i> depends on gravity</i>	103
3.5	<i><i>egt1</i> and <i>egt2</i> segregates like a Mendelian recessive trait</i>	105
3.6	<i><i>EGT1</i> encodes a Tubby-like F-box protein</i>	105
3.7	<i><i>EGT2</i> encodes a SAM Domain-Containing Protein</i>	106
3.8	<i><i>egt1</i> is involved in the adaptation of root growth angle to the environment</i>	109
3.9	<i><i>EGT1</i> and <i>EGT2</i> functions are conserved in durum wheat</i>	110
4.	DISCUSSION	113
5.	REFERENCES	116

ABSTRACT

Induced mutagenesis has been exploited for crop improvement and for investigating gene function and regulation. To unravel molecular mechanisms of stress resilience, we applied state-of-the-art genomics-based gene cloning methods to barley mutant lines showing altered root and shoot architecture and disease lesion mimic phenotypes.

With a novel method that we named complementation by sequencing, we cloned *NEC3*, the causal gene for an orange-spotted disease lesion mimic phenotype. *NEC3* belongs to the *CYP71P1* gene family and it is involved in serotonin biosynthesis. By comparative phylogenetic analysis we showed that *CYP71P1* emerged early in angiosperm evolution but was lost in some lineages including *Arabidopsis thaliana*. By BSA-Seq, we cloned the gene whose mutation increased leaf width, and we showed that the gene corresponded to the previously cloned *BROADLEAF1*. By BSA coupled to WGS sequencing, we cloned *EGT1* and *EGT2*, two genes that regulate root gravitropic set point angle. *EGT1* encodes a Tubby-like F-box protein and *EGT2* encodes a Sterile Alpha Motive protein; *EGT2* is phylogenetically related to *AtSAM5* in *Arabidopsis* and to *WEEP* in peach where it regulates branch angle. Both *EGT1* and *EGT2* are conserved in wheat. We hypothesized that both participate to an anti-gravitropic offset mechanism since their disruption causes mutant roots to grow along the gravity vector. By the MutMap+ method, we cloned the causal gene of a short and semi-rigid root mutant and found that it encodes for an endoglucanase and is the ortholog of *OsGLU3* in rice whose mutant has the same phenotype, suggesting that the gene is conserved in barley and rice.

The mutants and the corresponding genes which were cloned in this work are involved in the response to stress and can potentially contribute to crop adaptation.

CHAPTER 1. Cloning the barley *nec3* disease lesion mimic mutant

The results of this work were published in: Rosignoli, S., Cosenza, F., Moscou, M. J., Civolani, L., Musiani, F., Forestan, C., Milner, S. G., Savojardo, C., Tuberosa, R., & Salvi, S. (2022). Cloning the barley *nec3* disease lesion mimic mutant using complementation by sequencing. *Plant Genome*, 15, e20187. <https://doi.org/10.1002/tpg2.20187>

1 INTRODUCTION

Collections of artificially (chemically or physically) random-induced mutants have proved extremely valuable for basic biology investigations as well as for crop improvement and varietal release (Lundqvist, 2014; Mba, 2013; Oladosu et al., 2016; Parry et al., 2009). Disease lesion mimic (DLM) mutants are a heterogenous class of mutants showing colored spots, necrosis or other types of spontaneous lesions, mainly on leaf blades, similar to disease-related phenotypes (Balint-Kurti, 2019; Bruggeman et al., 2015). Tens of DLM mutants have been identified in barley, maize, rice, and *Arabidopsis*, (Bruggeman et al., 2015; Zheng et al., 2021) and occasionally in other species, including groundnut (Badigannavar et al., 2002), soybean (Al Amin et al., 2019), tomato (Spassieva & Hille, 2002), and switchgrass (Liu et al., 2017). In many cases, the DLM phenotype can be described as a form of the well-known hypersensitive response, characterized by a rapid and localized cell death. Thus, DLM mutants usually suffer negative pleiotropic effects including reduced photosynthesis, retarded growth, and increased susceptibility to necrotrophic pathogens (Balint-Kurti, 2019). This notwithstanding, DLM-causing alleles were occasionally shown to contribute to resistance to pathogens, as demonstrated for the barley *mlo* and *nec1* recessive genes for powdery mildew (*Blumeria graminis* f. sp. *hordei*) and bacterial pathogens, respectively (Büschges et al., 1997; Keisa et al., 2011; Kumar et al., 2001). Similarly, DLM *Spl17* and *Spl26* confer resistance to *Magnaporthe oryzae* and *Xanthomonas oryzae* in rice (Wu et al., 2008), *lm3* confers powdery mildew (*Blumeria graminis* f. sp. *tritici*) resistance in wheat (Wang et al., 2016), *Lm5* enhances resistance to powdery mildew and stripe rust (*Puccinia striiformis* f.sp. *tritici*) in wheat (Li et al., 2021), and *Rp1-D21* confers resistance to rust (*Puccinia sorghi*) in maize (Smith et al., 2010). In wheat, the complementary genes *Necrosis 1* (*Ne1*) and *Necrosis 2* (*Ne2*) cause hybrid necrosis (Chu et al., 2006; Tsunewaki, 1970), a type of hybrid postzygotic incompatibility associated with necrosis on the leaves of F₁ seedlings, stunted growth and sometimes

lethality, caused by deleterious epistatic interaction with a range of symptoms connected to multiple alleles at both loci. The *Ne2* gene was recently cloned and demonstrated to be the same gene as *Lr13* (Hewitt et al., 2021; Si et al., 2021), the widely distributed resistance gene against leaf rust caused by *Puccinia triticina*.

Contemporary to the publication of our work, Ameen et al. (2021) published the clonation of *nec3* in barley and determined that the orange necrotic phenotype is not a spontaneous DLM trait but it is induced by several species of *Ascomycete* and by *Xanthomonas translucens*. They also observed that the *nec3* mutants have an unstable cutin layer that possibly peels away from the leaf surface when in contact with the pathogen *Bipolaris sorokiniana* germ tubes.

Cloning genes responsible for chemically or physically induced mutations showing simple Mendelian inheritance has been carried out using positional cloning approaches, which have been recently complemented by mapping-by-sequencing and its different implementations (Bettgenhaeuser & Krattinger, 2019; Schneeberger, 2014). Cloning a gene by mapping-by-sequencing relies on (i) production of a mapping population (e.g., an F₂, from a cross between two inbred lines, one carrying the target yet unknown mutation), (ii) bulk segregant analysis (BSA), (Michelmore et al., 1991) using next generation sequencing (NGS) approaches for high density SNP genotyping, and (iii) identification of SNPs with significantly altered allele frequencies between wild-type and mutant DNA bulks. Ideally, mapping-by-sequencing is expected to highlight the causative SNP, leading to gene cloning. If this is not the case, SNPs genetically linked to the causative gene are however expected to be identified. Although mapping-by-sequencing was very successful in both model and crop species (Mascher et al., 2014; Schneeberger, 2014), it still requires the production of experimental cross populations and genetic mapping information, which could be quite demanding for some species. Attempts to circumvent this bottleneck, i.e., cloning by sequencing without mapping, have been recognized as possible if alternative methods exist to confirm the target gene function in the species (Candela et al., 2015). This approach was first applied in *Drosophila* where a gene controlling egg-shell morphology was identified by WGS sequencing of independent EMS-induced mutants showing the same egg phenotype, followed by confirmation by complementation (Blumenstiel et al., 2009). Similar experiments were carried out in other model species, e.g., in *Caenorhabditis* (Sarin et al., 2008). Despite these promising results, this approach has yet to be fully extended to plants, although some attempts were made. For example, in barley and wheat, a combination of WGS sequencing and chromosome flow sorting, named ‘MutChromSeq’ was applied to

multiple mutants to clone the underlying gene, provided that the chromosome carrying the target gene was known (Sánchez-Martín et al., 2016). An optimized combination of NGS for induced SNP discovery and progeny testing enabled Heuermann et al. (2019) to clone maize mutant genes, but this still required the production of controlled experimental crosses followed by genome-sequencing 16 plants. In *Arabidopsis*, a protocol named ‘mutagenomics’ was recently developed that combined EMS mutagenesis, phenotypic screening, WGS sequencing, and progeny testing (Hodgens et al., 2020).

Here we describe a novel collection of DLM mutants in barley and develop a phenotype-driven, WGS sequencing-based approach, which we named ‘complementation by sequencing’ (CBS), suitable for identifying candidate genes for target mutations without using genetic information, experimental cross populations, and/or progeny testing. We applied this method to clone the gene responsible for three independent orange-blotch DLM mutations, and we showed that this gene corresponds to the historical barley *nec3* mutant (Lundqvist et al., 1997).

2 OBJECTIVES

1. Production and characterization of a collection of disease lesion mimic mutants from the TILLMore barley mutant population.
2. Mapping and cloning the barley *nec3* disease lesion mimic mutant.
3. Developing and testing the novel mapping method: complementation by sequencing

3 MATERIALS AND METHODS

3.1 Plant material and growth conditions

All the barley necrotic mutants, with the exception of BW630, belong to the TILLMore collection of barley (TM) obtained with sodium azide mutagenesis on the cultivar Morex (Talamè et al., 2008). Two F₂ mapping populations were generated from the cross TM599 × Barke and TM4118 × Barke. The F₁ from the cross TM599 × BW630, and the F₁ from TM185 × TM599 and TM599 × TM1000 were created to perform complementation tests. BW630 is a Bowman backcross-derived line (Druka et al., 2011) carrying an orange blotch DLM *nec3* allele originally generated by X-ray mutagenesis on the cv. Villa (Häuser & Fischbeck, 1976). BW630 seeds were kindly supplied by Luke Ramsay, from the James

Hutton Institute, Invergowrie, UK and are deposited at NordGen, the Nordic Genetic Resource Center, Sweden. In order to morphologically classify the DLM mutants, necrosis were observed in terms of their approximate shape, margin (distinct or blurred), dimension (small: main axis < 3mm; medium: main axis between 3 and 6 mm, included; large: main axis > 6 mm) and color.

The entire TILLMore collection, and the cultivars Morex and Barke were grown in open field in Cadriano (Lat.: N 44°33'03'', Lon.: E 11°24'36'', 33 m a.s.l), Italy, in the spring of 2016 and again in the spring of 2019, following standard agronomic practices, in 0.6 m long two-row plots with a randomized design. The two F₂ populations and their parental lines were grown in the open field in Cadriano, Italy, in the spring of 2018. About 200 seeds of each F₂ were sown in rows, with an interspacing of 15 cm and an inter-row distance of 1 m. F₁ plants from TM599 × BW630, TM185 × TM599 and TM599 × 1000 were grown in the greenhouse, in a peat and vermiculite growing medium (Vigorplant Irish and Baltic peat-based professional mix) in 15 × 15 × 30 cm polyethylene pots with a day temperature of 22°C (16 h) and a night temperature of 18°C (8 h). Greenhouse lighting was a mix of natural light supplemented with artificial light by 400 watt high-pressure sodium lamps (Sylvania SHP-TS 400W Grolux).

3.2 Phenotyping of the F₂ populations

To determine the segregation of the TM599 and TM4118 necrotic traits, the number of mutated and wild-type plants were counted at flowering time, Zadoks growth stage 6, in the field trial. To calculate the percentage of necrotic leaf area, the third leaf from the top of each necrotic F₂ and six parental plants was collected, scanned with a Canon LiDE120 scanner, and their images were analyzed with the software LNC-Leaf Necrosis Classifier (Obořil, 2017). The vigor index was calculated as number of culms times plant height. Culms were counted if taller than 40 cm, including awns. Plant height was measured on the tallest culm, including awns.

3.3 Whole genome shotgun (WGS) sequencing and variant calling

TM185, TM599, TM1000, BW630, and barley cv. Villa were WGS sequenced. Genomic DNA was extracted from leaf samples using a commercial kit (Nucleospin Plant II, Macherey-Nagel, Germany). The DNA was sequenced with Illumina HiSeq PE150. Reads were trimmed using TrimmomaticPE version 0.39 (Bolger et al., 2014). The line TM599

produced a total of 342,940,495 reads with a SNP rate of one every 182 Kb. Reads were aligned to the third version of barley cv. Morex genome (Mascher et al., 2021) with BWA 0.7.12-r1039 (Li & Durbin, 2009) and variants in the genomic space were called with GATK 4.2.0.0 (McKenna et al., 2010), filtering for a minimum read depth of 9×, minimum PHRED quality of 40 and minimum quality normalized on depth (QD) of 20.

In this work, mutation density (see Results) is defined as the probability that a gene is affected by moderate (missense or missense and splice region variant) or strong (stop gained, stop lost, start lost, splice acceptor, or splice donor variant) mutations, as predicted by SNPEff v5.0d, across the genome, considering a total number of protein coding genes of 81,687 as in Morex v.3 (Mascher et al., 2021).

3.4 Bulk segregant analysis (BSA) and fine mapping

Bulk segregant analysis (Michelmore et al., 1991) was carried out to map the orange-spotted DLM mutant phenotype showed by TM599. The F₂ population obtained from the cross TM599 × Barke was grown in the field. Plants were visually inspected at flowering time, Zadoks growth stage 6, when 15 *nec3* plants and 15 wild-type plants were selected. Their leaf DNA was individually extracted with the Macherey-Nagel Nucleospin Plant II kit and added to two bulks in the same quantity for each single plant, reaching a final concentration of 50 ng/μl for both bulks. The bulks were genotyped with the 9k Illumina Infinium iSelect barley SNP array (Comadran et al., 2012) by TraitGenetics GmbH, Gatersleben, Germany. The analysis of SNP signal was carried out with GenomeStudio (Illumina, San Diego, Inc.), using the theta value as in (Hyten et al., 2008) and calculating delta theta as the squared difference between the wild-type bulk theta and the necrotic bulk theta. To reduce the candidate interval, a KASP analysis was performed using 47 markers on individual DNAs from the same F₂ population and the cv. Barke and Morex.

3.5 PCR amplification and Sanger sequencing

Primers were designed with the aid of the online tools Primer3 version 4.1.0 (Untergasser et al., 2012) and Benchling (www.benchling.com) for the purpose of obtaining two amplicons of about 760 bp (Table 8). We used the Phusion High-fidelity PCR kit (Thermo Fischer Scientific, Waltham, Inc.) and ran 35 cycles with a denaturation temperature of 98° C for 5 s, an annealing temperature of 66° C for 20 s and an extension temperature of 72° C for 16 s. The resulting DNA was sequenced with the Sanger method.

3.6 Homology modelling calculations

Template search was performed using the HHsearch method implemented in the HHpred server (Söding et al., 2005). The server performs up to eight iterative PSI-BLAST (Altschul et al., 1997) searches through filtered versions of the non-redundant (nr) database from the NCBI. Using the final target alignment, a profile hidden Markov model (HMM) (Eddy, 1998; Krogh et al., 1994) is calculated. Homologous templates are identified by searching through a weekly updated database containing HMMs for a representative subset of PDB sequences. Finally, HHsearch ranks database matches by the probability of the match to be homologous to the target sequence. This is useful to distinguish homologous from non-homologous matches. HHpred identified ferruginol synthase from *Salvia miltiorrhiza* (Chinese sage) as the best template structure for NEC3. For this protein, a high-resolution X-ray structure is available (PDB ID 5YLW, resolution 1.70 Å) (<https://www.rcsb.org/structure/5ylw>) and the sequence identity with NEC3 (29%) allows the generation of a model through homology modelling. The target and template sequences were realigned using the Promals3D server (Pei et al., 2008). The obtained alignment (Figure 9) was then used to calculate 100 models of NEC3 using the Modeller 9.21 software (Šali & Blundell, 1993). The heme group solved in the template structure, as well as a water molecule completing the iron ion coordination sphere, was included in the modelling. The best model was selected using the DOPE potential function included in Modeller (Shen & Sali, 2006). A loop optimization routine was used to refine the regions that showed higher than average energy as calculated using the DOPE potential function. The stereochemical quality of the model structure was established using ProCheck (Laskowski et al., 1993). The results of this analysis confirm the reliability of the model structure (Table 9). The analysis on the model structure, as well as the molecular graphics reported in this article, was performed by using UCSF Chimera (Pettersen et al., 2004).

3.7 Phylogenetic analysis of CYP71P1 gene family

A collection of 123 sequenced angiosperm species characterized by Zhao et al. (2020) were analyzed. Genomes were downloaded and queried using BLAST+ (v2.11.0) with default parameters using barley CYP41P1 as query. Multiple sequence alignment was performed using kalign (v3.3) using default parameters. To reduce the alignment to informative sites, the Python script QKphylogeny_alignment_analysis.py

(<https://github.com/matthewmoscou/QKphylogeny/>) was used to extract residues in the alignment that were present in at least 20% of species. Phylogenetic analysis was performed with iqtree v1.6.12 (Nguyen et al., 2015). Model selection identified JTT+I+G4 as the appropriate best fit model using Bayesian Information Criterion. Bootstrapping was performed using ultrafast bootstrapping with a total of 1,000 bootstraps. The phylogenetic tree was visualized using iTOL (<https://itol.embl.de/>).

4 RESULTS

4.1 Collection of leaf disease lesion mimic (DLM) mutants in barley

The chemically mutagenized TILLMore population (TM; 3,800 M₅-M₆ lines) was screened in the field in two different years (2016 and 2019) by visual observation for leaf necrosis at the adult stage (from stem elongation to heading) and 34 lines were identified showing stable leaf DLM phenotypes. Necrosis varied in shape, dimension, color, margins and localization on the leaf blade (Figure 1 and Table 1). We classified mutant lines into three main categories based on necrosis size, namely (i) ‘spots’, (ii) ‘blotches’, or (iii) ‘extended necrosis’ on leaf blade. The ‘spots’ category include 19 mutant lines with small, regular size necrosis, as in TM588 shown in Figure 1. In the following, underlined IDs corresponds to lines shown in Figure 1. Among the ‘spotted’ lines, four showed lesions that concentrate on the leaf mid vein (TM588, TM849, TM2095, and TM2424), three lines showed lesions grouped around the main leaf vein (TM537, TM2290, and TM2508), 12 lines showed scattered lesions across the leaf blade (TM361, TM904, TM1326, TM1403, TM1428, TM2268, TM2286, TM2695, TM3033, TM3474, TM4118, and TM5617). The ‘blotches’ category included 10 lines showing medium to large necrotic blotches on leaf blade, as in TM1120 shown in Figure 1. Three mutants showed orange blotches (TM185, TM599, and TM1000), three burnt orange to light brown blotches (TM1120, TM5721, and TM5866), and four mutants brown to dark brown blotches (TM1674, TM1847, TM2140, and TM5776). When blotch margin was considered, four lines (TM1674, TM1847, TM2140, and TM5866) showed blurred margins, while the remaining six showed net margins. Five lines (TM1120, TM1674, TM2140, TM5721, and TM5866) showed lesions that appeared encircled in a yellow halo. The ‘extended necrosis’ category included five mutants (TM327, TM982, TM1708, TM1797, and TM3684).

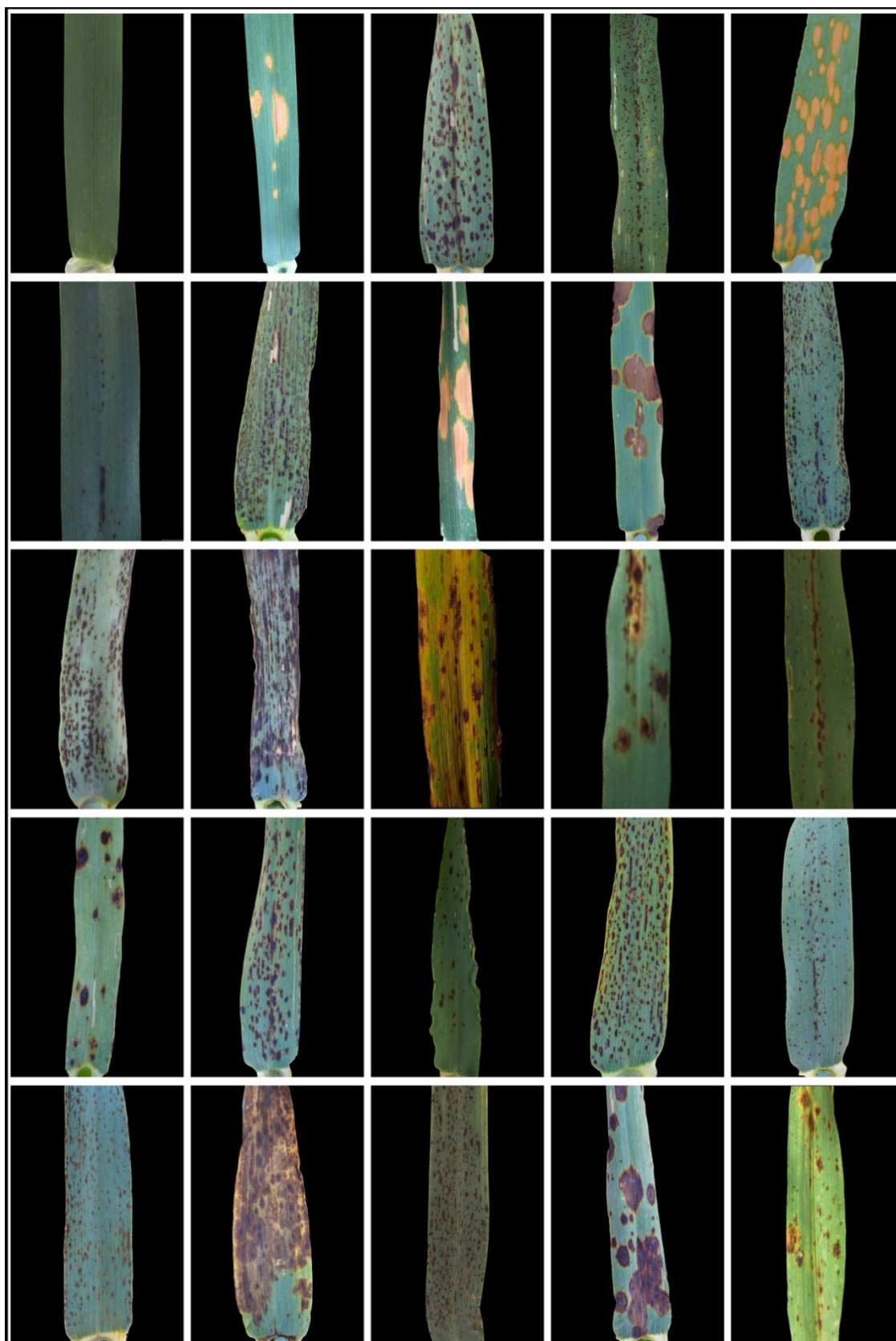


Figure 1. Representative images of the TILLMore disease lesion mimic (DLM) mutant collection. Plants were grown in the field and in the greenhouse, and representative leaves were photographed at flowering time (Zadoks growth stage 6). First row from the top, from

left to right: cv. Morex (wild-type), TM185, TM361, TM588, and TM599; second row: TM849, TM904, TM1000, TM1120, and TM1326; third row: TM1403, TM1708, TM1797, TM1847, and TM2095; fourth row: TM2140, TM2268, TM2286, TM2290, and TM2424; fifth row: TM2695, TM3684, TM4118, TM5776, and TM5866.

Table 1. TILLMore Necrotic collection. Dimensions are based on the main axis of the lesion, small: main axis < 3 mm; medium: main axis between 3 and 6 mm, included; large: main axis > 6 mm.

	Shape	Margins	Dimension	Colour	Short description
TM185	irregular elliptic to circular blotches	distinct	large	orange	large irregular orange blotches with distinct margins
TM327	large irregular necrosis	distinct	large	brown/beige	small brown spots that coalesce into large beige papery area with brown margins
TM361	small to medium circular and elliptic necrosis	distinct	small	brown	small brown circular and elliptic spots that are sometimes bigger and tend to grow on the mid vein
TM537	spot to linear	distinct	small	brown/dark brown	small dark brown spots coalescent into segment > 1 cm parallel to leaf vein and visible from both adaxial and abaxial surface
TM588	small brown spots	distinct	small	brown	small spots that tend to coalesce on mid vein
TM599	irregular elliptic to circular blotches	distinct	large	orange	large irregular orange blotches with distinct margins
TM849	small brown spots	distinct	small	dark brown	very small spots that are rare on the leaf but coalesce on the first half of mid vein
TM904	very irregular	blurred	large	brown/dark brown	small brown spots/short segments forming near leaf lateral margins and leaf mid vein associate into a very irregular brown longitudinal necrosis with varied color intensity and blurred in some parts.
TM982	spots	distinct	small	bronze	small bronze spots develop on blade and sheath and their density increases conferring an overall irregular bronze color to all the surface

	Shape	Margins	Dimension	Colour	Short description
TM1000	irregular elliptic to circular blotches	distinct	large	orange	large irregular orange blotches with distinct margins
TM1120	irregular elliptic to circular blotches	distinct	large	brown to burnt orange	large irregular burnt orange blotches having irregular oily margins turning to burnt orange blotches with yellow halo
TM1326	short segments / irregular	distinct	small	dark brown to black	small very dark spots converge into irregular short segments parallel to the vein
TM1403	small to medium spots/ irregular	distinct	small	dark brown to black	small dark brown spots converge into medium irregular shapes
TM1428	small to medium spots	distinct	small	dark brown	small brown spots sometimes converge into short segments especially on leaf margins or enlarge to medium spots
TM1674	small spot to large stripes	blurred	large	brown	small brown spots with yellow halo that transforms into irregular cluster of spots or big longitudinal stripes
TM1708	small to medium ellipses	blurred	medium	dark brown to black	small dark elliptic lesions that enlarge and coalesce into big irregularly shaped black lesions
TM1797	brown blotches	blurred	big	brown to burnt orange	medium to big brown to burnt orange blotches and leaf decoloration
TM1847	brown blotches	blurred	big	brown	few big brown blotches with blurred margins and some smaller lesion
TM2095	small brown spots	distinct	small	brown	small light brown lesion mainly on midvein, coalescing
TM2140	large elliptic to circular necrosis	blurred	large	brown	small brown spots evolve to big elliptic-circular brown spots with orange-yellow halo
TM2268	small brown spots	distinct	small	brown	small very dark spots converge into irregular dark brown short segments or blotches
TM2286	small brown spots	distinct	small	brown	sparse brown spots of varying size, discolored and curled leaf margins
TM2290	small bronze spots/short lines	distinct	small	bronze	small brown spots converge into irregular bronze small blotches or

	Shape	Margins	Dimension	Colour	Short description
					short segments parallel to the vein
TM2424	small brown spots + central vein	distinct	small	brown	small brown spots scattered on the leaf that coalesce in a central line on the mid vein
TM2508	small brown spots	distinct	small	brown	small brown spots that tend to be distributed along the leaf veins
TM2695	small brown spots	blurred	small	brown	small brown spots that sometimes coalesce in short segments
TM3033	small brown spots	distinct	small	brown	small brown spots sparsely scattered
TM3474	small brown ellipses	distinct	small	brown	small brown spots that evolve into elliptic lesions
TM3684	large brown lesions	blurred	large	brown and light brown	big brown blotches enlarge and coalesce covering almost the entire leaf
TM4118	small dark brown spots	distinct	small	brown to dark brown	small dark brown to elliptic spots
TM5617	small burnt orange spots and blotches	distinct	small	burnt orange	small burnt orange spots sometimes grow to larger irregular lesions
TM5721	irregular elliptic to circular blotches	distinct	large	brown to burnt orange	large irregular burnt orange blotches having irregular oily margins turning to burnt orange blotches with yellow halo
TM5776	large dark brown to black elliptic to circular blotches	distinct	large	dark brown to black	large dark brown to black elliptic to circular blotches with varied shape and dimension within the same leaf
TM5866	medium-large burnt orange lesions	blurred	large	burnt orange	medium to large burnt orange irregularly shaped lesions with yellow halo

4.2 Mendelian inheritance and impact on plant vigour of the necrotic trait

Two mutants (TM599, orange blotches), and TM4118 (brown spots) were tested for Mendelian inheritance by outcrossing to a different barley cultivar (Barke), F₁ were selfed, and F₂ populations grown and phenotyped (Figure 2). In both cases, necrotic:wild-type plants adhered to the expected ratio of 1:3 for the segregation of a recessive gene ($\chi^2 = 0.40$, $p = 0.52$ and $\chi^2 = 0.17$, $p = 0.68$, respectively; Table 2).

In Table S1 are the results from the phenotyping of the two F₂ populations, which include measurement of number of culms (height > 40 cm), plant height and percentage of necrotic

area. Vigor index, calculated as the number of culms higher than 40 cm times plant height, is not correlated to the percentage of necrotic area ($R^2 = 0.21$ for TM599; $R^2 = 0.0002$ for TM4118) or to the number of necrotic spots ($R^2 = 0.15$ for TM599) and it does not differ between the mutant and the wild-type group of plants: for TM599 the average is, respectively, 298.8 and 248.7 cm, t -test = 1.08, $p = 0.28$; for TM4118 the average is, respectively, 335.3 and 353.5 cm, t -test = 1.97, $p = 0.62$ (Table 3).

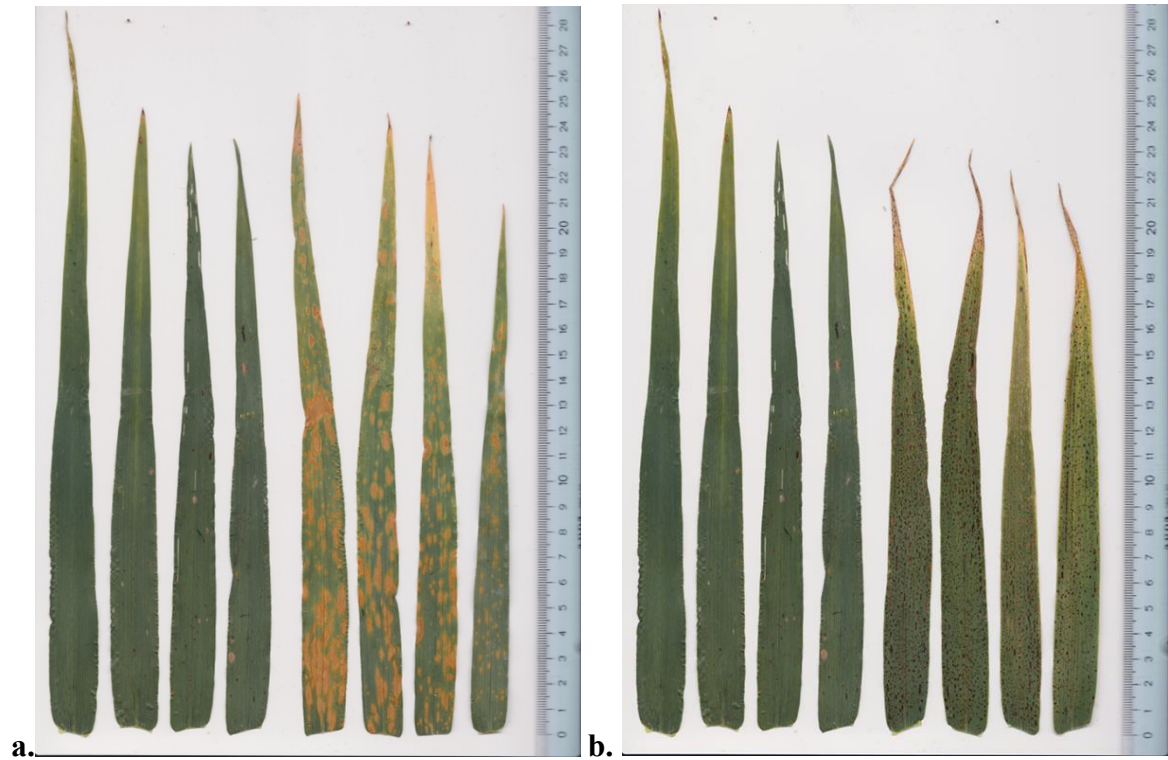


Figure 2. Example of mutant (first four from the right) and wild-type leaves (first four from the left) from the two F_2 populations used for BSA of TM599 (a) and TM4118 (b). Third leaves from the top were collected at flowering time and images were acquired with a digital scanner.

Table 2. Mendelian inheritance of necrotic mutations carried by TM599 (large orange blotches) and TM4118 (small brown spots).

ID F_2	Wild-type	Mutant	Total	Ratio	χ^2	P
TM599 \times Barke	149	43	192	0.29	0.40	0.52
TM4118 \times Barke	114	48	162	0.42	0.17	0.68

Table 3. Difference in vigor index between wild-type and mutants in the two F_2 populations.

ID F_2	Vigor index wt(cm)		Vigor index		P
	Wild-type	Mutant	wt	mutant	

				mut (cm)		
TM599 × Barke	149	298.8	43	248.7	1.08	0.28
TM4118 × Barke	114	335.3	48	353.5	1.97	0.62

4.3 BSA-based mapping of necrotic mutants

To genetically map the causative loci, BSA using a high-density SNP array was performed on F₂ plants from both populations. The locus for TM599 was mapped on chromosome 6H, between markers BOPA2_12_30697 and BOPA2_12_10803 (at ~21.5 Mb and ~404.0 Mb, respectively, on Morex ref.3. Figure 3.a). The locus for TM4118 was mapped on chromosome 1H between markers BOPA1_ConsensusGBS0342-1 and SCRI_RS_188218 (~83.3 and ~478.8 Mb, respectively, on Morex ref.3. Figure 3.b), and following KASP markers development, to an interval of approximately 15 Mb encompassing 116 genes. Additional investigations (Paragraph 4.4) showed that TM4118 corresponds to a new allele of the previously cloned *necl* (Rostoks et al., 2006). These results indicate that our DLM mutant collection includes mutants under a simple genetic control amenable to gene cloning.

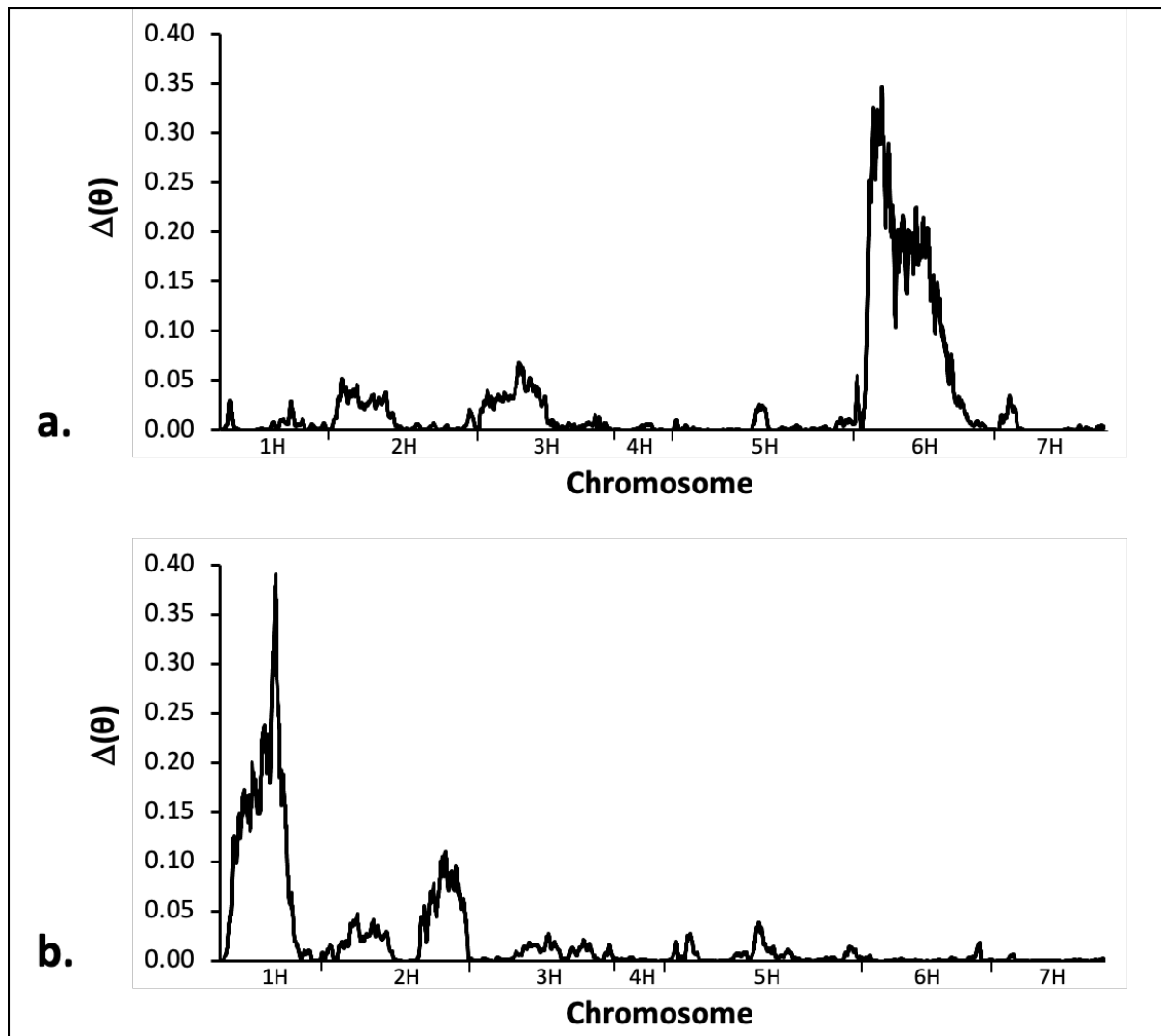


Figure 3. Results of genetic mapping by BSA combined with high-density SNP array of disease lesion mimic (DLM) mutants TM599 (a) and TM4118 (b). The y-axis (delta theta) value represents allele frequency deviation from null (50:50) at each SNP marker, derived following Hyten et al. (2008) with modification (see Materials and Methods).

4.4 TM4118 has the same causal gene as the previously described *nec1* mutant

TM4118 displays the same necrotic brown spots of the *nec1* barley mutant which has previously been described and cloned (Rostoks et al., 2006). The F₂ from TM4118 × Barke demonstrates the Mendelian recessive inheritance of *nec1-like* ($\chi^2 = 0.14$, $n = 162$). Bulked segregant analysis on the same F₂ population followed by fine mapping with 16 KASP markers identified an interval of 5.3 Mb on chromosome 1H between markers BOPA2_12_10166 and BOPA1_1670-369 and between positions 468.3 Mb and 473.6 Mb; within this interval 154 high confidence genes are contained. This region corresponds with the previously mapped and cloned DLM *Nec1* locus (Rostoks et al., 2006), encoding a cyclic

nucleotide-gated channel. We proceeded with WGS sequencing of TM4118 with Illumina HiSeq PE150. A total of 7,549 of SNPs were mapped. The estimated mutation load on the whole TM4118 genome is 11280.1, equivalent to one mutation every 443 kb (very close to the mean mutation density estimated after TILLING experiments in TILLMore, 1/350 kb. Talamè et al. 2008). Only one SNP was mapped inside the TM4118 target physical interval found by fine mapping: a G>A substitution at position 1H: 469,802,123 which, based on current barley reference genome annotation, causes a stop-gain mutation on *Nec1* (gene model *HORVU.MOREX.r3.1HG0067420*). Therefore, we conclude that TM4118 carries a novel *nec1* mutant allele.

4.5 Cloning orange blotch mutations by complementation by sequencing (CBS)

We cloned the gene responsible for the orange-blotched *nec3* phenotype starting from a genomic-based approach that we named ‘complementation by sequencing’ (CBS, summarized in Figure 4). This approach relies on i) the feasibility to obtain all the induced mutations in a chemically mutagenized line, and ii) the low probability that different mutagenized lines share the same mutated genes. Operatively, CBS includes three steps. Step 1) a chemically mutagenized population is produced; step 2) mutant lines sharing the same target phenotype are identified; step 3) selected mutant lines undergo WGS sequencing and SNPs are identified by comparison with the genomic sequence of the wild-type (background) line. A gene mutated in all the selected mutant lines will be considered as candidate given the low probability that this will happen by chance. For example, mutation density (probability that a gene is affected by a moderate or strong mutation, that is, a mutation that impacts a splice site, creates a non-synonymous mutation, frameshift, or early stop codon) can be estimated based on mutation rate. For a mutation density of 0.01 in a chemically mutagenized line, the probability that two lines share independent mutations in any of their genes is $0.01 \times 0.01 \times 30,000 = 3$ (with 30,000 = approximate number of genes in a plant diploid genome), or 0.03 in case of three independent lines.

Given the Mendelian inheritance of the orange spot *nec3*-like phenotype showed by TM599, and the availability of two additional lines showing the same phenotype (TM185 and TM1000, from the same TILLMore population (Figure 1), we applied CBS to clone the underlying gene. WGS sequencing and SNP extraction resulted in a total of 369, 234, and 77 functionally mutated genes in TM185, TM599, and TM1000, respectively, corresponding to a mutation density of 0.005, 0.003, and 0.001, respectively (average mutation density = 0.003).

After comparison, the three lines were shown to share mutations only in one gene on chromosome 6H, (Table 7; Figure 5 and Figure 6), gene model *HORVU.MOREX.r3.6HG0554760*, annotated as encoding a cytochrome P450. Table 7 lists the induced SNPs on the gene found in the three mutants. TM185 has the substitution of guanine with thymine at position 1384 compared to Morex, it causes a missense moderate mutation and an amino acid replacement of glycine at position 450 with tryptophan. TM599 has the substitution of cytosine with thymine at position 341 that causes a moderate mutation and the replacement of serine at position 114 with a phenylalanine. TM1000 has the substitution of guanine with thymine at position 1261 that causes a stop gained strong mutation and the replacement of glutamic acid at 421 with a stop codon. These mutations were confirmed by target Sanger sequencing (Figure 8). Notably, this gene lies in the same 6H chromosome region highlighted by BSA.

Comparing the number of variants per chromosome (Table 6), it was evident that the initial seed stock used for mutagenesis contained plural contaminations from backgrounds that are different from Morex. In particular, TM185 appears to be contaminated on chromosome 6H and TM1000 on chromosomes 3H, and likely on 6H and 7H. This did not represent a limitation to the finding of the candidate gene, but we decided to leave those chromosomes out when determining the TS and TV percentages, otherwise the number of induced mutations would have been outnumbered by the pre-existent natural variants. Details on mutation density calculation are reported in Table 5.

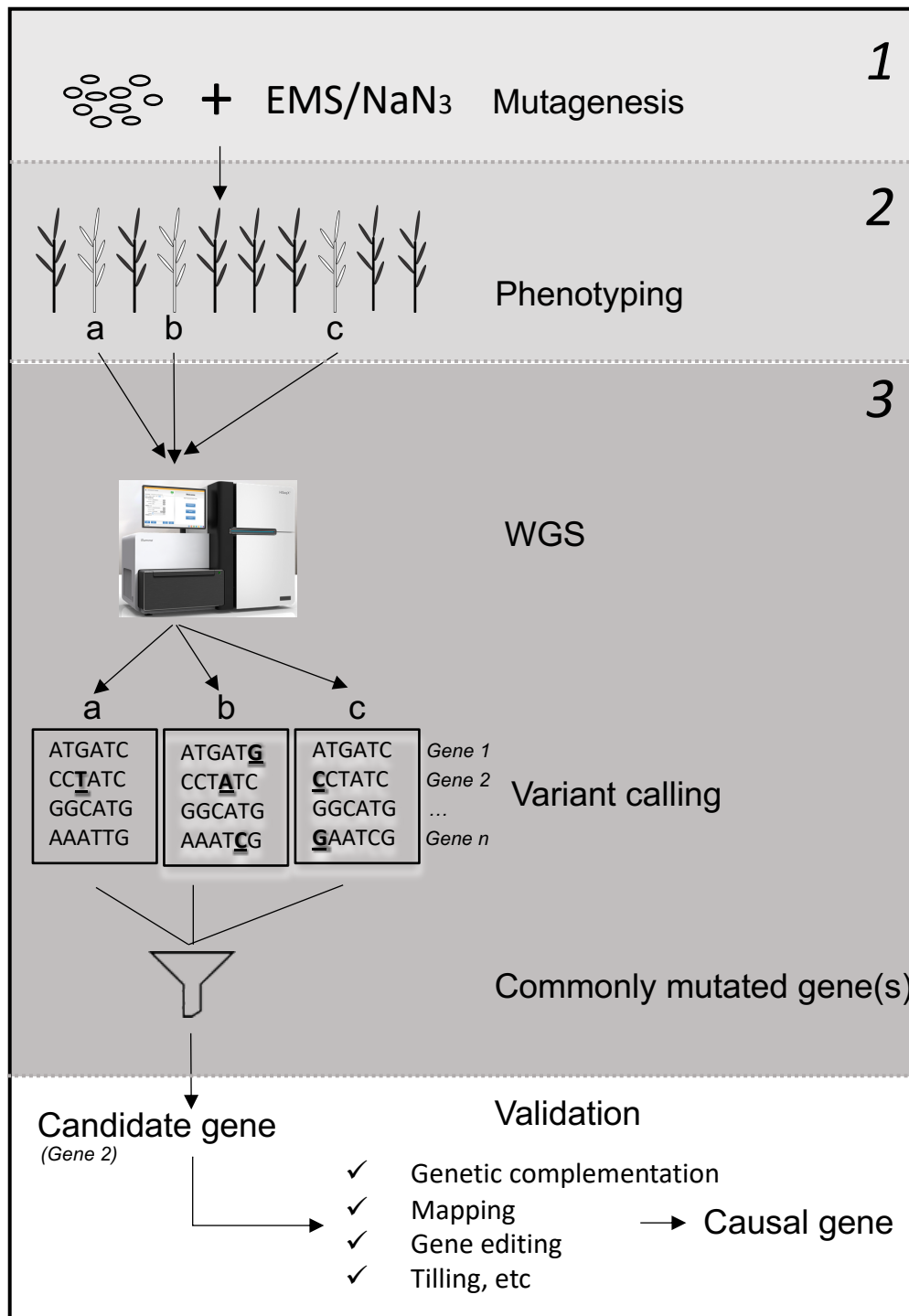


Figure 4. A schematic overview of the complementation by sequencing (CBS) method that was used to identify the candidate gene responsible for the orange blotch DLM mutations and the *nec3* locus.

Table 4. Mutation discovery by WGS in the three orange blotch DLM mutants identified within the chemically mutagenized population TILLMore.

Mutant	Mutation density (kb) ^(a)	Functional ^(b)	High effect ^(c)	Moderate effect ^(d)	TS ^(e)	TS (%) ^(f)
TM185	108.2	375	21	354	32,248	95.23
TM599	182.2	234	19	215	21,842	94.17
TM1000	310.1	78	5	73	6,917	89.01

(a) Ratio of genomic region length to number of SNPs on genes, in kilobases.

(b) Includes high and moderate effect mutations on genes.

(c) Includes stop gained, stop lost, start lost, splice acceptor or splice donor variant.

(d) Includes missense variant or missense and splice region variant. Both^(c) and^(d) according to SNPEff (see Materials and Methods).

(e) Number of transitions.

(f) Percentage of transitions on the total number of mutations in (a). Transversion number is the difference between (a) and (e).

Table 5. Values involved in mutation density (Table 4) calculation.

Mutant	SNPs ^(a)	Excluded chromosomes ^(b)	Remaining SNPs ^(c)	Remaining region (bp) ^(d)	Mutation density on remaining region (kb) ^(e)
TM185	338,095	6H	33,863	3,663,811,204	108.2
TM599	23,195	/	23,195	4,225,605,719	182.2
TM1000	49,640	3H, 6H, 7H	7,771	2,409,754,137	310.1

(a) Total number of SNPs for each mutant line.

(b) Chromosomes excluded from TS count and percentage because likely containing variants pre-existent to mutagenesis.

(c) Number of SNPs remaining after the exclusion of chromosomes.

(d) Length of the remaining region after the exclusion of chromosomes.

(e) New mutation density, as shown in Table1, calculated as the ratio of remaining region length to remaining SNPs number.

Table 6. Number of SNPs and mutation density (genomic region length/number of SNPs) in kilobases, for each chromosome, of the mutants TM185, TM599 and TM1000. Density is high on chromosome 6H of TM185 and chromosomes 3H, 6H and 7H of TM1000.

MUTANT	CHROMOSOME	SNPs	MUTATION DENSITY (kb/mutations)
TM185	1H	5,295	97.5
	2H	6,212	107.1
	3H	5,547	112.0
	4H	5,375	113.6
	5H	5,656	104.0
	6H	304,232	1.8
	7H	5,391	117.3
	Un	387	75.2
	TM599	1H	2,984
2H		4,109	162.0
3H		3,351	185.5
4H		2,719	224.5
5H		3,631	162.0
6H		3,068	183.1
7H		3,268	193.6
Un		65	447.9
TM1000	1H	1723	299.8
	2H	2022	329.2
	3H	32002	19.4
	4H	1958	311.7
	5H	2022	290.9
	6H	4253	132.1
	7H	5614	112.7
	Un	46	632.8

Table 7. Mutations identified in the candidate gene *nec3* *HORVU.MOREX.r3.6HG0554760*, in the three orange blotch DLM mutants.

Line	CHR	POS	REF ^(a)	ALT ^(b)	Q ^(c)	DP ^(d)	AD ^(e)	VARIANT ^(f)	MAGNITUDE ^(g)	SEQ ^(h)	PROT ⁽ⁱ⁾
TM185	6H	41417210	G	T	659	17	0.17	missense	moderate	c.1348G>T	p.Gly450Trp
TM599	6H	41416044	C	T	841	22	0.22	missense	moderate	c.341C>T	p.Ser114Phe
TM1000	6H	41417123	G	T	890	21	0.21	stop gain	high	c.1261G>T	p.421Glu*

(a) Reference base(s).

(b) Alternative base(s).

(c) Quality: Phred-scaled quality score for the assertion made in ALT. i.e. $-10\log_{10}\text{prob}$ (call in ALT is wrong).

(d) Read depth at this position.

(e) Allelic depths for the ref and alt alleles, in the order listed.

(f) Protein-coding gene transcript effect predictions according to SNPEff: missense_variant = change of one or more bases, resulting in a different amino acid sequence, transcript length is preserved. stop_gain = at least one base of a codon is changed, resulting in a premature stop codon, leading to a shortened transcript.

(g) Putative variant impact according to SNPEff (see Materials and Methods).

(h) Relative position inside the gene and sequence of the mutation.

(i) Position and sequence of the mutation on the protein.

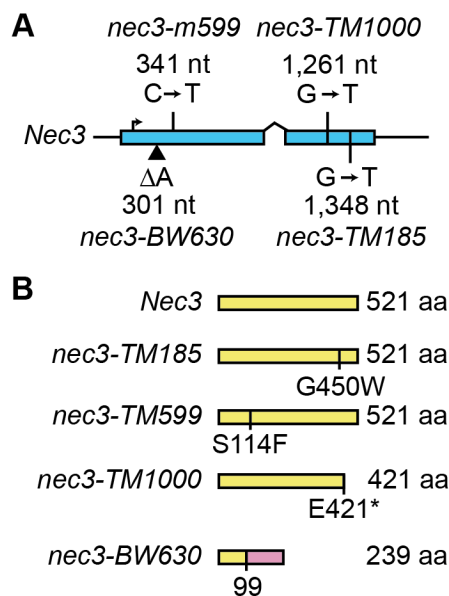


Figure 5. Gene model of *Nec3* (*HORVU.MOREX.r3.6HG0554760.1*) annotated with mutations of BW630, TM185, TM599, and TM1000. (A) Mutations at DNA sequence level

(B) Mutations at amino acid sequence level. TM185 has the substitution of guanine with thymine at position 1384 compared to Morex, it causes a missense moderate mutation and an amino acid replacement of glycine at position 450 with tryptophan. TM599 has the substitution of cytosine with thymine at position 341 that causes a moderate mutation and the replacement of serine at position 114 with a phenylalanine. TM1000 has the substitution of guanine with thymine at position 1261 that causes a stop gained strong mutation and the replacement of glutamic acid at 421 with a stop codon. BW630 has the deletion of an adenine that causes an altered open reading frame of 242 amino acids in nec3 compared to the wild type, cv. Villa.

a.

Morex	1 ATGGAGATGGAGCTGAACCTAGTCTCGTACGTGTCCATCGCCCTCTTCGTGCTCTCCGGCGGTACGTCTACCAACGGACGGCGGAGCCGGTCCCGGAGGCAGCGGCTCCC	110
TM185	1	110
TM599	1	110
TM1000	1	110
Morex	111 GCCGGCGCCGCCGGGTGGCCCGTGATCGGCCACCTCCACCTGCTGACGGACATGCCCCACCACGGCTCGGGAGCTGGCCAAGACCATGGCGCCCGCTGCTCCGGC	220
TM185	111	220
TM599	111	220
TM1000	111	220
Morex	221 TCCAGCTCGGCAGCGTCCCGCCGTTGGTGTCTCCAAGCCCGACCTTCCCGCGCCGGCGCTCACAGCAACGACGGCCATGGCGTCCCGCCCGACCTCCTCTCCGGC	330
TM185	221	330
TM599	221	330
TM1000	221	330
Morex	331 CAGTTCCTCTCTTCCGGTGTCCGACGTACGTTCCGCCCGCCGGGCGGTACCACCGCATGGCCGGCGGGTGGTGTCTCCGAGCTCCTCTCCGGCGCCCGCTCGC	440
TM185	331	440
TM599	331	440
TM1000	331	440
Morex	441 CACCTACGGCAGCTCCGGGCAAGGAGTCCGGCCCTGCTCGGCCACTCACCAAGAACACGGCCGGGAACCCCGTGCACCTAGCGAGTGCTTCTCAACCTCG	550
TM185	441	550
TM599	441	550
TM1000	441	550
Morex	551 CCAACGACGTCTCTCCCGGTGGCCCTTCGGCGCCGGTCCCGCACGGCAAGGACGACAAGCTCGCCGGGTGCTCGCCGAGGCCAGGACCTCTTCCCGGGTTACC	660
TM185	551	660
TM599	551	660
TM1000	551	660
Morex	661 GTGGGGACTTCTTCCCGAGCTGGAGCCCTTCGGGACACCGTACCAGGTCTCCGGCGCCGGTGAAGAGCTGCCTCGCCGACCTCCCGGAGGTCTGCGACGACATCGT	770
TM185	661	770
TM599	661	770
TM1000	661	770
Morex	771 CGAGGAGCAGTGAGCGGCAAGCAGGAGCCCTCCCGCGGACCGGACGAGGACTTCGTGGACGTCTCTCCGCGTCCAGAAGTCCCGCCGACCTCGAGGTCCCGCTCA	880
TM185	771	880
TM599	771	880
TM1000	771	880
Morex	881 CCGACGACACTCAAAGCCCTCGTCTGGACATGTTGTCGCCGGCACGGACAGGACTTCGGACGCTGGAGTGGTGTGACGGAGCTGGTGGCCACCCCGCCATC	990
TM185	881	990
TM599	881	990
TM1000	881	990
Morex	991 CTGAAAAGGGCGCAGGACGAGTCCGGCGTGTGTCGGCGCAAGGACGGGTGGAGGAGTCCGACCTGGCGGAGCTCCACTACATGCGGGCCATCATCAAGGAGACCTT	1100
TM185	991	1100
TM599	991	1100
TM1000	991	1100
Morex	1101 CCGGCTGACCCGGCGGTGCCGCTGCTGGTCCCGGGAGACCGTGGCGGCTGCACGCTGGCGGCTACGACATCCCGGCCAAGACCCGGGTCTTCAACAACCTTCG	1210
TM185	1101	1210
TM599	1101	1210
TM1000	1101	1210
Morex	1211 CCATGGCCGGGACCCGGAGATCTGGGAGGACCCGCTGGAGTACTCGCCGAGCGGTTGAGGTGCCCGGTGCCGGCGGAGATCGACCTCAAGGACCCGGACTACAAG	1320
TM185	1211	1320
TM599	1211	1320
TM1000	1211	1320
Morex	1321 CTGCTGCCGTTCCGGCGCGGGGAGGGGTTGCCCGGGTACACGTTCCGGCTGGCCACGGTGCAGGTGTCGCTGGCCAGCCTGCTGTACCCTTCGAGTGGCGCTGCC	1430
TM185	1321	1430
TM599	1321	1430
TM1000	1321	1430
Morex	1431 CGCCGGCTGCCGCCGAGGACGTGAGCGTGGAGGAGCTTCGGCTGGCCACCAGGAAGAAGACCCGCTCTTCGTGCCGTGAGGAAGAGCGAGTGTACGGCTTCA	1540
TM185	1431	1540
TM599	1431	1540
TM1000	1431	1540
Morex	1541 ACGGGGAGGAGCTCAACGAGGTTTAA	1566
TM185	1541	1566
TM599	1541	1566
TM1000	1541	1566

b.

```

Morex      1 MEMELNLVSYVSIALFVLSGAYVYHATRSRSPRQRLPPAPPWPVIGHLHLLTDMPHHALAEAKTMRAPLLRLQLGSPAVVI SKPDLARAALTSNDAAMASRPHLLSG 110
TM185     1 ..... 110
TM599     1 ..... 110
TM1000    1 ..... 110

Morex     111 QFLSFGCS DVT FAPAGPYHRMARRVVVSELLSARRVATYGSVRGKELRRLLAHLTKNTAPGTPVDLSECFNLANDVLCRVAFGRRFPHGKDDKLA AVLAE AQDLFAGFT 220
TM185    111 ..... 220
TM599    111 . . . F . . . . . 220
TM1000   111 ..... 220

Morex     221 VGDFFPELEPFASVTGLRRRLKSLADLREVCDDIVEEHVSGKHERLPGRDEDVVDLLRVQKSPDLEVPLTDDNLKALVLDMFVAGTDTTFFATLEWVMT ELVRHPR I 330
TM185    221 ..... 330
TM599    221 ..... 330
TM1000   221 ..... Q . . . . . 330

Morex     331 LKRAQDEVRRVVGKGRVEESDLAELHYMRAIIKETFR LHPAVPLLVPRETVAAC TGGYDIPAKTRVFINTFAMGRDPEIWEDPLEYSPERFEVAGGGEIDLKDPDYK 440
TM185    331 ..... 440
TM599    331 ..... 440
TM1000   331 ..... D . . . . * 421

Morex     441 LLPFGGRRGCPGYTFALATVQVSLASLLYHFEWALPAGVRAEDVSV EESFGLATRKKDPLFVAVRKS DVYAFNGEELNEV* 522
TM185    441 ..... W . . . . . 522
TM599    441 ..... 522
TM1000   441 ..... 522

```

Figure 6. Multialignment of *nec3* alleles. Alignment of the **a)** coding sequences and **b)** proteic sequences of the *Nec3* gene from TM185, TM599 and TM1000 to the reference sequence (Morex, wild-type). The layout was generated with Jalview v.2.11 (Waterhouse et al., 2009). TM1000 has three SNPs compared to Morex, only the third one (c.1261G>T) causing a STOP codon has been caused by mutagenesis whilst the other two, causing missense variants, were previously present, derived from natural heterogeneity (see Table 6).

4.6 Functional validation of cytochrome P450 as causal gene for the orange blotch and the historical *nec3* barley mutations

Functional validation of *cytochrome P450* was obtained following three approaches. Firstly, we fine mapped the causal DLM locus in TM599 by developing and mapping KASP markers down to a region of ~165 kb interval on chromosome 6H, between markers 1_0355_120_R and morex_contig_6964_765_F, at 41,293,242 and 41,458,908 bp, respectively, which included six genes. Among these genes, only *HORVU.MOREX.r3.6HG0554760* showed a mutation in TM599 (the C>T substitution at position 41,416,044 that was highlighted above). Second, complementation tests were carried out by producing all the crosses between the three orange blotched DLM lines. All the F₁ plants displayed the typical orange necrotic phenotype, meaning no complementation occurs (Figure 7), thus suggesting that the three lines share the same causal gene. Third, we carried out a complementation test between TM599 and BW630 (Figure 7), which carries an historical *nec3* mutant allele that exhibits a similar orange spot DLM phenotype to TM185, TM599, and TM1000 (Druka et al., 2011). Also in this case, no complementation was observed in the F₁ plants, suggesting that BW630 shares the same causal gene as our three DLM mutants. Lastly, we searched for mutations in

cytochrome P450 in BW630 which was shown to carry a deletion of an adenine that causes an altered open reading frame of 242 amino acids in *nec3* (Figure 5) as compared to its wild-type sequence (from the cv. Villa), in agreement with the X-ray-based random mutagenesis that was utilized (Häuser & Fischbeck, 1976). Taken together, these results validate that *HORVU.MOREX.r3.6HG0554760*, a predicted cytochrome P450 encoding gene, as the causal gene responsible for the orange blotch DLM mutations and the historical *nec3* barley locus. In turn, these results validate the CBS approach for identifying candidate genes in chemically mutagenized populations.



Figure 7. Results of complementation test between *nec3* mutants. From left to right: F₁ plants for TM599 × BW630, TM599 × TM1000, TM185 × TM599. All F₁ plants from the three crosses between the four *DLM nec3*-like mutants showed the distinctive orange blotch phenotype.

Table 8. PCR primers used in the validation of mutant alleles of *nec3*.

ID	SEQUENCE
TAN_F1	CCACCTCCACCTGCTGAC
TAN_R1	AGGTTGTCGTCGGTGAGC
TAN_F2	ACAACCTCAAAGCCCTCGT
TAN_R2	GGTCCTTCTTCCTGGTGG

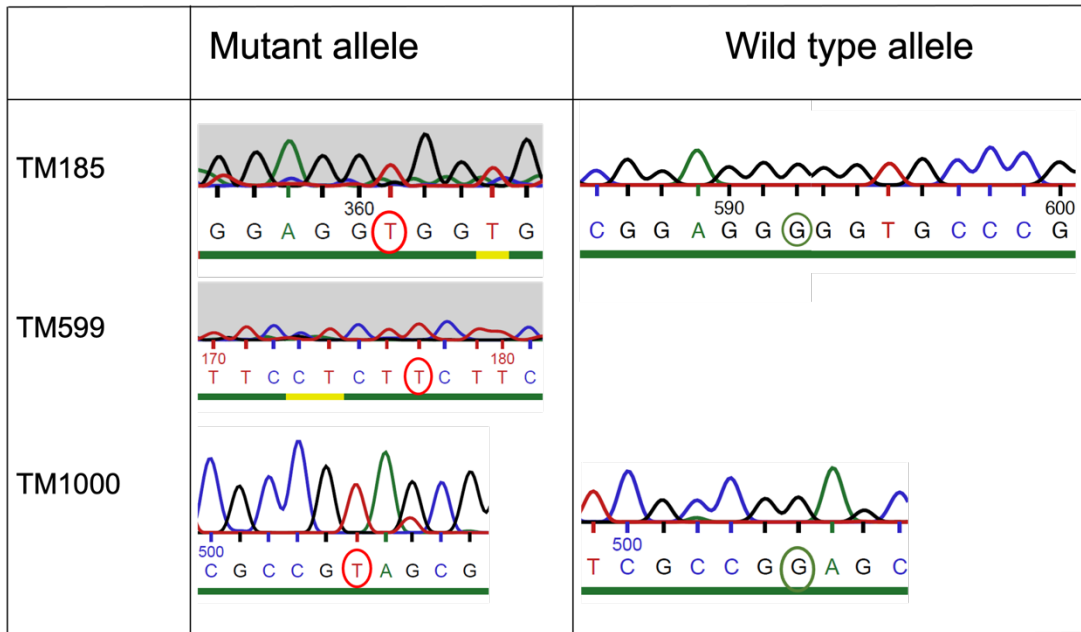


Figure 8. Sanger sequencing results of the *NEC3* alleles. On the left column: chromatograms of sequences from mutant plants in the region of previously identified SNPs. In red circle: SNPs mutations. On the right column: chromatograms of sequences from wild-type Morex plants in the same region as on the left. In green circle: reference base corresponding to mutations in the red circle.

4.7 Homology modelling of *NEC3*

The structural determinants associated with mutations in *nec3* were analysed through structural modelling of the protein. The *NEC3* protein model structure has the typical tertiary structure of globular proteins and is composed almost entirely by α -helices and by three small antiparallel β -sheets (Figure 10). The heme group is hosted in a large cavity in the centre of the protein and is held in place through the formation of a coordination bond between the side chain of Cys451 and the central iron ion. The iron ion is also bound to a water molecule completing a slightly distorted octahedral coordination geometry of the metal. The heme group is also H-bonded to Arg104, Arg379, and Gly446, further stabilizing the binding pose of the prosthetic group in its pocket. The mutation identified in the TM185 mutant line (G450W) can interfere with the positioning of the heme group. Indeed, Gly450 is located in the heme pocket and a substitution with a larger residue, such as a tryptophan, can impede the correct collocation of the heme group. Moreover, Gly450 is next to the iron-coordinating residue Cys451 and a mutation at this position can impair the conformation of the loop hosting Cys451 and subsequently change the position of the heme group. In the case of

residues (E, F, I, K, L, M, Q, R, W, Y): b; positively charged (K, R, H): +; negatively charged (D, E): -; charged (D, E, K, R, H): c.

Table 9. Model structure evaluation. Results of the Procheck and Prosa analysis done on the NEC3 model structure and on the ferruginol synthase from *Salvia miltiorrhiza* (Chinese sage) structure (PDB id 5YLW).

Protein	Procheck Ramachandran plot				Procheck G-factor	Prosa Z-score
	Most favored	Additionally allowed	Generously allowed	Disallowed		
NEC3	92.8%	6.9%	0.2%	0.0%	-0.12	-9.27
5YLW	95.1%	4.1%	0.0%	0.0%	-0.23	-9.79

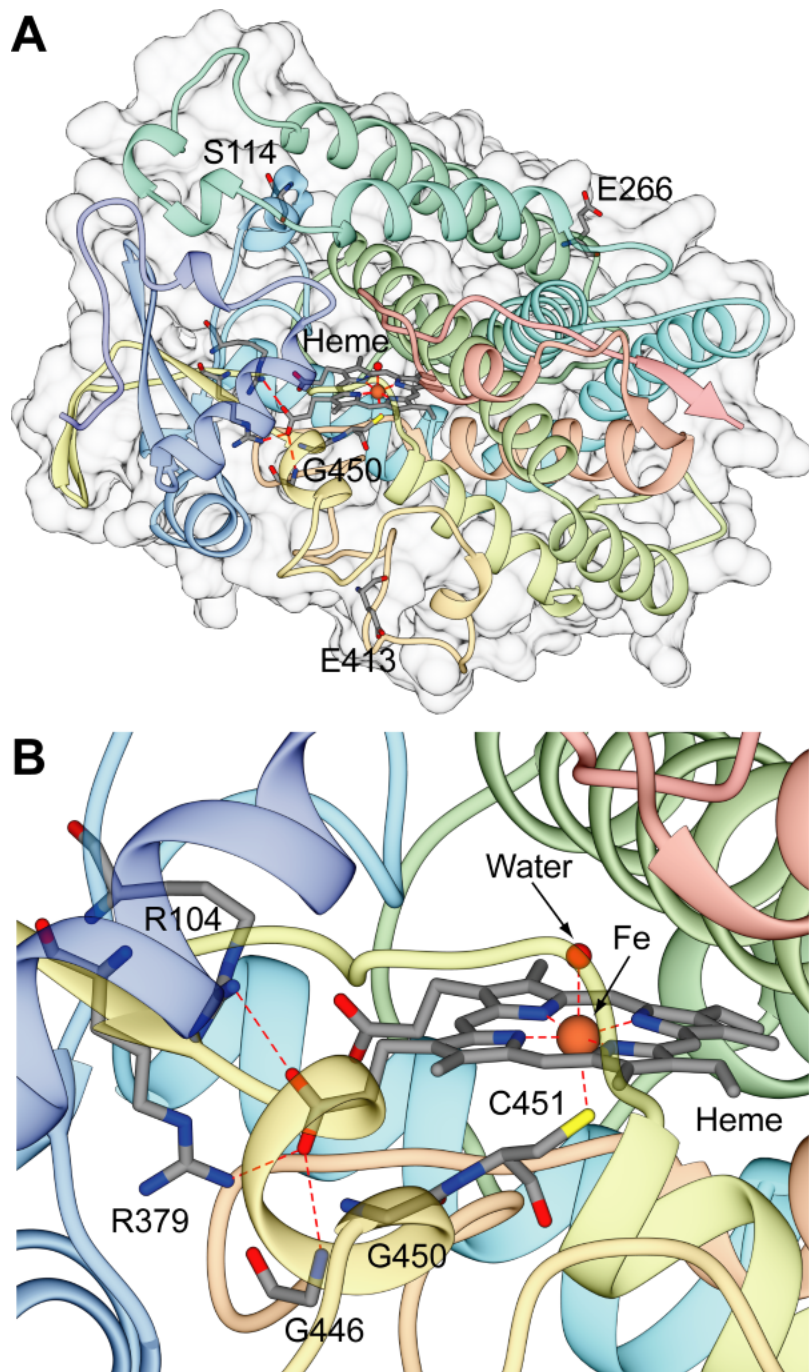


Figure 10. NEC3 model structure. a) Ribbon diagram and molecular surface of the NEC3 model structure. The ribbons are colored from blue to red by going from the N- to the C-terminal. The heme group and the residues cited in the text are reported as sticks colored according to the atom type. b) Detail of the heme group and of the residues coordinating the iron ion or H-bonding the heme group.

4.8 P450 and its evolution in plants

To identify the evolutionary origin of *nec3*, we identified cytochrome P450 domain-containing proteins from barley (400 proteins), rice (*Oryza sativa*; 409 proteins), and

Brachypodium distachyon (347 proteins). The maximum likelihood tree using the multiple sequence alignment of cytochrome P450 found that *Nec3* belongs to the *CYP71P1* gene family (Fujiwara et al., 2010). Previous work in rice found that the necrotic lesion mutant *sekiguchi lesion (sl)* encodes *CYP71P1*, which catalyzes the conversion of tryptamine to serotonin (Fujiwara et al., 2010). Barley *nec3* mutants phenocopy the rice *sl* mutants with having orange lesions on leaves (Kiyosawa, 1970; Sekiguchi & Furuta, 1965). The presence of *CYP71P1* in rice and barley indicates that this gene family emerged prior to the divergence of these two species. Previous work had found orthologs of *CYP71P1* in *Triticum aestivum* (wheat), *Brachypodium distachyon*, *Setaria italica*, *Sorghum bicolor*, and *Zea mays*, but absent in *Arabidopsis thaliana*, *Brassica napus*, *Glycine max*, and *Medicago truncatula* (Lu et al., 2018). To define the boundaries of the presence/absence variation of the *CYP71P1* gene family, we used BLAST to identify putative orthologs of *HvCYP71P1* in angiosperms based on a set of 123 species (52 families; 31 orders) used by Zhao et al. (2020).

Phylogenetic analysis of putative orthologs found that alignment identity closely matched presence within the *CYP71P1* gene family (Figure 11). The *CYP71P1* gene family phylogeny largely reflects the species tree of the angiosperms, split into monocots and dicots. No evidence was found for the presence of the *CYP71P1* gene family in gymnosperms, ferns, lycophytes, or bryophytes. The most substantial lineage-specific expansions occur within the monocots, including an ancient duplication within the Panicoideae (subfamily 1 and subfamily 2), a duplication of *CYP71P1* from chromosome group 6 to chromosomes 4B and 5A in *Triticum turgidum*, and a recent expansion in *Echinochloa crus-galli* (cockspur grass). Several families are absent in the *CYP71P1* gene family phylogeny. Overlay of the presence or absence of the *CYP71P1* gene family found substantial variation throughout angiosperms (Figure 12). Evaluation of all families where at least two species are present showed that five families lack *CYP71P1*: Brassicaceae (9 species), Cleomaceae (2 species), Orchidaceae (2 species), Fabaceae (12 species), and Cucurbitaceae (4 species). Taken together, these results show that *CYP71P1* is only found in angiosperms, is widely present in diverse monocot and dicot species, and has been dispensable in some lineages.

The domain structure of *CYP71P1* includes a predicted chloroplast localization signal peptide, proline-rich region, K-helix, and heme-binding motifs. We re-evaluated the mutational landscape in *CYP71P1* family members in rice and barley compared to conservation in amino acid composition in the multiple sequence alignment (Figure 13). The barley mutant S114F is a highly conserved position (86 Ser, 4 Ala, and 1 Phe) with the 4 Ala (ZmayB, PhaC, PviB, TrdcD) and 1 Phe (GraB) in species with multiple *CYP71P1* genes.

Rice mutant T314I (CM2229) is highly conserved with 89 Thr and 1 Ala, with the single Ala in PhaA from a member of the gene family in *P. hallii*). A gap in the position was observed in TrdcD (another duplication from polyploidization and likely a pseudogene). Rice mutant G455D in the heme-binding motif was invariant in 89 CYP71P1 proteins except for a gap in TrdcD. These results show that all loss-of-function mutations that we identified in this study occur in highly conserved sites in CYP71P1.

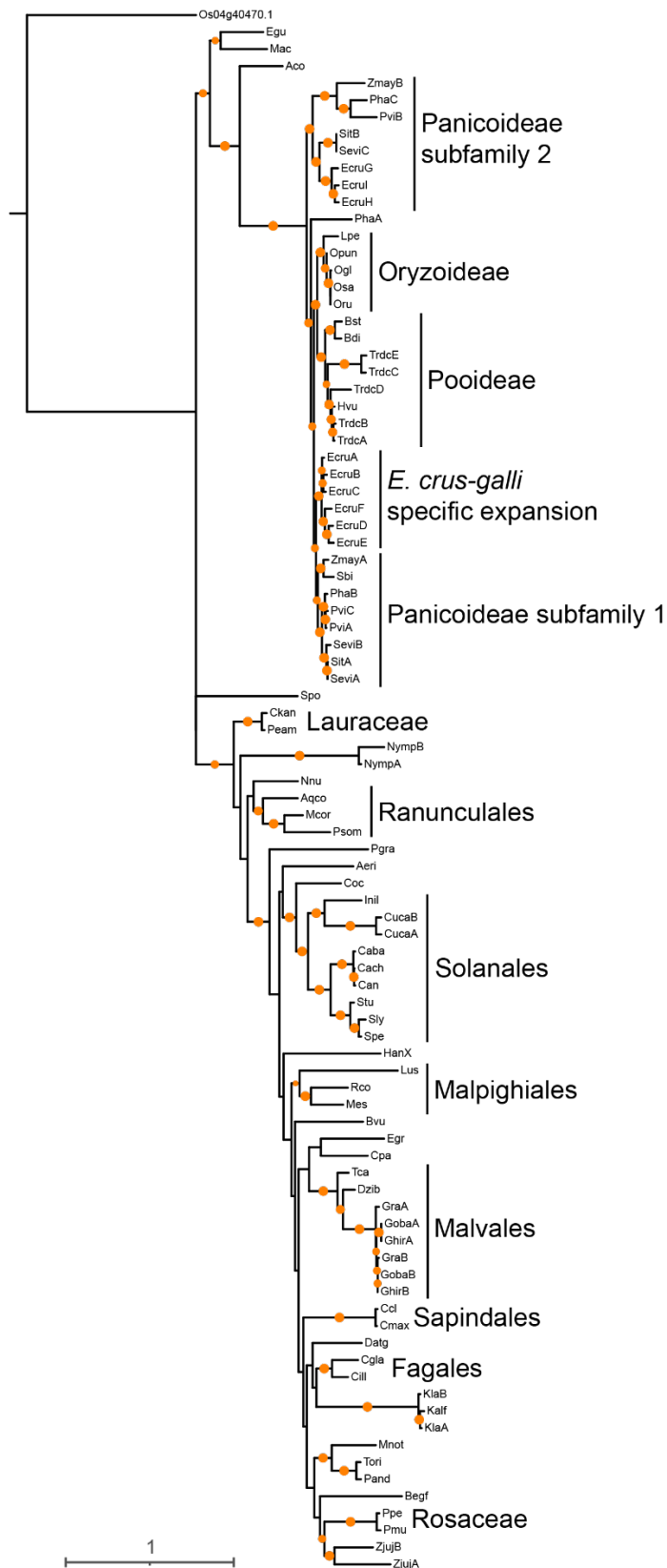


Figure 11. Phylogenetic tree of the *CYP71P1* protein family. Multiple sequence alignment was performed using MUSCLE (v3.8.31). Phylogenetic tree was constructed using iqtree (v1.6.12). Support is based on 1,000 bootstraps with orange circles indicating at least 80%

support. Order and family are annotated when all members are present within a clade with bootstrap support. Rice *Os04g40470* was used as outgroup.

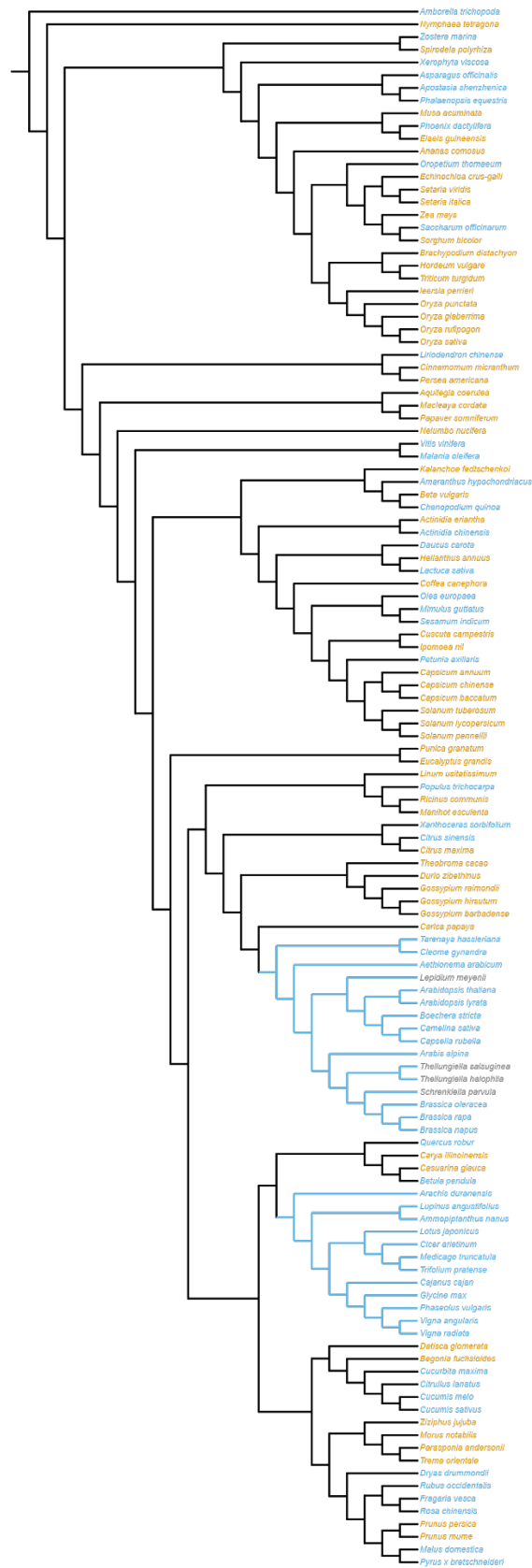


Figure 12. Substantial presence/absence variation in the *CYP71P1* gene family throughout angiosperms. Presence (orange) or absence (blue) is based on iterative BLAST analysis to identify putative *CYP71P1* homologs and phylogenetic analysis to confirm orthology. Grey indicates that the genome was inaccessible. Angiosperm phylogenetic tree is from Zhao *et al.* (2020).

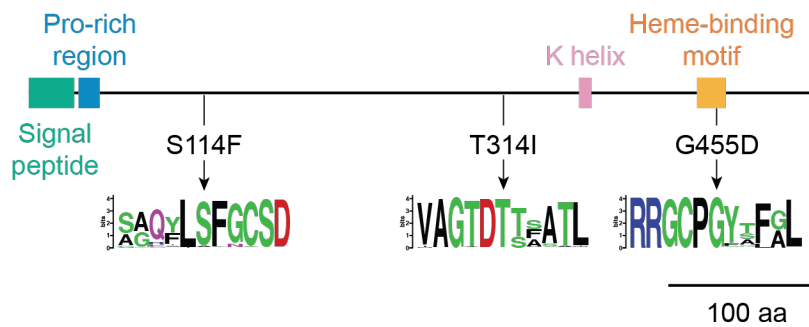


Figure 13. Mutational landscape of the *CYP71P1* gene family. *CYP71P1* carries a predicted chloroplast localization signal peptide, proline-rich region, K-helix, and heme-binding motifs. Barley mutant S114F is a highly conserved position (86 Ser, 4 Ala, and 1 Phe) with the 4 Ala (ZmayB, PhaC, PviB, TrdcD) and 1 Phe (GraB) in species with multiple *CYP71P1* genes. Rice mutant T314I (CM2229) is highly conserved with 89 Thr and 1 Ala, with the single Ala in PhaA from a member of the gene family in *P. hallii*). A gap in the position was observed in TrdcD (another duplication from polyploidization and likely a pseudogene). Rice mutant G455D in the heme-binding motif was invariant in 89 *CYP71P1* proteins except for a gap in TrdcD.

5 DISCUSSION

DLM mutants are invaluable tools to dissect the plant defence mechanisms. The collection of 34 DLM barley mutant lines presented in this study significantly integrates existing resources in barley, where approximately 30 DLM mutant lines were previously described (Druka *et al.*, 2011; Lundqvist *et al.*, 1997; Rostoks *et al.*, 2003). Once thoroughly characterized, our collection is expected to unveil new loci and new alleles at known loci. In this work, TM4118 was shown to be a new allele of the known DLM gene *nec1* (Rostoks *et al.*, 2006), whereas TM185, TM599, and TM1000 contributed three independent alleles of *nec3* and allowed us to clone the underlying gene. *nec3* or *necrotic leaf spot 3* is a historical barley mutation (Häuser & Fischbeck, 1976) for which different induced alleles are available, causing tan,

orange, or brown necrotic blotches on leaf sheath and blade, persisting to maturity (Lundqvist et al., 1997). Some *nec3* alleles were shown to have a negative effect on plant vigor (Druka et al., 2011). By CBS, here we have shown that *nec3* corresponds to the *cytochrome P450 CYP71P1*. Interestingly, the rice ortholog *Os12g16720*, was found as the causal gene for DLM mutants both in japonica (Cui et al., 2021; Fujiwara et al., 2010), and indica (Tian et al., 2020; Zheng et al., 2021) genetic backgrounds. These works clarified that CYP71P1 has tryptamine 5-hydroxylase enzyme activity and catalyzed the conversion of tryptamine to serotonin (Fujiwara et al., 2010). When CYP71P1 is defective, high endogenous oxidation level leads to cell death occurrence and blotches formation, which is consistent with the role of serotonin as an effective internal ROS scavenger (Tian et al., 2020). Other work suggested a potential role of P450 CYP71P1 on insect resistance through its serotonin synthesis effect (Lu et al., 2018) and on chloroplast development or function (Cui et al., 2021). In this work, we have identified three *HvCYP71P1* alleles and confirmed their genetic relationship with the historical mutant *nec3*. Our work shows that *nec3* is likely conserved in function between rice and barley, which facilitates further work aimed at elucidating its role in response to biotic and abiotic stresses.

Ameen et al. (2021) found that the *nec3* mutant is not a spontaneous DLM but it is induced by a reaction to pathogens, to several species of *Ascomycete* and to *Xanthomonas translucens*; *nec3* has an unstable cutin layer that possibly peels away from the leaf surface when in contact with the pathogen *Bipolaris sorokiniana* germ tubes.

Serotonin (5-hydroxytryptamine) is widely found in animals and plants, playing a role in a diverse range of physiological activities (Akula et al., 2011). The biosynthesis of serotonin in plants occurs through a two-step process: tryptophan is catalyzed into tryptamine by tryptophan decarboxylase (TDC; EC 4.1.1.28) (Berlin et al., 1993; De Luca et al., 1989), succeeded by catalysis of tryptamine by tryptamine 5-hydroxylase (T5H) to form serotonin (Schröder et al., 1999). Investigations in the biosynthesis of serotonin in St. John's wort (*Hypericum perforatum*) identified a similar pathway as mammals involving 5-hydroxytryptophan (Murch et al., 2000). Using phylogenetic analysis of the *CYP71P1* gene family, we discovered that it is an ancient gene family that emerged early in angiosperm evolution. While CYP71P1 is found in both monocots and dicots, it has been lost in several lineages. The independent loss of CYP71P1 in different plant lineages does not appear to be correlated with substantial reduction in serotonin levels (Erland et al., 2016). This supports the hypotheses that at least two pathways exist for serotonin biosynthesis or alternatively,

another enzyme exists with T5H activity. In part, serotonin biosynthesis may occur via TDC, which has both TDC and T5H activity (Park et al., 2008).

We propose complementation by sequencing (CBS) as a novel non-genetic, sequencing-only method to rapidly identify a candidate gene responsible for a mutant phenotype provided the existence of two or more individuals showing the same phenotype and originating from the same mutant collection. CBS relies on the simple rationale that it is possible to identify most or all induced mutations and that individuals sharing the same phenotype should also share the same mutated gene, albeit with different within-gene mutations. CBS can be applied to any species that can undergo random mutagenesis and is not restricted to a specific pedigree or generational step (although homozygous mutations should be available in order to target recessive mutations). As detailed below, CBS can be applied to most TILLING populations. Additionally, as CBS is not based on meiotic recombination, it can target genes located anywhere in the genome, including highly repetitive, low recombinogenic regions, usually not accessible to fine genetic mapping and positional cloning (Taagen et al., 2021).

The CBS approach depends on some assumptions that may limit its applicability. First, theoretically, CBS works best if mutation load is limited, otherwise a pair or a triplet of individuals sharing the same phenotype would also share too many mutations, preventing any candidate gene prioritization. Assessing the effect of mutation load is straightforward by applying the formula $SMG = FMD^n \times g$, where SMG = number of functionally (missense or stronger) mutated genes shared between lines; FMD = functional mutation density, i.e., probability of a gene to carry a functional mutation; n = number of plants showing a given phenotype; and g = number of genes in the genome. Functional mutation density can be derived empirically by sequencing data or by TILLING results (Wang et al., 2012). Chemical mutagenesis in plants was shown to reach an induced SNP density of c. 1/100 kb, beyond which sterility and viability become limiting (Schreiber et al., 2019; Wang et al., 2012). At this SNP density, a homozygous line will carry on average 210 functionally mutated genes, corresponding to $FMD = 0.006$ ($210/35,000$), thus, SMG between two lines will be approximately one, likely allowing to identify the effective candidate gene. For the most common lower induced SNP densities (i.e. approx. 1/500 kb) (Wang et al., 2012) the number of mutated genes per line will be in the order of 50 and SMG between two lines will drop to <1 , strongly reducing the risk of a false positive candidate gene identification. Second, population sizes should be large enough to warrant the presence of a second or third individual independently mutated in the same gene (this condition known as saturation), given a known mutation density. Estimates of mutant population sizes reaching saturation

have been thoroughly worked out and range from few thousands to 10,000 individuals (Wang et al., 2012). Third, CBS, like any other forward- or reverse-genetics approach, will be impacted by the complexity of the genetic architecture underlying a given phenotype (i.e., whenever different mutated genes would cause the same phenotype). While in this situation CBS will not identify a common gene, the increasing knowledge of biochemical metabolic pathways, including their regulation, could at least lead to the identification of the relevant biochemical pathway and gene network where the different mutations act. For this purpose, tools to explore gene knowledge, i.e., (Hassani-Pak et al., 2020) and metabolic networks, i.e., PMN, Plant Metabolic Pathway Databases (Schlöpfer et al., 2017), are available for many model and crop species. A fourth assumption is the availability of a high reference genome, which is necessary for reliable SNP calling in CBS step 3. However, the current favourable trend of cost reduction and throughput increase should soon make this point less relevant for most species, as exemplified in barley (Mascher et al., 2021).

6 REFERENCES

- Akula, R., Giridhar, P., & Ravishankar, G. A. (2011). Phyto serotonin. *Plant Signaling & Behavior*, 6(6), 800-809. <https://doi.org/10.4161/psb.6.6.15242>
- Al Amin, G., Kong, K., Sharmin, R. A., Kong, J., Bhat, J. A., & Zhao, T. (2019). Characterization and rapid gene-mapping of leaf lesion mimic phenotype of spl-1 mutant in soybean (*Glycine max* (L.) Merr.). *International journal of molecular sciences*, 20(9), 2193. <https://doi.org/10.3390/ijms20092193>
- Altschul, S. F., Madden, T. L., Schäffer, A. A., Zhang, J., Zhang, Z., Miller, W., & Lipman, D. J. (1997). Gapped BLAST and PSI-BLAST: a new generation of protein database search programs. *Nucleic Acids Research*, 25(17), 3389-3402. <https://doi.org/10.1093/nar/25.17.3389>
- Ameen, G., Solanki, S., Sager-Bittara, L., Richards, J., Tamang, P., Friesen, T.L. and Brueggeman, R.S., 2021. Mutations in a barley cytochrome P450 gene enhances pathogen induced programmed cell death and cutin layer instability. *PLoS genetics*, 17(12). <https://doi.org/10.1371/journal.pgen.1009473>
- Ashley-Koch, A., Yang, Q., & Olney, R. S. (2000). Sickie Hemoglobin (Hb S) Allele and Sickie Cell Disease: A HuGE Review. *American Journal of Epidemiology*, 151(9), 839-845. <https://doi.org/10.1093/oxfordjournals.aje.a010288>
- Badigannavar, A. M., Kale, D., Eapen, S., & Murty, G. (2002). Inheritance of disease lesion mimic leaf trait in groundnut. *Journal of Heredity*, 93(1), 50-52. <https://doi.org/10.1093/jhered/93.1.50>
- Balint-Kurti, P. (2019). The plant hypersensitive response: concepts, control and consequences. *Molecular Plant Pathology*, 20(8), 1163-1178. <https://doi.org/10.1111/mpp.12821>
- Berlin, J., Rügenhagen, C., Dietze, P., Fecker, L. F., Goddijn, O. J. M., & Hoge, J. H. C. (1993). Increased production of serotonin by suspension and root cultures of *Peganum harmala* transformed with a tryptophan decarboxylase cDNA clone from *Catharanthus roseus*. *Transgenic Research*, 2(6), 336-344. <https://doi.org/10.1007/BF01976175>
- Bettgenhaeuser, J., & Krattinger, S. G. (2019). Rapid gene cloning in cereals. *Theoretical and Applied Genetics*, 132(3), 699-711. <https://doi.org/10.1007/s00122-018-3210-7>
- Blumenstiel, J. P., Noll, A. C., Griffiths, J. A., Perera, A. G., Walton, K. N., Gilliland, W. D., . . . Staehling-Hampton, K. (2009). Identification of EMS-induced mutations in *Drosophila melanogaster* by whole-genome sequencing. *Genetics*, 182(1), 25-32. <https://doi.org/10.1534/genetics.109.101998>
- Bruggeman, Q., Raynaud, C., Benhamed, M., & Delarue, M. (2015). To die or not to die? Lessons from lesion mimic mutants. *Frontiers in plant science*, 6, 24. <https://doi.org/10.3389/fpls.2015.00024>
- Büschges, R., Hollricher, K., Panstruga, R., Simons, G., Wolter, M., Frijters, A., . . . Schulze-Lefert, P. (1997). The Barley *Mlo* Gene: A Novel Control Element of Plant Pathogen Resistance. *Cell*, 88(5), 695-705. [https://doi.org/10.1016/S0092-8674\(00\)81912-1](https://doi.org/10.1016/S0092-8674(00)81912-1)
- Candela, H., Casanova-Sáez, R., & Micol, J. L. (2015). Getting started in mapping-by-sequencing. *Journal of integrative plant biology*, 57(7), 606-612. <https://doi.org/10.1111/jipb.12305>
- Chu, C.-G., Faris, J., Friesen, T., & Xu, S. (2006). Molecular mapping of hybrid necrosis genes Ne1 and Ne2 in hexaploid wheat using microsatellite markers. *Theoretical and Applied Genetics*, 112(7), 1374-1381.
- Cingolani, P., Platts, A., Wang, I. L., Coon, M., Nguyen, T., Wang, L., . . . Ruden, D. M. (2012). A program for annotating and predicting the effects of single nucleotide polymorphisms, SnpEff: SNPs in the genome of *Drosophila melanogaster* strain w1118; iso-2; iso-3. *Fly (Austin)*, 6(2), 80-92. <https://doi.org/10.4161/fly.19695>
- Comadran, J., Kilian, B., Russell, J., Ramsay, L., Stein, N., Ganal, M., . . . Waugh, R. (2012). Natural variation in a homolog of *Antirrhinum CENTRORADIALIS* contributed to spring growth habit and environmental adaptation in cultivated barley. *Nat Genet*, 44(12), 1388-1392. <https://doi.org/10.1038/ng.2447>
- Cui, Y., Peng, Y., Zhang, Q., Xia, S., Ruan, B., Xu, Q., . . . Zeng, D. (2021). Disruption of

- EARLY LESION LEAF 1*, encoding a cytochrome P450 monooxygenase, induces ROS accumulation and cell death in rice. *The Plant Journal*, 105(4), 942-956. <https://doi.org/10.1111/tpj.15079>
- De Luca, V., Marineau, C., & Brisson, N. (1989). Molecular cloning and analysis of cDNA encoding a plant tryptophan decarboxylase: comparison with animal dopa decarboxylases. *Proceedings of the National Academy of Sciences*, 86(8), 2582. <https://doi.org/10.1073/pnas.86.8.2582>
- Druka, A., Franckowiak, J., Lundqvist, U., Bonar, N., Alexander, J., Houston, K., . . . Waugh, R. (2011). Genetic dissection of barley morphology and development. *Plant Physiology*, 155(2), 617-627. <https://doi.org/10.1104/pp.110.166249>
- Eddy, S. R. (1998). Profile hidden Markov models. *Bioinformatics*, 14(9), 755-763. <https://doi.org/10.1093/bioinformatics/14.9.755>
- Erland, L. A. E., Turi, C. E., & Saxena, P. K. (2016). Serotonin: An ancient molecule and an important regulator of plant processes. *Biotechnology Advances*, 34(8), 1347-1361. <https://doi.org/https://doi.org/10.1016/j.biotechadv.2016.10.002>
- Fujiwara, T., Maisonneuve, S., Isshiki, M., Mizutani, M., Chen, L., Wong, H. L., . . . Shimamoto, K. (2010). Sekiguchi Lesion Gene Encodes a Cytochrome P450 Monooxygenase That Catalyzes Conversion of Tryptamine to Serotonin in Rice. *Journal of Biological Chemistry*, 285(15), 11308-11313. <https://doi.org/10.1074/jbc.M109.091371>
- Hassani-Pak, K., Singh, A., Brandizi, M., Hearnshaw, J., Parsons, J. D., Amberkar, S., . . . Rawlings, C. (2020). KnetMiner: a comprehensive approach for supporting evidence-based gene discovery and complex trait analysis across species. *Plant Biotechnology Journal*. <https://doi.org/10.1111/pbi.13583>
- Heuermann, M. C., Rosso, M. G., Mascher, M., Brandt, R., Tschiersch, H., Altschmied, L., & Altmann, T. (2019). Combining next-generation sequencing and progeny testing for rapid identification of induced recessive and dominant mutations in maize M2 individuals. *The Plant Journal*, 100(4), 851-862. <https://doi.org/10.1111/tpj.14431>
- Hewitt, T., Zhang, J., Huang, L., Upadhyaya, N., Li, J., Park, R., . . . Zhang, P. (2021). Wheat leaf rust resistance gene Lr13 is a specific Ne2 allele for hybrid necrosis. *Molecular Plant*, 14(7), 1025-1028. <https://doi.org/https://doi.org/10.1016/j.molp.2021.05.010>
- Hodgens, C., Chang, N., Schaller, G. E., & Kieber, J. J. (2020). Mutagenomics: A rapid, high-throughput method to identify causative mutations from a genetic screen. *Plant Physiology*, 184(4), 1658-1673. <https://doi.org/10.1104/pp.20.00609>
- Hyten, D. L., Song, Q., Choi, I. Y., Yoon, M. S., Specht, J. E., Matukumalli, L. K., . . . Cregan, P. B. (2008). High-throughput genotyping with the GoldenGate assay in the complex genome of soybean. *Theor Appl Genet*, 116(7), 945-952. <https://doi.org/10.1007/s00122-008-0726-2>
- Häuser, J., & Fischbeck, G. (1976). Untersuchungen zur Lokalzielung einiger Mutationen von Gerste (*Hordeum sativum*). *Zeits. für Pflanzenzüchtung*, 77, 269-280.
- Keisa, A., Kanberga-Silina, K., Nakurte, I., Kunga, L., & Rostoks, N. (2011). Differential disease resistance response in the barley necrotic mutant *necl*. *BMC Plant Biology*, 11(1), 1-10. <https://doi.org/10.1186/1471-2229-11-66>
- Kiyosawa, S. (1970). Inheritance of a particular sensitivity of the rice variety, Sekiguchi Asahi, to pathogens and chemicals, and linkage relationship with blast resistance genes. *Bull. natn. Inst. agric. Sci., Tokyo*, 21, 61-72.
- Krogh, A., Brown, M., Mian, I. S., Sjölander, K., & Haussler, D. (1994). Hidden Markov Models in Computational Biology: Applications to Protein Modeling. *Journal of Molecular Biology*, 235(5), 1501-1531. <https://doi.org/https://doi.org/10.1006/jmbi.1994.1104>
- Kumar, J., Hüchelhoven, R., Beckhove, U., Nagarajan, S., & Kogel, K.-H. (2001). A compromised Mlo pathway affects the response of barley to the necrotrophic fungus *Bipolaris sorokiniana* (teleomorph: *Cochliobolus sativus*) and its toxins. *Phytopathology*, 91(2), 127-133. <https://doi.org/10.1094/PHYTO.2001.91.2.127>
- Laskowski, R. A., MacArthur, M. W., Moss, D. S., & Thornton, J. M. (1993). PROCHECK: a program to check the stereochemical quality of protein structures. *Journal of Applied Crystallography*, 26(2), 283-291. <https://doi.org/https://doi.org/10.1107/S0021889892009944>
- Li, C., Liu, H., Wang, J., Pan, Q., Wang, Y., Wu, K., . . . Ma, J. (2021). Characterization and fine mapping of a lesion mimic mutant (Lm5) with enhanced stripe rust and powdery mildew

- resistance in bread wheat (*Triticum aestivum* L.). *Theoretical and Applied Genetics*.
<https://doi.org/10.1007/s00122-021-03973-1>
- Li, H. (2011). A statistical framework for SNP calling, mutation discovery, association mapping and population genetical parameter estimation from sequencing data. *Bioinformatics*, 27(21), 2987-2993. <https://doi.org/10.1093/bioinformatics/btr509>
- Li, H., & Durbin, R. (2009). Fast and accurate short read alignment with Burrows-Wheeler transform. *Bioinformatics*, 25(14), 1754-1760. <https://doi.org/10.1093/bioinformatics/btp324>
- Li, H., Handsaker, B., Wysoker, A., Fennell, T., Ruan, J., Homer, N., . . . Subgroup, G. P. D. P. (2009). The Sequence Alignment/Map format and SAMtools. *Bioinformatics*, 25(16), 2078-2079. <https://doi.org/10.1093/bioinformatics/btp352>
- Liu, S., Fu, C., Gou, J., Sun, L., Huhman, D., Zhang, Y., & Wang, Z.-Y. (2017). Simultaneous downregulation of MTHFR and COMT in switchgrass affects plant performance and induces lesion-mimic cell death. *Frontiers in plant science*, 8, 982. <https://doi.org/10.3389/fpls.2017.00982>
- Lu, H.-p., Luo, T., Fu, H.-w., Wang, L., Tan, Y.-y., Huang, J.-z., . . . Shu, Q.-y. (2018). Resistance of rice to insect pests mediated by suppression of serotonin biosynthesis. *Nature Plants*, 4(6), 338-344. <https://doi.org/10.1038/s41477-018-0152-7>
- Lundqvist, U. (2014). Scandinavian mutation research in barley - a historical review. *Hereditas*, 151(6), 123-131. <https://doi.org/10.1111/hrd2.00077>
- Lundqvist, U., Franckowiak, J. D., & Konishi, T. (1997). New and revised description of barley genes. *Barley Genetics Newsletter*, 26.
- Mascher, M., Gundlach, H., Himmelbach, A., Beier, S., Twardziok, S. O., Wicker, T., . . . Stein, N. (2017). A chromosome conformation capture ordered sequence of the barley genome. *Nature*, 544(7651), 427-433. <https://doi.org/10.1038/nature22043>
- Mascher, M., Jost, M., Kuon, J. E., Himmelbach, A., Aßfalg, A., Beier, S., . . . Stein, N. (2014). Mapping-by-sequencing accelerates forward genetics in barley. *Genome Biol*, 15(6), R78. <https://doi.org/10.1186/gb-2014-15-6-r78>
- Mascher, M., Wicker, T., Jenkins, J., Plott, C., Lux, T., Koh, C. S., . . . Stein, N. (2021). Long-read sequence assembly: a technical evaluation in barley. *The Plant Cell*. <https://doi.org/10.1093/plcell/koab077>
- Mba, C. (2013). Induced mutations unleash the potentials of plant genetic resources for food and agriculture. *Agronomy*, 3(1), 200-231. <https://doi.org/10.3390/agronomy3010200>
- Michelmore, R. W., Paran, I., & Kesseli, R. V. (1991). Identification of markers linked to disease-resistance genes by bulked segregant analysis: a rapid method to detect markers in specific genomic regions by using segregating populations. *Proc Natl Acad Sci U S A*, 88(21), 9828-9832. <https://doi.org/10.1073/pnas.88.21.9828>
- Murch, S. J., KrishnaRaj, S., & Saxena, P. K. (2000). Tryptophan is a precursor for melatonin and serotonin biosynthesis in in vitro regenerated St. John's wort (*Hypericum perforatum* L. cv. Anthos) plants. *Plant Cell Reports*, 19(7), 698-704. <https://doi.org/10.1007/s002990000206>
- Nguyen, L.-T., Schmidt, H. A., Von Haeseler, A., & Minh, B. Q. (2015). IQ-TREE: a fast and effective stochastic algorithm for estimating maximum-likelihood phylogenies. *Molecular biology and evolution*, 32(1), 268-274. <https://doi.org/10.1093/molbev/msu300>
- Obořil, M. (2017). Quantification of leaf necrosis by biologically inspired algorithms. https://inc.proteomics.ceitec.cz/non_source_files/LNC_presentation_short.pdf.
- Oladosu, Y., Rafii, M. Y., Abdullah, N., Hussin, G., Ramli, A., Rahim, H. A., . . . Usman, M. (2016). Principle and application of plant mutagenesis in crop improvement: a review. *Biotechnology & Biotechnological Equipment*, 30(1), 1-16. <https://doi.org/10.1080/13102818.2015.1087333>
- Park, M., Kang, K., Park, S., & Back, K. (2008). Conversion of 5-Hydroxytryptophan into Serotonin by Tryptophan Decarboxylase in Plants, *Escherichia coli*, and Yeast. *Bioscience, Biotechnology, and Biochemistry*, 72(9), 2456-2458. <https://doi.org/10.1271/bbb.80220>
- Parry, M. A., Madgwick, P. J., Bayon, C., Tearall, K., Hernandez-Lopez, A., Baudo, M., . . . Ouabbou, H. (2009). Mutation discovery for crop improvement. *Journal of Experimental Botany*, 60(10), 2817-2825. <https://doi.org/10.1093/jxb/erp189>

- Pei, J., Kim, B.-H., & Grishin, N. V. (2008). PROMALS3D: a tool for multiple protein sequence and structure alignments. *Nucleic Acids Research*, *36*(7), 2295-2300. <https://doi.org/10.1093/nar/gkn072>
- Pettersen, E. F., Goddard, T. D., Huang, C. C., Couch, G. S., Greenblatt, D. M., Meng, E. C., & Ferrin, T. E. (2004). UCSF Chimera--a visualization system for exploratory research and analysis. *J Comput Chem*, *25*(13), 1605-1612. <https://doi.org/10.1002/jcc.20084>
- Rostoks, N., Schmierer, D., Kudrna, D., & Kleinhofs, A. (2003). Barley putative hypersensitive induced reaction genes: genetic mapping, sequence analyses and differential expression in disease lesion mimic mutants. *Theoretical and Applied Genetics*, *107*(6), 1094-1101. <https://doi.org/10.1007/s00122-003-1351-8>
- Rostoks, N., Schmierer, D., Mudie, S., Drader, T., Brueggeman, R., Caldwell, D. G., . . . Kleinhofs, A. (2006). Barley necrotic locus *necl* encodes the cyclic nucleotide-gated ion channel 4 homologous to the *Arabidopsis* HLM1. *Mol Genet Genomics*, *275*(2), 159-168. <https://doi.org/10.1007/s00438-005-0073-9>
- Sarin, S., Prabhu, S., O'meara, M. M., Pe'er, I., & Hobert, O. (2008). *Caenorhabditis elegans* mutant allele identification by whole-genome sequencing. *Nature methods*, *5*(10), 865-867. [10.1038/nmeth.1249](https://doi.org/10.1038/nmeth.1249)
- Schläpfer, P., Zhang, P., Wang, C., Kim, T., Banf, M., Chae, L., . . . Bernard, T. (2017). Genome-wide prediction of metabolic enzymes, pathways, and gene clusters in plants. *Plant physiology*, *173*(4), 2041-2059. <https://doi.org/10.1104/pp.16.01942>
- Schneeberger, K. (2014). Using next-generation sequencing to isolate mutant genes from forward genetic screens. *Nature Reviews Genetics*, *15*(10), 662-676. <https://doi.org/10.1038/nrg3745>
- Schreiber, M., Barakate, A., Uzrek, N., Macaulay, M., Sourdille, A., Morris, J., . . . Waugh, R. (2019). A highly mutagenised barley (cv. Golden Promise) TILLING population coupled with strategies for screening-by-sequencing. *Plant methods*, *15*(1), 1-14. <https://doi.org/10.1186/s13007-019-0486-9>
- Schröder, P., Abele, C., Gohr, P., Stuhlfauth-Roisch, U., & Grosse, W. (1999). Latest on enzymology of serotonin biosynthesis in walnut seeds. *Adv Exp Med Biol*, *467*, 637-644. https://doi.org/10.1007/978-1-4615-4709-9_81
- Sekiguchi, Y., & Furuta, T. (1965). On a mutant rice cultivar with particular sensitivity against fungal pathogens. *Ann. Phytopath. Soc. Japan*, *30*, 71-72.
- Shen, M.-y., & Sali, A. (2006). Statistical potential for assessment and prediction of protein structures. *Protein Science*, *15*(11), 2507-2524. <https://doi.org/10.1110/ps.062416606>
- Si, Y., Zheng, S., Niu, J., Tian, S., Gu, M., Lu, Q., . . . Ling, H.-Q. (2021). *Ne2*, a typical CC-NBS-LRR-type gene, is responsible for hybrid necrosis in wheat. *New Phytologist*, *232*(1), 279-289. <https://doi.org/10.1111/nph.17575>
- Smith, S. M., Steinau, M., Trick, H. N., & Hulbert, S. H. (2010). Recombinant *Rpl* genes confer necrotic or nonspecific resistance phenotypes. *Molecular Genetics and Genomics*, *283*(6), 591-602. <https://doi.org/10.1007/s00438-010-0536-5>
- Spassieva, S., & Hille, J. (2002). A lesion mimic phenotype in tomato obtained by isolating and silencing an *Lls1* homologue. *Plant Science*, *162*(4), 543-549. [https://doi.org/10.1016/S0168-9452\(01\)00595-7](https://doi.org/10.1016/S0168-9452(01)00595-7)
- Sánchez-Martín, J., Steuernagel, B., Ghosh, S., Herren, G., Hurni, S., Adamski, N., . . . Wicker, T. (2016). Rapid gene isolation in barley and wheat by mutant chromosome sequencing. *Genome biology*, *17*(1), 1-7. <https://doi.org/10.1186/s13059-016-1082-1>
- Söding, J., Biegert, A., & Lupas, A. N. (2005). The HHpred interactive server for protein homology detection and structure prediction. *Nucleic Acids Research*, *33*(suppl_2), W244-W248. <https://doi.org/10.1093/nar/gki408>
- Taagen, E., Tanaka, J., Gul, A., & Sorrells, M. E. (2021). Positional-based cloning 'fail-safe' approach is overpowered by wheat chromosome structural variation. *Plant Genome*. 2021; 1-22. <https://doi.org/10.1002/tpg2.20106>

- Talamè, V., Bovina, R., Sanguineti, M. C., Tuberosa, R., Lundqvist, U., & Salvi, S. (2008). TILLMore, a resource for the discovery of chemically induced mutants in barley. *Plant Biotechnol J*, 6(5), 477-485. <https://doi.org/10.1111/j.1467-7652.2008.00341.x>
- Tian, D., Yang, F., Niu, Y., Lin, Y., Chen, Z., Li, G., . . . Wang, M. (2020). Loss function of SL (sekiguchi lesion) in the rice cultivar Minghui 86 leads to enhanced resistance to (hemi) biotrophic pathogens. *BMC Plant Biology*, 20(1), 1-14. <https://doi.org/10.1186/s12870-020-02724-6>
- Tsunewaki, K. (1970). Necrosis and chlorosis genes in common wheat and its ancestral species. *Seiken Ziho*(22), 67-75.
- Untergasser, A., Cutcutache, I., Koressaar, T., Ye, J., Faircloth, B. C., Remm, M., & Rozen, S. G. (2012). Primer3--new capabilities and interfaces. *Nucleic Acids Res*, 40(15), e115. <https://doi.org/10.1093/nar/gks596>
- Wang, F., Wu, W., Wang, D., Yang, W., Sun, J., Liu, D., & Zhang, A. (2016). Characterization and genetic analysis of a novel light-dependent lesion mimic mutant, lm3, showing adult-plant resistance to powdery mildew in common wheat. *PLoS One*, 11(5). <https://doi.org/10.1371/journal.pone.0155358>
- Wang, T. L., Uauy, C., Robson, F., & Till, B. (2012). TILLING in extremis. *Plant Biotechnol J*, 10(7), 761-772. <https://doi.org/10.1111/j.1467-7652.2012.00708.x>
- Waterhouse, A. M., Procter, J. B., Martin, D. M., Clamp, M., & Barton, G. J. (2009). Jalview Version 2--a multiple sequence alignment editor and analysis workbench. *Bioinformatics*, 25(9), 1189-1191. <https://doi.org/10.1093/bioinformatics/btp033>
- Wu, C., Bordeos, A., Madamba, M. R. S., Baraoidan, M., Ramos, M., Wang, G.-l., . . . Leung, H. (2008). Rice lesion mimic mutants with enhanced resistance to diseases. *Molecular Genetics and Genomics*, 279(6), 605-619. <https://doi.org/10.1007/s00438-008-0337-2>
- Zhao, T., Xue, J., Kao, S.-m., Li, Z., Zwaenepoel, A., Schranz, M. E., & Van de Peer, Y. (2020). Novel phylogeny of angiosperms inferred from whole-genome microsynteny analysis. *bioRxiv*, 2020.2001.2015.908376. <https://doi.org/10.1101/2020.01.15.908376>
- Zheng, Y., Xu, J., Wang, F., Tang, Y., Wei, Z., Ji, Z., . . . Zhao, K. (2021). Mutation Types of CYP71P1 Cause Different Phenotypes of Mosaic Spot Lesion and Premature Leaf Senescence in Rice. *Frontiers in plant science*, 12, 488. <https://doi.org/10.3389/fpls.2021.641300>
- Šali, A., & Blundell, T. L. (1993). Comparative Protein Modelling by Satisfaction of Spatial Restraints. *Journal of Molecular Biology*, 234(3), 779-815. <https://doi.org/https://doi.org/10.1006/jmbi.1993.162>

7 SUPPLEMENTARY MATERIAL

Supplemental Table S1 . Phenotyping of the F₂ populations derived from TM599 × Barke (a) and TM4118 × Barke (b) in the field at flowering time.

F₂ TM599 × Barke

Plant	WT/mutant	Number of culms > 40 cm	Plant height (cm)	Vigor index	Necrotic area (%)	Number of necrotic lesions	Selected for BSA
1	WT	1	66	66			
2	WT	1	45	45			
3	WT	6	85	510			
4	WT	1	52	52			
5	WT	2	53	106			
6	WT	9	83	747			
7	mut	1	51	51			
8	WT	4	67	268			
9	WT	8	70	560			
10	mut	6	75	450	39.4	13	X
11	mut	3	66	198			
12	WT	15	74	1110			
13	WT	9	75	675			
14	WT	6	74	444			
1414	WT	6	74	444			
14	WT	3	71	213			
15	WT	1	52	52			
16	WT	5	69	345			
17	WT	5	103	515			
18	WT	0	20	0			
19	WT	2	69	138			
20	WT	5	68	340			
21	WT	5	67	335			
22	WT	1	62	62			
23	mut	8	86	688	10.5	19	X
24	mut	5	81	405	16.2	18	
25	WT	3	41	123			
26	WT	0	38	0			
27	WT	9	70	630			
28	WT	4	78	312			
29	WT	2	55	110			
30	mut	2	54	108	4.6	5	X
31	mut	3	60	180	9.2	25	
32	WT	3	73	219			
33	WT	3	68	204			
34	WT	3	63	189			
35	WT	14	91	1274			
36	WT	9	63	567			
37	WT	6	99	594			
38	mut	3	70	210			
39	WT	2	49	98			
40	WT	4	70	280			
41	WT	4	61	244			
42	WT	1	45	45			X
43	WT	7	78	546			
44	WT	1	72	72			

45	WT	2	65	130			
46	WT	1	54	54			
47	WT	4	62	248			
48	mut	2	56	112	2.7	11	
49	WT	6	62	372			
50	WT	0	37	0			
51	WT	3	61	183			
52	WT	9	86	774			X
53	WT	2	61	122			
54	WT	3	58	174			
55	WT	6	104	624			
56	WT	4	85	340			
57	WT	3	51	153			
58	WT	4	61	244			
59	WT	3	60	180			
60	WT	4	52	208			
61	WT	3	72	216			
62	mut	6	67	402			X
63	mut	0	33	0			X
64	WT	2	77	154			
65	WT	2	54	108			
66	WT	0	5	0			
67	WT	6	64	384			
68	WT	6	79	474			
69	WT	7	58	406			
70	WT	4	58	232			
71	WT	2	84	168			
72	WT	5	52	260			
73	WT	1	40	40			
74	WT	3	74	222			
75	WT	2	56	112			
76	mut	4	58	232			
77	WT	5	75	375			
78	mut	4	90	360	31.9	4	X
79	WT	0	39	0			
80	WT	2	50	100			
81	WT	3	66	198			
82	WT	12	75	900			X
83	WT	4	66	264			
84	WT	6	72	432			X
85	mut	3	56	168	4.5	11	
86	WT	3	53	159			
87	mut	3	61	183	3.4	2	
88	WT	0	28	0			
89	WT	9	79	711			
90	WT	2	88	176			
91	WT	2	51	102			
9191	WT	0	12	0			
92	WT	7	66	462			X
93	WT	3	70	210			
94	WT	7	95	665			
95	mut	2	74	148			X
96	mut	3	71	213	23.3	6	
97	WT	4	93	372			
98	WT	10	69	690			
99	WT	4	82	328			
100	WT	4	73	292			
101	mut	6	92	552	20.1	11	X
102	WT	4	74	296			
103	WT	2	50	100			X
104	WT	9	80	720			X
105	mut	0	23	0	2.1	2	
106	WT	0	21	0			
107	mut	0	39	0			

108	mut	2	51	102	8.2	16	
109	WT	3	60	180			
110	WT	2	50	100			
111	WT	1	46	46			
112	WT	1	55	55			
113	WT	7	67	469			X
114	WT	7	91	637			X
115	mut	7	77	539	41.0	32	
116	WT	5	60	300			
117	WT	3	60	180			
118	WT	1	50	50			
119	WT	0	5	0			
120	WT	2	55	110			
121	WT	3	62	186			
122	mut	1	54	54	4.9	4	X
123	WT	4	76	304			
124	mut	2	124	248			X
125	WT	5	79	395			
126	mut	3	77	231	26.7	3	
127	WT	2	62	124			
128	WT	3	85	255			
129	mut	4	64	256			
130	WT	0	20	0			
131	WT	3	46	138			
132	WT	4	74	296			
133	WT	0	5	0			
134	WT	3	76	228			
135	WT	12	93	1116			X
136	WT	11	87	957			X
137	mut	4	81	324			X
138	mut	7	87	609	24.5	6	X
139	WT	8	78	624			
140	mut	0	5	0	2.4	2	
141	WT	9	72	648			
142	WT	5	87	435			
143	mut	2	56	112			
144	mut	5	66	330	7.1	14	
145	WT	14	89	1246			
146	mut	10	81	810	44.3	40	X
147	mut	10	88	880	4.8	17	X
148	WT	9	105	945			
149	WT	10	75	750			X
150	mut	1	55	55	13.3	5	
151	WT	1	71	71			
152	WT	2	55	110			
153	WT	0	30	0			
154	WT	3	68	204			
155	mut	0	39	0	11.3	10	
156	mut	4	70	280	32.8	24	
157	WT	5	55	275			
158	WT	11	93	1023			X
159	WT	5	73	365			
160	WT	7	60	420			
161	mut	9	63	567	2.5	8	X
162	mut	2	59	118			
163	WT	1	70	70			
164	WT	4	68	272			
165	WT	4	75	300			
166	mut	0	32	0			
167	WT	2	55	110			
168	WT	4	65	260			
169	WT	1	59	59			
170	WT	1	46	46			
171	WT	7	74	518			X

172	WT	1	58	58			
173	WT	4	51	204			
174	WT	1	66	66			
175	WT	4	74	296			X
176	WT	2	59	118			
177	WT	3	74	222			
178	WT	3	60	180			
179	WT	2	54	108			
180	mut	2	61	122			
181	WT	2	80	160			
182	mut	1	44	44			
183	WT	2	90	180			
184	WT	2	53	106			
185	WT	3	66	198			
186	mut	1	61	61	4.7	11	
187	WT	12	86	1032			
188	mut	5	58	290	4.8	4	
189	WT	0	39	0			
190	WT	6	81	486			

b. F₂ TM4118 × Barke

Plant	WT/mutant	Number of culms	Plant height (cm)	Vigor index	Necrotic area (%)	BSA	Selected for
1	mut	6	75	450	6.01		X
2	wt	6	65	390	0.36		X
3	wt	3	54	162	0.16		X
4	wt	1	57	57	0.22		X
5	wt	2	63	126	0.60		
6	wt	4	72	288	0.90		X
7	wt	0	26	0	0.11		X
8	wt	7	68	476	0.97		X
9	wt	8	70	560	0.00		X
10	mut	3	80	240	5.50		X
11	wt	4	70	280	0.27		X
12	wt	7	75	525	0.60		X
13	wt	3	51	153	0.45		X
14	mut	0	35	0	21.03		X
15	mut	4	55	220	37.11		X
16	wt	6	62	372	0.03		X
17	wt	5	61	305	0.72		X
18	wt	8	55	440	0.20		
19	mut	5	53	265	29.31		X
19"	mut	5	75	375	7.41		X
20	wt	7	93	651	0.73		X
21	mut	2	65	130	23.49		X
22	wt	8	70	560	0.01		
23	wt	4	68	272	0.02		
24	wt	5	61	305	0.06		X
25	wt	1	56	56	0.19		
26	mut	5	55	275	26.24		X
27	mut	6	71	426	7.11		X
28	mut	10	66	660	20.79		X
29	wt	1	55	55	0.30		
30	wt	9	105	945	0.06		
31	wt	7	63	441	0.01		
32	wt	8	64	512	0.27		X

33	wt	2	56	112	0.20	
34	wt	2	60	120	0.06	
35	mut	5	70	350	33.35	X
36	wt	5	63	315	0.79	
37	wt	9	57	513	0.50	
38	wt	2	52	104	0.76	X
39	mut	8	64	512	7.41	
40	mut	5	60	300	13.89	
41	wt	7	65	455	0.60	X
42	mut	0	15	0	5.20	
43	wt	2	66	132	0.06	
44	wt	3	93	279	0.01	
45	wt	3	72	216	0.10	
46	wt	3	60	180	0.15	
47	wt	4	62	248	0.00	
48	wt	3	52	156	0.14	
49	wt	4	58	232	0.74	
50	mut	7	105	735	15.37	
51	wt	2	65	130	0.23	
52	wt	4	57	228	0.40	X
53	wt	8	63	504	0.03	
54	mut	5	63	315	7.17	X
55	wt	1	55	55	0.74	
56	wt	7	80	560	0.04	
57	wt	6	93	558	0.06	X
58	mut	6	70	420	3.11	
59	wt	6	66	396	0.90	
60	wt	4	75	300	0.85	
61	wt	2	60	120	0.08	
62	wt	3	69	207	0.98	X
63	wt	3	75	225	0.03	X
64	wt	2	66	132	0.80	
65	mut	6	73	438	2.64	X
66	wt	2	55	110	0.04	
67	wt	2	73	146	0.01	
68	wt	7	79	553	0.00	
69	wt	2	59	118	0.12	
70	wt	2	54	108	0.69	
71	mut	6	87	522	21.70	
72	wt	5	73	365	0.11	
73	mut	5	62	310	8.94	X
74	wt	4	56	224	0.01	
75	mut	1	81	81	5.09	
76	mut	4	58	232	5.97	
77	mut	2	46	92	6.44	
78	mut	4	48	192	37.59	X
79	wt	5	59	295	0.72	
80	wt	4	68	272	0.03	
81	wt	4	65	260	0.02	
82	wt	8	92	736	0.69	
83	mut	7	74	518	10.92	X
84	mut	9	75	675	6.97	X
85	wt	1	53	53	0.01	
86	wt	4	62	248	0.02	
87	mut	3	68	204	4.04	X
88	mut	6	55	330	10.00	
89	wt	3	51	153	0.98	
90	mut	8	100	800	7.03	X

91	wt	2	50	100	0.02	
92	wt	6	73	438	0.78	
93	mut	3	48	144	15.64	X
94	wt	1	70	70	0.55	
95	wt	5	60	300	0.01	
96	mut	1	57	57	11.60	
97	wt	6	80	480	0.62	
98	wt	5	60	300	0.09	
99	mut	7	60	420	5.76	
100	mut	8	85	680	7.60	X
101	mut	3	76	228	5.81	
102	wt	9	90	810	0.00	
103	wt	7	67	469	0.02	
104	wt	8	80	640	0.13	
105	wt	8	70	560	0.01	
106	mut	7	93	651	7.20	X
107	mut	5	60	300	8.18	X
108	mut	8	97	776	10.40	X
110	mut	2	40	80	14.00	
111	wt	1	47	47	0.20	
112	wt	0	18	0	0.18	
113	wt	1	49	49	0.00	
114	mut	3	57	171	7.36	
115	wt	8	55	440	0.19	
116	wt	7	70	490	0.05	
117	mut	8	90	720	15.00	X
118	wt	7	60	420	0.01	
119	wt	3	65	195	0.01	
120	wt	2	43	86	0.01	
121	wt	5	59	295	0.67	
122	wt	4	65	260	0.01	
123	wt	5	69	345	0.23	
124	wt	8	91	728	0.33	
125	wt	3	73	219	0.36	X
126	wt	9	58	522	0.44	
127	wt	4	66	264	0.00	
128	wt	4	59	236	0.48	
129	wt	2	58	116	0.88	
130	wt	5	68	340	0.02	
131	wt	8	52	416	0.07	
132	mut	4	77	308	11.46	
133	wt	7	62	434	0.77	
134	wt	9	73	657	0.23	
135	wt	8	83	664	0.30	
136	wt	6	67	402	0.11	
137	wt	4	63	252	0.26	
138	mut	3	55	165	20.58	X
139	wt	7	65	455	0.40	
140	mut	6	58	348	49.53	X
141	mut	4	65	260	29.00	X
142	mut	6	65	390	16.00	X
143	mut	7	60	420	30.60	X
144	wt	6	75	450	0.02	
145	wt	2	55	110	0.19	
146	wt	7	57	399	0.01	
147	wt	6	70	420	0.56	
148	wt	8	97	776	0.36	
149	wt	9	77	693	0.01	

150	mut	3	75	225	11.19	
151	wt	9	93	837	0.09	
152	wt	6	95	570	0.03	
153	wt	1	57	57	0.08	
154	wt	8	80	640	0.02	
155	wt	7	77	539	0.12	
156	wt	3	57	171	0.02	
157	wt	5	71	355	0.19	
158	wt	7	78	546	0.04	
159	wt	0	38	0	0.02	
160	wt	7	68	476	0.45	
161	wt	8	80	640	0.08	
162	mut	7	80	560	11.47	

Supplemental Table S2. Chromosome length for Morex v3 reference genome, as available from (Mascher et al., 2021) .

CHROMOSOME	LENGTH
1H	516,505,932
2H	665,585,731
3H	621,516,506
4H	610,333,535
5H	588,218,686
6H	561,794,515
7H	632,540,561
Un	29,110,253

- Ameen, G., Solanki, S., Sager-Bittara, L., Richards, J., Tamang, P., Friesen, T. L., & Brueggeman, R. S. (2021). Mutations in a barley cytochrome P450 gene enhances pathogen induced programmed cell death and cutin layer instability. *PLOS Genetics*, *17*(12), e1009473. <https://doi.org/10.1371/journal.pgen.1009473>
- Mascher, M., Wicker, T., Jenkins, J., Plott, C., Lux, T., Koh, C. S., . . . Stein, N. (2021). Long-read sequence assembly: a technical evaluation in barley. *The Plant Cell*. <https://doi.org/10.1093/plcell/koab077>
- Rostoks, N., Schmierer, D., Mudie, S., Drader, T., Brueggeman, R., Caldwell, D. G., . . . Kleinhofs, A. (2006). Barley necrotic locus nec1 encodes the cyclic nucleotide-gated ion channel 4 homologous to the Arabidopsis HLM1. *Mol Genet Genomics*, *275*(2), 159-168. <https://doi.org/10.1007/s00438-005-0073-9>
- Waterhouse, A. M., Procter, J. B., Martin, D. M., Clamp, M., & Barton, G. J. (2009). Jalview Version 2--a multiple sequence alignment editor and analysis workbench. *Bioinformatics*, *25*(9), 1189-1191. <https://doi.org/10.1093/bioinformatics/btp033>
- Zhao, T., Xue, J., Kao, S.-m., Li, Z., Zwaenepoel, A., Schranz, M. E., & Van de Peer, Y. (2020). Novel phylogeny of angiosperms inferred from whole-genome microsynteny analysis. *bioRxiv*, 2020.2001.2015.908376. <https://doi.org/10.1101/2020.01.15.908376>

CHAPTER 2. Mapping and cloning the TILLMore broad leaf barley mutant TM2544

1 INTRODUCTION

Leaves are the primary photosynthetic organs and leaf blade area (LA) is a complex trait strategic for yield and adaptation improvement as it affects photosynthesis and response to water stress.

Previous studies focused on the correlation between LA and yield component. In maize grown under optimal conditions, increased leaf area is beneficial for yield, especially in shorter growing seasons (Hunter, 1980). In barley, Alqudah and Schnurbusch (2015) found that LA impacts single plant yield; for both six and two row-type barley, they reported positive correlations between LA per main culm and grain yield of the main culm. A study on main culm leaf area in a spring barley association panel grown under long day provided evidence that natural variation of leaf area is an important source for improving grain yield, adaptation and canopy architecture of temperate cereals (Alqudah et al., 2018). However, augmented LA affects leaf area index (LAI, the total one-sided area of leaf tissue per unit ground surface area) and the canopy function and, while higher LAI during canopy development benefits light interception/capture and reduce competition from weeds (Haefele et al., 2004), at maturity it could negatively affect light harvesting reducing its penetration to the bottom leaves (Berdahl et al., 1972). Under drought stress, a reduced leaf area can be beneficial due to improved WUE via dehydration avoidance, that is, the plant uses less water, but the yield is not improved (Blum, 2005; George-Jaeggli et al., 2017). Stomatal density, conductance and size should also be considered (Caine et al., 2019; Hughes et al., 2017; Liu et al., 2012).

Several mutants for leaf size and shape, among others grouped into narrow leaves, rolled leaves, dwarf/short leaves, have been described in rice (Kurata et al., 2005), maize (Neuffer et al., 1997) and barley (Shaaf et al., 2019). A number of genes and QTLs controlling leaf size have been reported in rice (Qi et al., 2008; Wang et al., 2022; Zhao et al., 2016; Zheng et al., 2021) and maize (S. Li et al., 2018; W. Li et al., 2018; Nelissen et al., 2016; Strable, 2021; Sun et al., 2017; Zhang et al., 2018) and knowledge is expanding in barley. In wheat, several QTLs have been related to flag leaf length and width (Hu et al., 2020; Liu et al., 2018; Ma et al., 2020; Wang et al.; Yan et al., 2020; Zhao et al., 2018). In barley, Liu et al.

(2015) identified two pleiotropic genomic regions on chromosome 2H and 7H controlling flag leaf length and width. Alqudah et al. (2018) applied GWAS on 215 spring barley accessions and found several QTLs with major effects on LA variation, close to heading time, phytohormone- and sugar-related genes. Du et al. (2019) found QTLs for leaf length and area for different leaves and concluded that the top four leaves were significantly positively correlated with plant height and some yield-related traits. Makhtoum et al. (2022) identified one QTL for flag leaf length in optimal conditions, and one for both flag leaf length and width under drought. Digel et al. (2016) demonstrated that the *PHOTOPERIOD-H1* (*Ppd-H1*) gene affecting flowering time in response to photoperiod (Turner et al., 2005) does also impact leaf size under long days, as its recessive mutant allele confers a longer leaf growth period that increases leaf cell number and consequently leaf length (Digel et al., 2016). *VRS1*, the gene that codes for row-type in barley, increases leaf area in six-row cultivars by greater leaf width while two-rowed leaf primordia has impaired cell proliferation (Thirulogachandar et al., 2017). *NLD1* encodes a WUSCHEL-RELATED HOMEODOMAIN 3 (WOX3), an ortholog of the maize *NARROW SHEATH* gene, whose mutation causes narrow leaves due to defects in the development of leaf marginal regions (Yoshikawa et al., 2016). *MND1*, *MND4* and *MND8* are three genes whose mutation is responsible for a shortened plastochron and reduced leaf length (Hibara et al., 2021). *BLF1* on chromosome 5H codes for a transcriptional regulator in the indeterminate domain protein family which acts as a regulator of leaf width (Jöst et al., 2016). The *blf1* recessive mutant has wider and slightly shorter leaves caused by an increased number of cell files in the medial-lateral axis.

2 OBJECTIVES

Leaf blade area is an important trait that can be used to improve yield in cereals and barley. Within the barley chemically mutagenized collection TILLMore available at the University of Bologna, a mutant line (TM2544) showing an obvious broad leaf phenotype was identified based on visual screening. Our objectives were to genetically map and clone the barley broad leaf mutant TM2544.

3 MATERIALS AND METHODS

3.1 Plant material and growth conditions

The barley broad leaf mutant TM2544 belongs to the TILLMore collection of mutants obtained with sodium azide mutagenesis on the cultivar Morex (Talamè et al., 2008).

The F₁ was generated with the outcross of TM2544 × Barke. The F₂ mapping population (F2B2544) derived from self-pollination of that F₁.

TM2544 was first identified by visual inspection as a broad leaf mutant in the field in Cadriano (Lat.: N 44°33'03'', Lon.: E 11°24'36'', 33 m a.s.l), Italy, in the spring of 2019, where it was grown with the entire TILLMore collection and Morex, following standard agronomic practices, in 0.6 m long two-row plots; the trait appeared consistently in every plant of the plot and was confirmed by measurement. TM2544, F₁ and F₂ plants, with Morex and Barke were subsequently grown in the greenhouse, in a peat and vermiculite growing medium (Vigorplant Irish and Baltic peat-based professional mix) in 15 × 15 × 30 cm polyethylene pots with a day temperature of 22°C (16 h) and a night temperature of 18°C (8 h). Greenhouse lighting was a mix of natural light supplemented with artificial light by 400 watt high-pressure sodium lamps (Sylvania SHP-TS 400W GroLux).

3.2 Phenotyping

Leaf maximum width was manually measured after their full emergence from the main culm for 20 TM2544 plants, 16 Morex, 6 F₁(from 4th leaf upwards), 125 F₂ plants grown in the greenhouse (4th, 5th, 6th, flag -1, i.e., the second leaf from the top, and flag leaf). Leaf length from the tip of the distal region to the proximal region near the ligule was manually measured. 10 flag -1 leaves from the main culm of TM2544 and 10 leaves from Morex were collected and their image was acquired with a Canon LiDE120 scanner, and their images were analyzed with the software ImageJ (Schneider et al., 2012).

3.3 BSA-Seq and Whole Genome Sequencing (WGS)

BSA-Seq (Klein et al., 2018) was carried out to map the broad leaf mutant phenotype showed by TM2544. 125 plants from the F₂ population from the cross TM2544 × Barke were phenotyped in the greenhouse. The nine plants with the most extreme phenotype were selected for each of the mutant and the wildtype bulk. Their leaf DNA was individually extracted with the Macherey-Nagel Nucleospin Plant II kit and added to two bulks in the same quantity for each single plant, reaching a final concentration of 50 ng/μl for both bulks. The whole genomic DNA was sequenced with Illumina MiSeq PE300, ≈ 30× of coverage, by

IGA Technologies Services, Udine, Italy. After the alignment with BWA 0.7.17 (Li & Durbin, 2009) on the reference Morex v2 (Monat et al., 2019), variants in the genomic space were called with Samtools 1.9, filtering for a minimum read depth of 10× and minimum PHRED quality of 40, and data were analyzed with the SNP Index method (Takagi et al., 2013), where the index of each SNP is calculated as the ratio between the number of alternate reads at the position and the total number of reads. The Δ SNP Index is the difference between the indexes of the mutant bulk and the index of the wild type bulk. The greater this difference, the more likely it is that this SNP is associated with the trait of interest. For WGS of TM2544, leaf DNA was extracted as above and it was sequenced with Illumina HiSeq PE150 by Novogene, Cambridge, UK, with 20× of coverage. The variant calling analysis was carried out by the Bioinformatics Group of the Future Food Beacon of Excellence, at the University of Nottingham. Reads were aligned to the first version of barley cv. Morex reference genome (Mascher et al., 2017) and variants were filtered for a minimum quality normalized on depth (QD) of 20 and a depth between 10 and 200. Effects were predicted with SNPEff (Cingolani et al., 2012).

4 RESULTS

4.1 Phenotyping TM2544 and of F₁ and F₂ populations

At a first visual inspection, **TM2544** leaf appeared broader than the wild type Morex, consistently in all the leaves starting from the 4th upwards and in all the culms. Its leaves were longer and with a wider insertion angle with the culm (Figure 1 and Figure 3). The mutant plants were healthy and vigorous in both field and greenhouse environments, producing long spikes with fertile florets, comparable to the wild type. The height of the plant in the field was slightly reduced compared to the wild type (Figure 1). Some leaves showed morphological anomalies in the form of crinkles and creases on the sheath, that sometimes could be more pronounced especially in the flag leaf, causing defects in the heading of the spike (Figure 2).

To compare maximum leaf width, ten TM2544 flag -1 leaves (second leaf from top) from ten independent plants were measured in the field and 20 in the greenhouse, together with, respectively, 87 and 16 leaves of Morex. The results are shown in Figure 4. TM2544 average width of 3.6 ± 0.13 cm in the field ($n = 10$ plants, one leaf per plant) was significantly greater

than the average of 2.1 ± 0.12 cm of Morex ($n = 87$ plants), with an average increase of 71% (Mann-Whitney-Wilcoxon test, $W = 53.5$, $p < 2.2 \times 10^{-16}$).

In pots, TM2544 average leaf width of 2.6 ± 0.50 cm ($n = 20$ plants, 79 leaves in total) was also significantly greater than the average Morex leaf width of 1.6 ± 0.22 cm ($n = 16$ plants, 70 leaves in total) with an average increase of 63% (Mann-Whitney-Wilcoxon test, $W = 53.5$, $p < 2.2 \times 10^{-16}$).

To compare leaf blade length, 19 TM2544 plants and 16 Morex plants in pots were measured at flowering stage. Results are shown in Figure 5. The average blade length of 25.3 ± 6.8 cm for TM2544 ($n = 19$ plants, 91 leaves in total) was significantly greater than the average of 18.5 ± 4.5 cm for Morex ($n = 16$ plants, 76 leaves in total) with an average increase of 37% (Mann-Whitney-Wilcoxon test, $W = 1344.5$, $p = 1.094 \times 10^{-11}$).

To better quantify the difference in leaf shape between mutant and wt, we elaborated the chart in Figure 6. One representative flag -1 leaf was collected from the mutant and the wild type and we measured the leaf width every 1 mm of distance from the ligule. The mutant leaf resulted larger than Morex at every distance from the ligule. Blade width reached the maximum value at 5 cm distance from the ligule in both mutant and wt.

All the plants in the F_1 populations from TM2544 \times Barke showed a broad leaf phenotype. The analysis of variance demonstrated that the leaf width in the F_1 , with an average leaf width of 2.4 ± 0.7 cm ($n = 6$ plants, 24 leaves in total) did not differ from TM2544 (Figure 7) (Kruskal – Wallis test, $\chi^2 = 163.02$, $p < 2.2 \times 10^{-16}$; Dunn test with Bonferroni adjustment, F_1 - TM2544 $Z = -1.968125$, $p_{\text{unadjusted}} = 4.905361 \times 10^{-2}$, $p_{\text{adjusted}} = 2.943216 \times 10^{-1}$, n.s). As for leaf length, the F_1 showed longer leaves compared to Morex and to both parentals TM2544 and Barke, with an average of 35.3 ± 10.1 cm, $n = 6$ plants, 24 leaves in total and an average increase of 91% compared to Morex, 39% compared to TM2544 and 25.2% compared to Barke (Kruskal-Wallis test, $\chi^2 = 70.695$, $p = 4.454 \times 10^{-16}$; Dunn's test with Bonferroni adjustment, F_1 B2544 – Morex, $p = 1.28 \times 10^{-13}$; F_1 B2544 – TM2544, $p = 3.3 \times 10^{-4}$; F_1 B2544 – Barke, $p = 2.28 \times 10^{-2}$).

The F_2 population of 125 plants from TM2544 \times Barke showed a transgressive segregation for leaf width, except for leaf 4 and leaf 5, with a minimum of 0.8 cm and a maximum of 3.5 cm (Figure 8). Data were plotted in histograms and two vertical lines were added with the average leaf width of the two parentals (Figure 9). The F_2 segregation of leaf width differed from the expected 3:1 ratio (in case broad leaf is dominant) between mutant and wild type (Table 1).

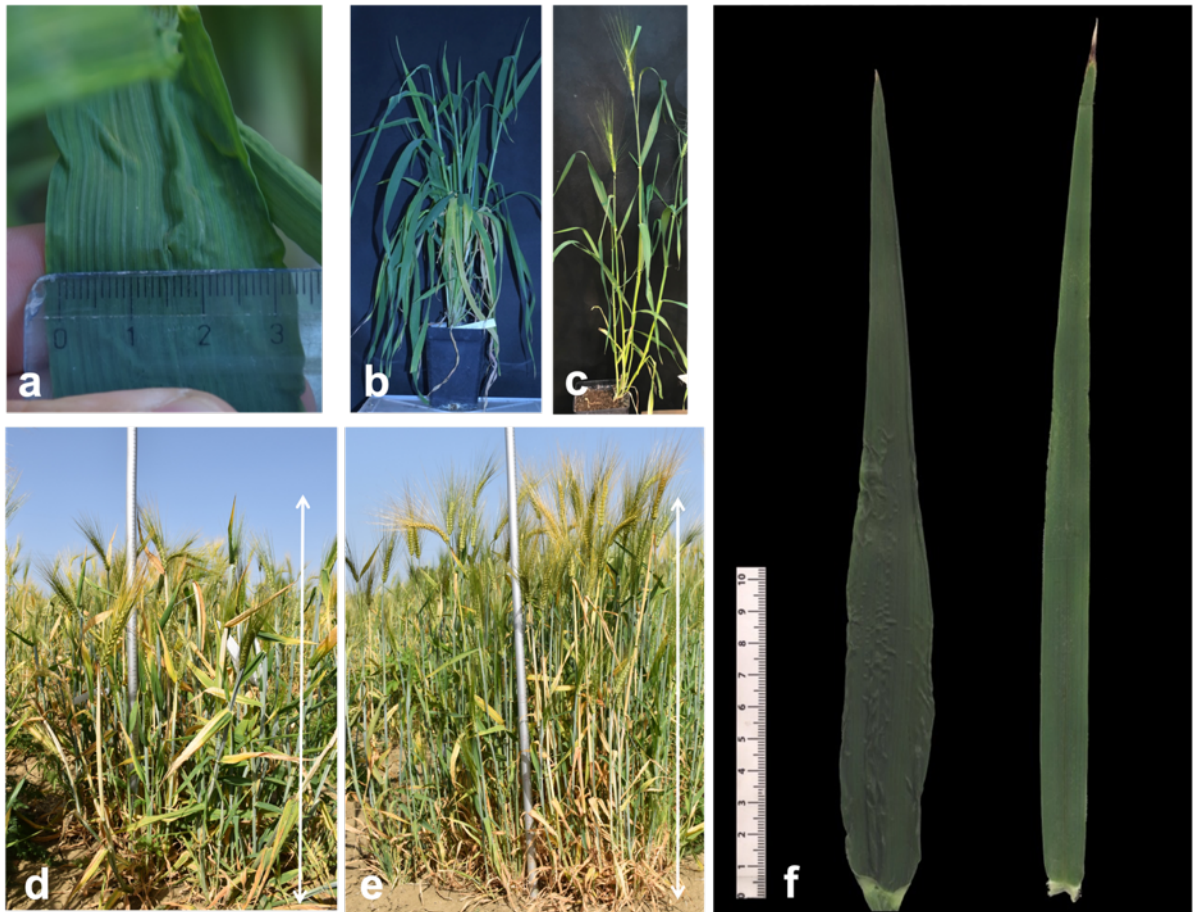


Figure 1. Representative images of the TILLMore broad leaf mutant TM2544. (a) Close up of a leaf – 1 (second leaf from top) from TM2544 at the maximum width point. (b) TM2544 grown in pot in the green house, compared to Morex (c). Mutant leaves appear longer and with a wider insertion angle of on the culm. (d) TM2544 grown in the field, compared to Morex (e). The mutant plants appear slightly shorter but healthy and vigorous, with spikes comparable to Morex. The white arrows are 1 m long. (f) Representative flag -1 leaf from the main culm of TM2544 (left) compared to Morex (right).

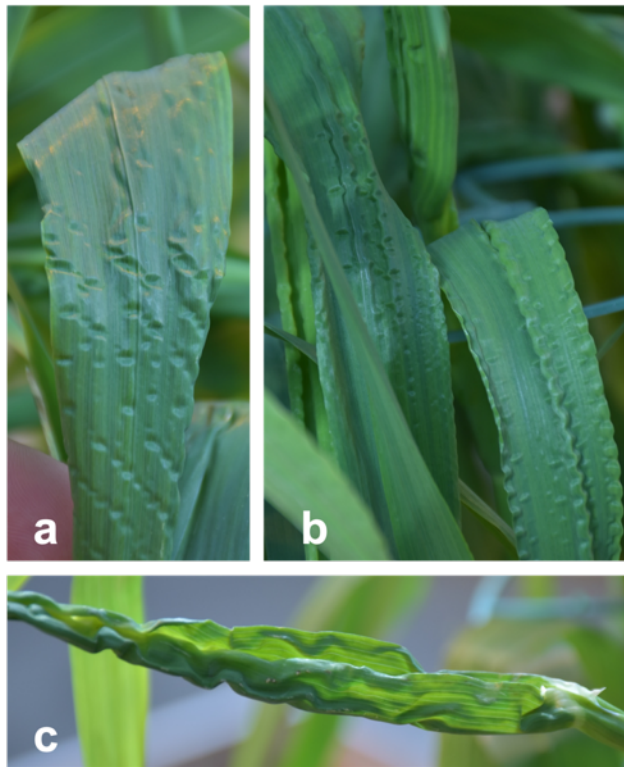


Figure 2. Examples of typical morphological anomalies of TM2544. (a), (b) Close up of small crinkles and creases on the leaves. (c) Pronounced undulations sometimes occur on the flag leaf, causing defects during heading resulting in the spike remaining partially or totally enclosed in the flag leaf.

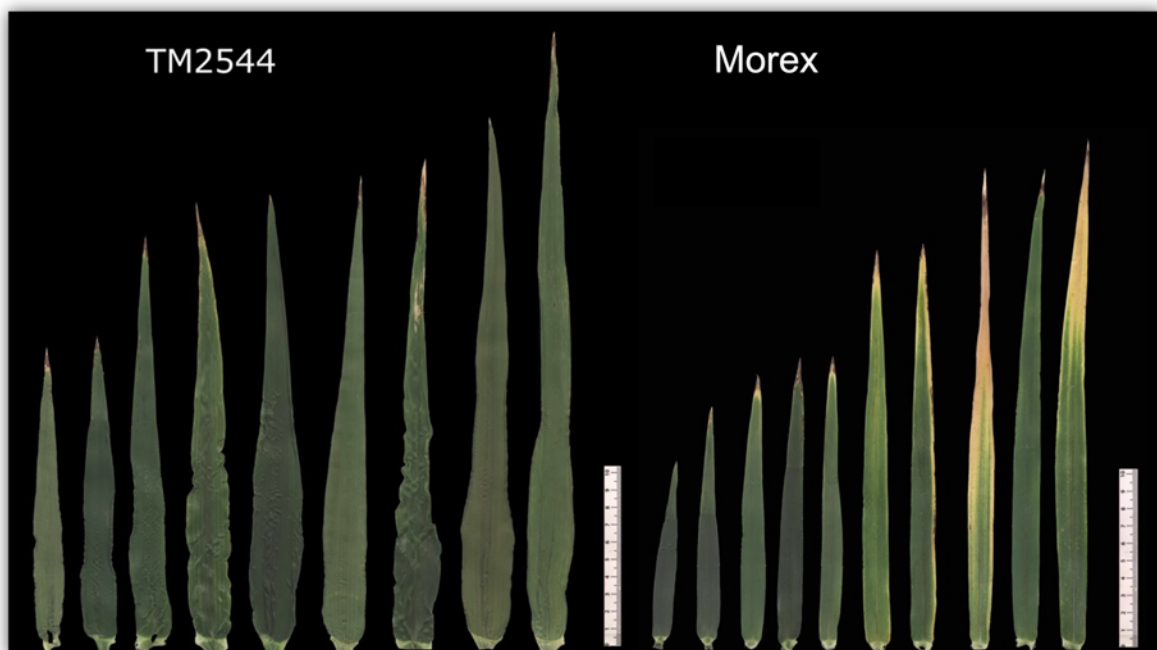


Figure 3. Leaves of TM2544 compared to cv. Morex. Flag -1 leaves were collected from the main culm at flowering stage and their image was acquired with a digital scanner.

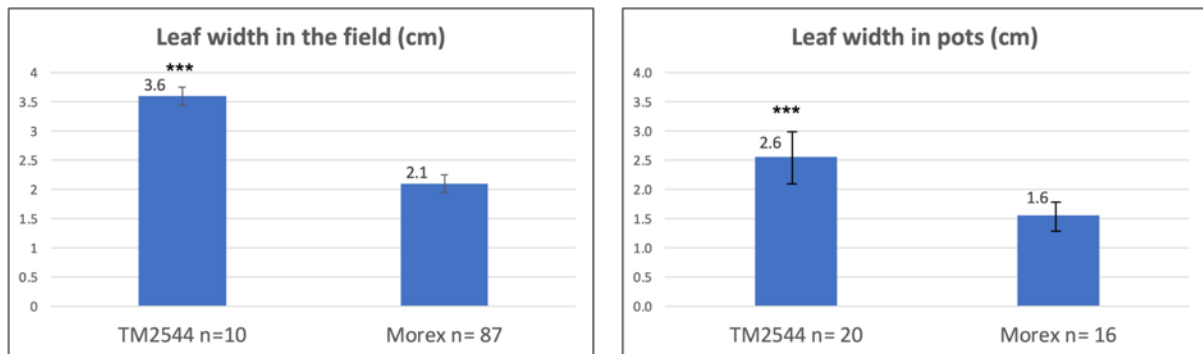


Figure 4. Maximum leaf width of TM2544 in the field and in pots compared to Morex. Flag -1 leaves were collected from the main culm at flowering stage. For TM2544 in pots, one 4th, 5th, 6th, flag -1 and flag leaves were collected. TM2544 showed an increased width leaf both in the field (+ 71%) and in pots (+ 63%) compared to Morex. Mann-Whitney-Wilcoxon test, $p = 1.21 \times 10^{-7}$ and $p < 2.2 \times 10^{-16}$, respectively.

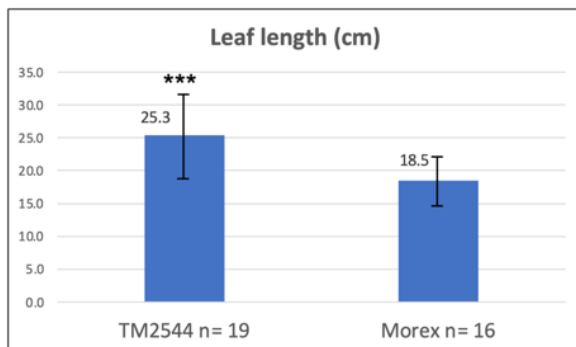


Figure 5. Leaf length of TM2544 measured in pots compared to Morex. Leaves from the 4th upwards were measured at flowering stage. TM2544 showed an increase in leaf length of 37%. Mann-Whitney-Wilcoxon test, $p = 1.094 \times 10^{-11}$.

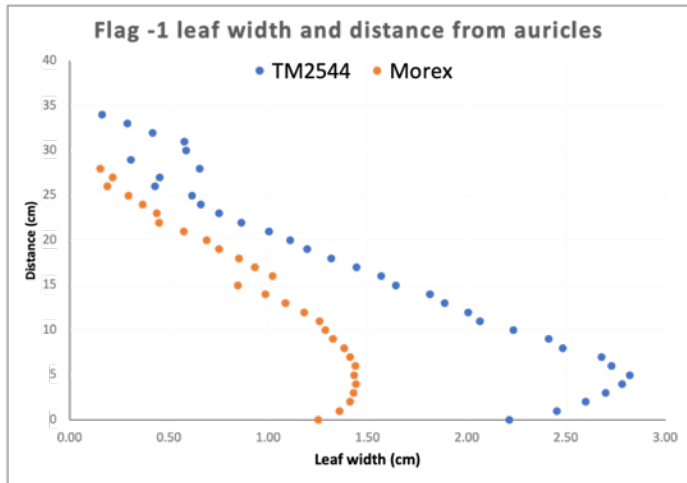


Figure 6. Leaf width of TM2544 and distance from auricles compared to Morex. One flag -1 leaf for each of the lines was collected from the main culm. Their scanned image was elaborated with ImageJ, and leaf width was measured for every millimetre of distance from the ligules.

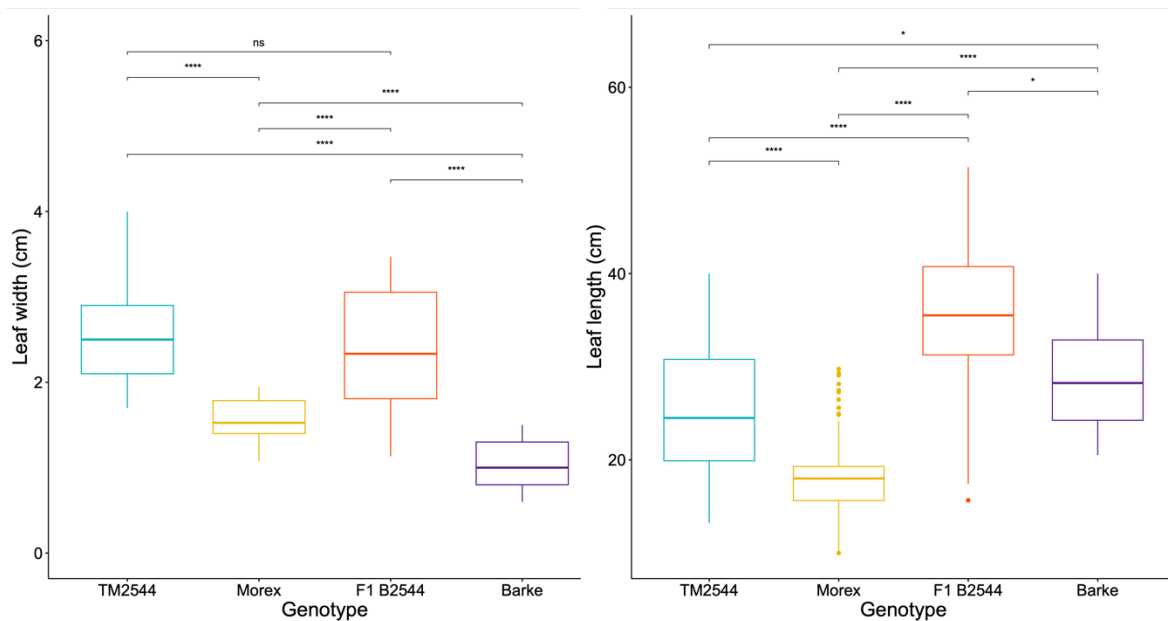


Figure 7. Leaf width and leaf length comparisons between TM2544, Morex, the F₁ population from TM2544 × Barke and Barke.

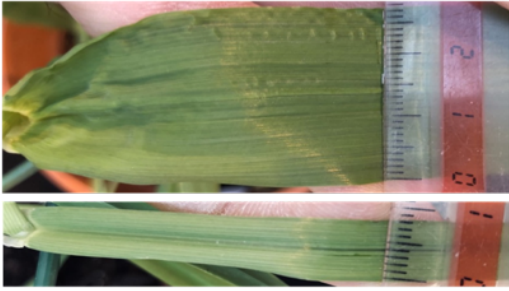


Figure 8. Maximum and minimum leaf width of F₂ B2544. Flag -1 leaves of the F₂ at flowering stage, in pots.

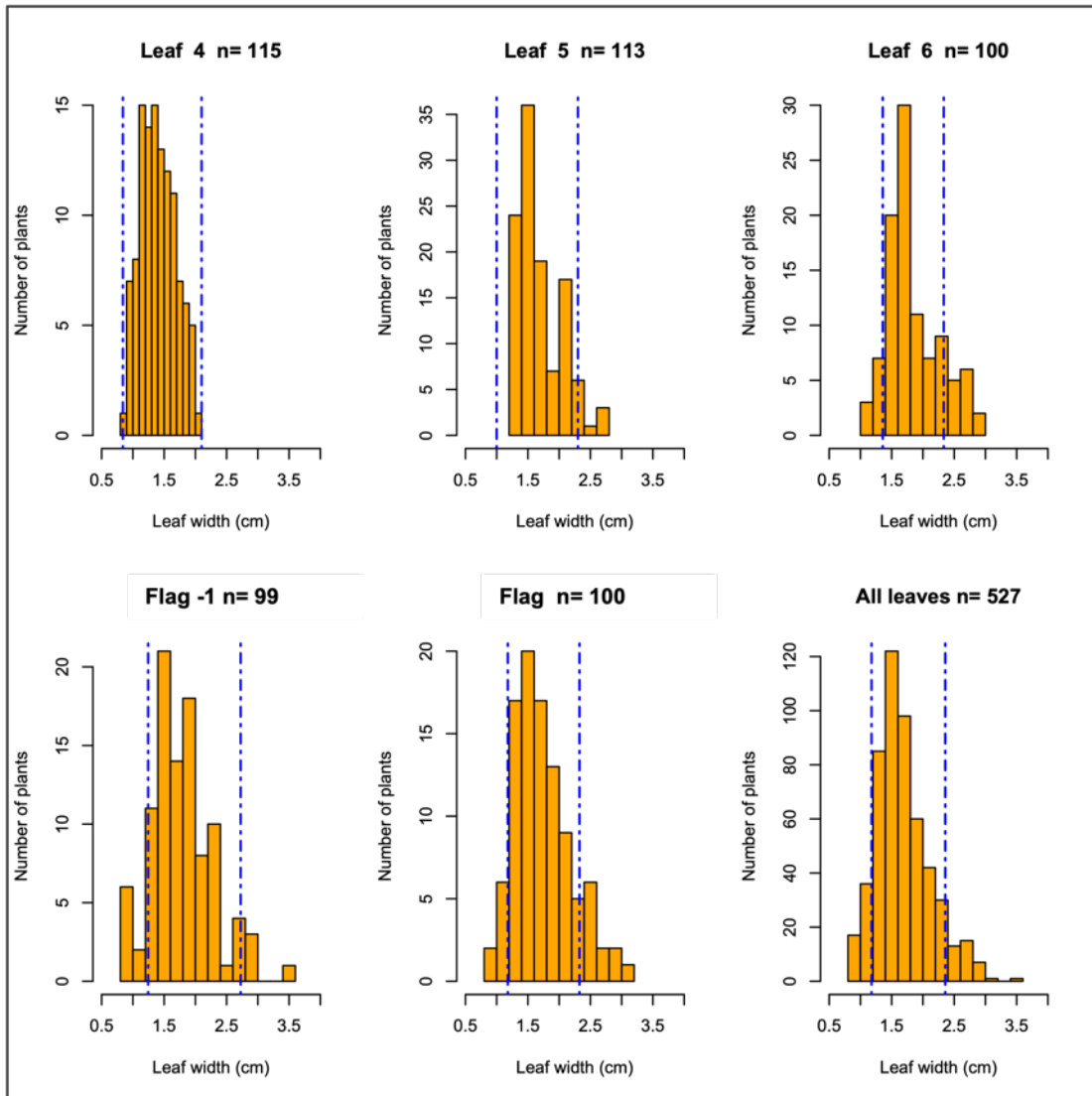


Figure 9. Leaf width distribution in the F₂ population TM2544 × Barke. A total of n = 125 plants and 527 leaves were measured from 4th leaf upwards. Blue dash-dotted lines are the mean width of the two parental lines.

Table 1. Leaf width segregation in the F₂, according to Morex avg. width = 1.57 cm (n = 50).

χ^2 goodness of fit test was applied to the expected 3:1 ratio (in case broad leaf is dominant) between mutant and wild type numbers.

Leaf	Mut	WT	Mut/WT	χ^2	p-value	Signif.
4	42	73	0.6	90.81	1.58E-21	***
5	68	45	1.5	13.24	2.74E-04	**
6	81	19	4.3	1.92	1.66E-01	n.s.
Flag -1	67	32	2.1	2.83	9.24E-02	n.s.
Flag	64	36	1.8	6.45	1.11E-02	*
all	322	205	1.6	54.3	1.72E-13	***

4.2 Whole genome sequencing

To find the SNPs of the broad leaf mutant TM2544, and to verify if it had a variant in the *BLF1* gene, which had been previously demonstrated to regulate leaf width (Jöst et al., 2016), we applied whole genome shotgun sequencing. Variant calling, carried out by the Bioinformatics Group of the Future Food Beacon of Excellence, at the University of Nottingham, returned 62 functional SNPs with a predicted high or moderate effect on the corresponding protein. Among these, we found no SNP on *BLF1* or its promoter. However, the gene was classified as low confidence on the reference Morex v.1, and this could explain why it was excluded. We did an extraction on the vcf file with AWK and found one SNP in the interval of *BLF1* with 31 reads out of 31 confirming the alternate allele (Table 2). We can conclude that, among other 62 candidate genes, TM2835 has a mutation in *BLF1*.

Table 2. Variant of TM2544 in *BLF1*.

CHROM	POS	REF	ALT	DP	AD
5H	463,047,028	C	T	31	0,31

CHR = chromosome; POS = position; REF = reference allele; ALT = alternative allele; DP = depth, or number of reads aligned to the position; AD = alternative depth or number of alternative reads.

4.3 BSA-Seq

To reduce the number of candidate genes, we applied BSA-Seq to the F2 from TM2544 × Barke. After phenotyping the F2, the nine individuals with broader leaves were selected to constitute the mutant bulk and the nine plants with narrower leaves were selected into the wild type bulk, their DNA was individually extracted and then bulked in the same quantity for each single plant. The two DNA bulks were sequenced with Illumina MiSeq PE300, ≈ 30× of coverage, by IGA Technologies Services, Italy.

The results of the Δ SNPIndex showed that the functional variant with the highest Δ SNPIndex of 0.90 (Table 2) was on *HORVU.MOREX.r2.5HG0402200*, the same gene that had been previously identified as *bfl1*, causing broad leaf in barley (Jöst et al., 2016). This SNP was a substitution of a cytosine with a thymine in position 5H: 463,047,028, that caused a predicted high effect variant due to the formation of a new stop codon (Table 3). For these reasons, *HORVU.MOREX.r2.5HG0402200* is the strongest candidate for TM2544.

Table 3. Result of BSA-Seq Δ SNPIndex. Only the functional SNPs with high Δ SNPIndex (from 0.90 to 0.50) are reported

CHR	POS	REF	ALT	VARIANT	MAGNITUDE	GENE	VAR_SEQ	Δ SNPIndex
5H	463047028	C	T	sg	H	HORVU.MOREX.r2.5HG0402200	c.232C>T	0.90
5H	305275826	C	T	mv	M	HORVU.MOREX.r2.5HG0382010	c.118C>T	0.73
5H	451543540	C	A	sg	H	HORVU.MOREX.r2.5HG0400650	c.310G>T	0.72
4H	248507780	C	T	mv	M	HORVU.MOREX.r2.4HG0304550	c.5030C>T	0.71
2H	548886074	C	T	mv	M	HORVU.MOREX.r2.2HG0146960	c.325G>A	0.63
6H	5240790	G	A	mv	M	HORVU.MOREX.r2.6HG0449570	c.346C>T	0.61
1H	447359980	A	C	mv	M	HORVU.MOREX.r2.1HG0054990	c.445A>C	0.59
1H	291671232	G	A	mv	M	HORVU.MOREX.r2.1HG0034560	c.458C>T	0.58
1H	447359978	T	C	mv	M	HORVU.MOREX.r2.1HG0054990	c.443T>C	0.56
1H	441260867	T	G	mv	M	HORVU.MOREX.r2.1HG0053870	c.84T>G	0.53
1H	451897676	C	T	mv	M	HORVU.MOREX.r2.1HG0056010	c.376G>A	0.53
1H	447359983	A	G	mv	M	HORVU.MOREX.r2.1HG0054990	c.448A>G	0.52
1H	451608856	G	A	mv	M	HORVU.MOREX.r2.1HG0055950	c.2858C>T	0.52
1H	451482367	A	G	mv	M	HORVU.MOREX.r2.1HG0055910	c.308T>C	0.51
1H	455408528	G	T	mv	M	HORVU.MOREX.r2.1HG0056930	c.1528G>T	0.50
1H	447359561	C	T	mv	M	HORVU.MOREX.r2.1HG0054990	c.26C>T	0.50

CHR = chromosome; POS = position; REF = reference allele; ALT = alternative allele; VARIANT type of consequence caused by the variant: mv = missense variant, sg = stop codon gained; MAGNITUDE = predicted effect on the protein: H = high, M = moderate; VAR SEQ = variation in the genomic sequence; Δ SNPIndex = SNPIndex(mut) – SNPIndex(wt) where SNPIndex = number of variant reads on depth.

5 DISCUSSION

We applied Illumina WGS sequencing and BSASeq to map and clone the broad leaf mutant TM2544 from the TILLMore collection. The F₁ population led us to think that the trait could be dominant, contrary to the already known *blfl* (Jöst et al., 2016), even if the segregation ratio in the F₂ from TM2544 × Barke did not adhere to the expected 3:1 Mendelian ratio of mutant to wild type. Moreover, contrary to *blfl-1*, TM2544 showed longer leaf compared to Morex.

However, WGS found, besides 62 possible candidates, a SNP in the interval of *BLF1* and BSASeq found the only peak for Δ SNPIndex > 0.8 inside *BLF1*, and the SNP is predicted to cause a high effect on the protein with the gain of a premature stop codon. Thus, *blfl* is likely the causal gene of our mutant. As for the segregation in the F₂, we must consider that Barke, the *cultivar* used for the outcross, is not neutral in terms of leaf width, in fact its leaf blade is narrower than Morex, the parental wild type. This can influence the leaf width in the F₂ with an effect contrary to that of the causal gene. For this study, it would have been adequate to choose a *cultivar* with a leaf width as similar as possible to that of the parental Morex.

Moreover, the increased leaf length in the mutant and F₁ could be caused by one of the other 62 functional mutations in a different gene, or, in the case of the F₁, it could be attributed to heterosis. For a further future test, we should obtain a knock-out mutant of *BLF1* in Morex with gene editing and investigate the effect of the other mutated genes on leaf length.

6 REFERENCES

- Alqudah, A. M., & Schnurbusch, T. (2015). Barley leaf area and leaf growth rates are maximized during the pre-anthesis phase. *Agronomy*, *5*(2), 107-129.
- Alqudah, A. M., Youssef, H. M., Graner, A., & Schnurbusch, T. (2018). Natural variation and genetic make-up of leaf blade area in spring barley. *Theoretical and Applied Genetics*, *131*(4), 873-886. <https://doi.org/10.1007/s00122-018-3053-2>
- Berdahl, J. D., Rasmusson, D. C., & Moss, D. N. (1972). Effects of Leaf Area on Photosynthetic Rate, Light Penetration, and Grain Yield in Barley1. *Crop Science*, *12*(2), crops1972.0011183X001200020006x. <https://doi.org/https://doi.org/10.2135/crops1972.0011183X001200020006x>
- Blum, A. (2005). Drought resistance, water-use efficiency, and yield potential—are they compatible, dissonant, or mutually exclusive? *Australian Journal of Agricultural Research*, *56*(11), 1159-1168.
- Caine, R. S., Yin, X., Sloan, J., Harrison, E. L., Mohammed, U., Fulton, T., . . . Coe, R. A. (2019). Rice with reduced stomatal density conserves water and has improved drought tolerance under future climate conditions. *New Phytologist*, *221*(1), 371-384.
- Cingolani, P., Platts, A., Wang, I. L., Coon, M., Nguyen, T., Wang, L., . . . Ruden, D. M. (2012). A program for annotating and predicting the effects of single nucleotide polymorphisms, SnpEff: SNPs in the genome of *Drosophila melanogaster* strain w1118; iso-2; iso-3. *Fly (Austin)*, *6*(2), 80-92. <https://doi.org/10.4161/fly.19695>
- Digel, B., Tavakol, E., Verderio, G., Tondelli, A., Xu, X., Cattivelli, L., . . . von Korff, M. (2016). Photoperiod-H1 (Ppd-H1) Controls Leaf Size. *Plant Physiology*, *172*(1), 405-415. <https://doi.org/10.1104/pp.16.00977>
- Du, B., Liu, L., Wang, Q., Sun, G., Ren, X., Li, C., & Sun, D. (2019). Identification of QTL underlying the leaf length and area of different leaves in barley. *Scientific Reports*, *9*(1), 4431. <https://doi.org/10.1038/s41598-019-40703-6>
- George-Jaeggli, B., Mortlock, M. Y., & Borrell, A. K. (2017). Bigger is not always better: Reducing leaf area helps stay-green sorghum use soil water more slowly. *Environmental and Experimental Botany*, *138*, 119-129. <https://doi.org/https://doi.org/10.1016/j.envexpbot.2017.03.002>
- Haefele, S. M., Johnson, D. E., M'Bodj, D., Wopereis, M. C. S., & Miezán, K. M. (2004). Field screening of diverse rice genotypes for weed competitiveness in irrigated lowland ecosystems. *Field Crops Research*, *88*(1), 39-56. <https://doi.org/https://doi.org/10.1016/j.fcr.2003.11.010>
- Hibara, K.-i., Miya, M., Benvenuto, S. A., Hibara-Matsuo, N., Mimura, M., Yoshikawa, T., . . . Itoh, J.-i. (2021). Regulation of the plastochron by three many-noded dwarf genes in barley. *PLoS genetics*, *17*(5), e1009292.
- Hu, J., Wang, X., Zhang, G., Jiang, P., Chen, W., Hao, Y., . . . Wang, H. (2020). QTL mapping for yield-related traits in wheat based on four RIL populations. *Theoretical and Applied Genetics*, *133*(3), 917-933. <https://doi.org/10.1007/s00122-019-03515-w>
- Hughes, J., Hepworth, C., Dutton, C., Dunn, J. A., Hunt, L., Stephens, J., . . . Gray, J. E. (2017). Reducing Stomatal Density in Barley Improves Drought Tolerance without Impacting on Yield. *Plant Physiology*, *174*(2), 776-787. <https://doi.org/10.1104/pp.16.01844>
- Hunter, R. (1980). Increased Leaf Area (Source) and Yield of Maize in Short-season Areas 1. *Crop science*, *20*(5), 571-574.
- Jöst, M., Hensel, G., Kappel, C., Druka, A., Sicard, A., Hohmann, U., . . . Lenhard, M. (2016). The INDETERMINATE DOMAIN Protein BROAD LEAF1 Limits Barley Leaf Width by Restricting Lateral Proliferation. *Curr Biol*, *26*(7), 903-909. <https://doi.org/10.1016/j.cub.2016.01.047>
- Klein, H., Xiao, Y., Conklin, P. A., Govindarajulu, R., Kelly, J. A., Scanlon, M. J., . . . Bartlett, M. (2018). Bulk-Segregant Analysis Coupled to Whole Genome Sequencing (BSA-Seq) for Rapid Gene Cloning in Maize. *G3 (Bethesda)*, *8*(11), 3583-3592. <https://doi.org/10.1534/g3.118.200499>

- Kurata, N., Miyoshi, K., Nonomura, K.-I., Yamazaki, Y., & Ito, Y. (2005). Rice mutants and genes related to organ development, morphogenesis and physiological traits. *Plant and cell physiology*, *46*(1), 48-62.
- Li, H., & Durbin, R. (2009). Fast and accurate short read alignment with Burrows-Wheeler transform. *Bioinformatics*, *25*(14), 1754-1760. <https://doi.org/10.1093/bioinformatics/btp324>
- Li, S., Zhao, Q., Zhu, D., & Yu, J. (2018). A DREB-like transcription factor from maize (*Zea mays*), ZmDREB4. 1, plays a negative role in plant growth and development. *Frontiers in plant science*, *9*, 395.
- Li, W., Yang, Z., Yao, J., Li, J., Song, W., & Yang, X. (2018). Cellulose synthase-like D1 controls organ size in maize. *BMC Plant Biology*, *18*(1), 239. <https://doi.org/10.1186/s12870-018-1453-8>
- Liu, J., Zhang, F., Zhou, J., Chen, F., Wang, B., & Xie, X. (2012). Phytochrome B control of total leaf area and stomatal density affects drought tolerance in rice. *Plant Molecular Biology*, *78*(3), 289-300. <https://doi.org/10.1007/s11103-011-9860-3>
- Liu, K., Xu, H., Liu, G., Guan, P., Zhou, X., Peng, H., . . . Du, J. (2018). QTL mapping of flag leaf-related traits in wheat (*Triticum aestivum* L.). *Theoretical and Applied Genetics*, *131*(4), 839-849. <https://doi.org/10.1007/s00122-017-3040-z>
- Liu, L., Sun, G., Ren, X., Li, C., & Sun, D. (2015). Identification of QTL underlying physiological and morphological traits of flag leaf in barley. *BMC Genetics*, *16*(1), 29. <https://doi.org/10.1186/s12863-015-0187-y>
- Ma, J., Tu, Y., Zhu, J., Luo, W., Liu, H., Li, C., . . . Lan, X. (2020). Flag leaf size and posture of bread wheat: genetic dissection, QTL validation and their relationships with yield-related traits. *Theoretical and Applied Genetics*, *133*(1), 297-315. <https://doi.org/10.1007/s00122-019-03458-2>
- Makhtoum, S., Sabouri, H., Gholizadeh, A., Ahangar, L., Katouzi, M., & Mastinu, A. (2022). Mapping of QTLs controlling barley agronomic traits (*Hordeum vulgare* L.) under normal conditions and drought and salinity stress at reproductive stage. *Plant Gene*, *31*, 100375. <https://doi.org/https://doi.org/10.1016/j.plgene.2022.100375>
- Mascher, M., Gundlach, H., Himmelbach, A., Beier, S., Twardziok, S. O., Wicker, T., . . . Stein, N. (2017). A chromosome conformation capture ordered sequence of the barley genome. *Nature*, *544*(7651), 427-433. <https://doi.org/10.1038/nature22043>
- Monat, C., Padmarasu, S., Lux, T., Wicker, T., Gundlach, H., Himmelbach, A., . . . Mascher, M. (2019). TRITEX: chromosome-scale sequence assembly of Triticeae genomes with open-source tools. *Genome Biol*, *20*(1), 284. <https://doi.org/10.1186/s13059-019-1899-5>
- Nelissen, H., Gonzalez, N., & Inzé, D. (2016). Leaf growth in dicots and monocots: so different yet so alike. *Current Opinion in Plant Biology*, *33*, 72-76. <https://doi.org/https://doi.org/10.1016/j.pbi.2016.06.009>
- Neuffer, M. G., Coe, E. H., & Wessler, S. R. (1997). *Mutants of maize*. Cold Spring Harbor Laboratory Press.
- Qi, J., Qian, Q., Bu, Q., Li, S., Chen, Q., Sun, J., . . . Li, X. (2008). Mutation of the rice Narrow leaf1 gene, which encodes a novel protein, affects vein patterning and polar auxin transport. *Plant Physiology*, *147*(4), 1947-1959.
- Schneider, C. A., Rasband, W. S., & Eliceiri, K. W. (2012). NIH Image to ImageJ: 25 years of image analysis. *Nat Methods*, *9*(7), 671-675. <https://doi.org/10.1038/nmeth.2089>
- Shaaf, S., Bretani, G., Biswas, A., Fontana, I. M., & Rossini, L. (2019). Genetics of barley tiller and leaf development. *Journal of Integrative Plant Biology*, *61*(3), 226-256. <https://doi.org/https://doi.org/10.1111/jipb.12757>
- Strable, J. (2021). Developmental genetics of maize vegetative shoot architecture. *Molecular Breeding*, *41*(3), 19. <https://doi.org/10.1007/s11032-021-01208-1>
- Sun, X., Cahill, J., Van Hautegeem, T., Feys, K., Whipple, C., Novák, O., . . . Nelissen, H. (2017). Altered expression of maize PLASTOCHRON1 enhances biomass and seed yield by extending cell division duration. *Nature Communications*, *8*(1), 14752. <https://doi.org/10.1038/ncomms14752>

- Takagi, H., Abe, A., Yoshida, K., Kosugi, S., Natsume, S., Mitsuoka, C., . . . Takuno, S. (2013). QTL-seq: rapid mapping of quantitative trait loci in rice by whole genome resequencing of DNA from two bulked populations. *The Plant Journal*, *74*(1), 174-183.
- Talamè, V., Bovina, R., Sanguineti, M. C., Tuberosa, R., Lundqvist, U., & Salvi, S. (2008). TILLMore, a resource for the discovery of chemically induced mutants in barley. *Plant Biotechnol J*, *6*(5), 477-485. <https://doi.org/10.1111/j.1467-7652.2008.00341.x>
- Thirulogachandar, V., Alqudah, A. M., Koppolu, R., Rutten, T., Graner, A., Hensel, G., . . . Kuhlmann, M. (2017). Leaf primordium size specifies leaf width and vein number among row-type classes in barley. *The Plant Journal*, *91*(4), 601-612. <https://doi.org/https://doi.org/10.1111/tpj.13590>
- Turner, A., Beales, J., Faure, S., Dunford, R. P., & Laurie, D. A. (2005). The pseudo-response regulator Ppd-H1 provides adaptation to photoperiod in barley. *Science*, *310*(5750), 1031-1034.
- Wang, F., Tang, Z., Wang, Y., Fu, J., Yang, W., Wang, S., . . . Yin, H. (2022). Leaf Mutant 7 Encoding Heat Shock Protein OsHSP40 Regulates Leaf Size in Rice. *International journal of molecular sciences*, *23*(8), 4446.
- Wang, J., Liu, H., Zhao, C., Tang, H., Mu, Y., Xu, Q., . . . Ma, J. Mapping and validation of major and stable QTL for flag leaf size from tetraploid wheat. *The Plant Genome*, *n/a*(n/a), e20252. <https://doi.org/https://doi.org/10.1002/tpg2.20252>
- Yan, X., Wang, S., Yang, B., Zhang, W., Cao, Y., Shi, Y., . . . Jing, R. (2020). QTL mapping for flag leaf-related traits and genetic effect of QFLW-6A on flag leaf width using two related introgression line populations in wheat. *Plos one*, *15*(3), e0229912.
- Yoshikawa, T., Tanaka, S.-Y., Masumoto, Y., Nobori, N., Ishii, H., Hibara, K.-I., . . . Taketa, S. (2016). Barley NARROW LEAFED DWARF1 encoding a WUSCHEL-RELATED HOMEODOMAIN 3 (WOX3) regulates the marginal development of lateral organs. *Breeding Science*, 16019.
- Zhang, D., Sun, W., Singh, R., Zheng, Y., Cao, Z., Li, M., . . . Zhang, Z. (2018). GRF-interacting factor1 Regulates Shoot Architecture and Meristem Determinacy in Maize. *The Plant Cell*, *30*(2), 360-374. <https://doi.org/10.1105/tpc.17.00791>
- Zhao, C., Bao, Y., Wang, X., Yu, H., Ding, A., Guan, C., . . . Cui, F. (2018). QTL for flag leaf size and their influence on yield-related traits in wheat. *Euphytica*, *214*(11), 209. <https://doi.org/10.1007/s10681-018-2288-y>
- Zhao, S., Zhao, L., Liu, F., Wu, Y., Zhu, Z., Sun, C., & Tan, L. (2016). NARROW AND ROLLED LEAF 2 regulates leaf shape, male fertility, and seed size in rice. *Journal of integrative plant biology*, *58*(12), 983-996.
- Zheng, Y., Xu, J., Wang, F., Tang, Y., Wei, Z., Ji, Z., . . . Zhao, K. (2021). Mutation Types of CYP71P1 Cause Different Phenotypes of Mosaic Spot Lesion and Premature Leaf Senescence in Rice. *Frontiers in plant science*, *12*, 488.

INTRODUCTION TO CHAPTERS 3 AND 4: Roots and root system architecture and anatomy in barley

1. Anatomy and structure of barley roots and their potential for plant breeding

Roots have multiple functions including water and nutrient acquisition (Knipfer & Fricke, 2010), plant anchorage (Shah et al., 2017; Stubbs et al., 2019), shaping of plant-soil microbiota interphase (Vives-Peris et al., 2020; Wang & Song, 2022), non-self-recognition (Anten & Chen, 2021), and others.

Barley and other cereals have a fibrous root system that is divided into embryonic and post-embryonic roots (Figure 1.a). Embryonic roots are initiated in the embryo and are composed by one primary root and a few (2-6) seminal roots; post-embryonic roots emerge from nodes in the lower portions of stems and tillers; all roots can generate lateral roots (Rossini et al., 2018). Roots are formed by the root apical meristem, where cells divide rapidly, before entering the partially overlapping elongation zone, where cells grow longitudinally and then reach the differentiation zone, which is marked by the presence of root hairs and where cells reach their final size and function (Hochholdinger et al., 2018). In the radial orientation at the differentiation zone, barley seminal roots consist of one layer of epidermis, one of exodermis, four layers of cortical cells and one of endodermis; the central stele has one central large metaxylem vessel and eight smaller peripheral vessels (Kirschner et al., 2017).

Root system architecture, the spatial distribution of roots in soil, is determined by different parameters including the number of axial roots and of lateral roots, lateral root distribution, root growth angle, root length, root diameter. Both root anatomy and root system architecture are potential targets to improve soil resources uptake (Lynch et al., 2021; Maqbool et al., 2022). For example, a steeper and deeper root system is useful in conditions of low nitrogen or water availability and is better for CO₂ sequestration; such root ideotype is facilitated by steeper root growth angles, fewer axial roots, reduced lateral branching (Lynch, 2022). A shallower root system is better for top soil foraging of the less mobile nutrients like phosphorus (Lynch et al., 2021) and for avoidance of saline stress (Kitomi et al., 2020); it is obtained with shallower root growth angles, more axial roots, and greater lateral branching are beneficial (Lynch, 2022), (Figure 1.b).

Root system architecture can be strongly affected by environmental cues like water and nutrient gradients (Huang & Zhang, 2020; Morris et al., 2017; von Wangenheim et al., 2020),

soil compaction (Pandey et al., 2021), salinity (Galvan-Ampudia et al., 2013; Van Zelm et al., 2020), light (Silva-Navas et al., 2016) and gravity (Zhang et al., 2019). While root growth angle can vary in relations to many of the aforementioned conditions, when it is determined by gravity it is called root gravitropic setpoint angle and it results from two competing mechanism: gravitropism and anti-gravitropic offset (Roychoudhry et al., 2013; Roychoudhry & Kepinski, 2015). Gravity is sensed in the root cap (Sack, 1991), with statoliths sedimentation, that triggers an auxin efflux established and maintained by various auxin influx and efflux transporters, generating a gradient up until the elongation zone. Here, the differential growth of epidermis cells between the top part of the root and the bottom part, causes the bending of the whole root towards gravity (Sato et al., 2014; Swarup & Bennett, 2009), (Figure 3). Anti-gravitropic offset counteracts gravitropism and gives the root an angle greater than zero (Roychoudhry et al., 2013).

Whilst root architectural traits are important for stress adaptation, root anatomy (Figure 2) and the phenotypes of specific root cell types can also play important roles in stress resilience, for example, a study on 192 spring barley accessions grown in water deficit found 58 QTLs for anatomical traits modification in response to stress, like increased diameter of the stele and of the number of meta-xylem vessels, root cortical aerenchyma, suberized endodermis (Oyiga et al., 2020). In maize grown under low phosphorous, reduced living cortical area was associated with increased soil exploration, phosphorus capture, biomass, and grain yield (Galindo-Castañeda et al., 2018); root cortical aerenchyma reduced the metabolic costs of soil exploration, improving rooting depth, water capture, and plant growth under drought (Chimungu et al., 2015). Root suberization and lignification was shown to negatively impact water conductivity and reduce drought stress in rice (Lee et al., 2016) and barley (Kreszies et al., 2020).

Root hair show variations in length and density between different accessions, they contributed to phosphorous uptake and yield stability in barley under drought stress (Marin et al., 2021).

Root anatomy is associated with differential effects on pathogens and mycorrhizal colonization of nodal roots in maize: root rots were positively correlated with cortical cell file number and inversely correlated with cortical cell size (Galindo-Castañeda et al., 2019), aerenchyma formation reduced the number of live cortex cells and therefore inhibited colonization by arbuscular mycorrhizal fungi but it also decreased the infection with pathogenic fungi (Kawa & Brady, 2022). Plant cell walls are components of both pre-existing

and inducible plant defence mechanisms against pathogen and modification of cell wall can altered the resistance to pathogens with different parasitic style (Molina et al., 2021).

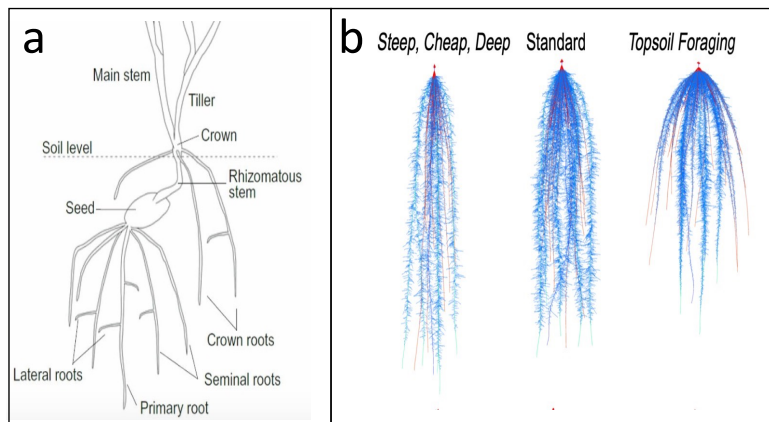


Figure 1. Roots and root system of cereals. (a) Schematic diagram of a barley roots at tillering phase, the root system is composed by seminal roots emerging from the seed, divided into primary and secondary roots, crown roots growing from the stem, and lateral roots emerging from other roots. From Rossini et al. (2018) (b) *Steep, Cheap, and Deep* and *Topsoil Foraging* ideotypes in maize at 42 d after germination as simulated by OpenSimRoot. The phenotype on the left is useful for the capture of subsoil resources, including water and leached nitrate, whereas the phenotype on the right is useful for the capture of topsoil resources including recently mineralized nitrate, ammonium, phosphorus, potassium, calcium, magnesium, and, in some cases, micronutrient metals. From Lynch (2019).

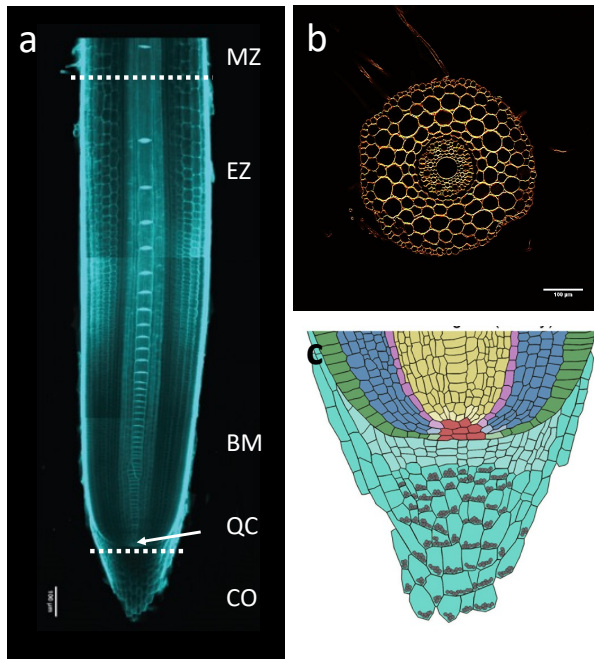


Figure 2. Developmental zones and anatomy of barley cv. Morex (a) Longitudinal confocal image of seminal root tip, basal meristem (BM), columella (CO), elongation zone (EZ), maturation zone (MZ), quiescent center (QC), Scale bar 100 μm. From Fusi et al. (2022) (b) Confocal cross section of seminal root tip of the maturation zone. Image courtesy of Riccardo Fusi (c) Models of barley root stem cell niche. Cell types are marked by color (red: quiescent centre, green: epidermis, blue: cortex, pink: endodermis, yellow: stele, turquoise: root cap), stem cells that give rise to different tissues are depicted in the respective light colors; gray spheres represent starch granules in the root; scale bar 100 μm. From Kirschner et al. (2017).

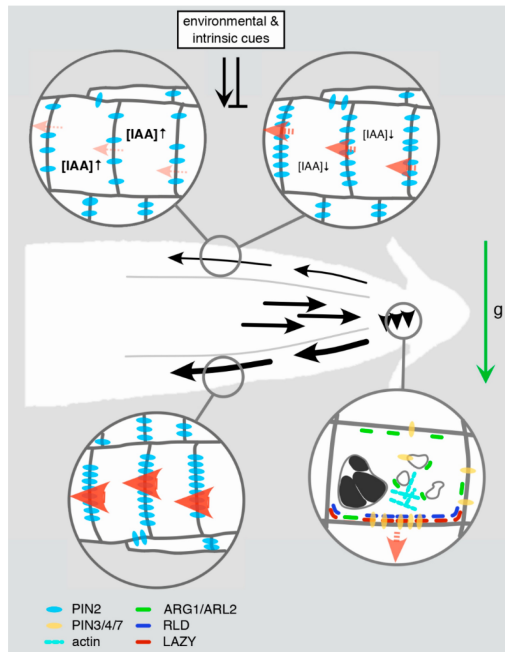


Figure 3. Gravitropic root bending and associated PIN relocation and expression in *Arabidopsis*. Upon gravistimulation (“g”, green arrow), a gradient of differential auxin fluxes is transiently established (black arrows and arrowheads), adjusting root growth direction via modulation of cell elongation. Within several minutes after gravistimulation, PIN proteins (dark yellow) in columella root cap statocytes undergo polarization at the plasma membrane at the cellular lower margin. This response appears to be triggered by starch-filled (black structures) statolith movement/sedimentation in accordance with the gravity vector. Molecular players involve ARG1/ARL2 J-domain proteins (green), which might link PIN transcytosis to vesicular transport and/or elements of the actin cytoskeleton (turquoise rods). LAZY (red) and RLD (dark blue) proteins represent another polarity determination module, whose concerted accumulation at the statocytes lower margin might precede polar accumulation of PINs. The resulting asymmetry in localized auxin distribution is transmitted into the root elongation zone, with elevated auxin levels transported at the root’s lower side (thick black arrows). A transient increase in the abundance of PIN2 (light blue), predominantly in epidermis cells at the lower side of the root meristem might result from diminished endocytosis and turnover of the protein. This could translate into elevated auxin flux rates (red arrowheads) in these cells, ultimately causing inhibition of cell elongation. At the root meristem’s upper side diminished levels of PIN2 are assumed to reduce auxin flux rates, promoting differential cell elongation at upper and lower and hence bending of the root. Variations in PIN2 abundance in these cells appear to be controlled by a combination of environmental and intrinsic cues, thereby impacting on intracellular auxin steady-state-levels

and causing adjustments in the lateral auxin gradient. Such spatiotemporal variations in auxin flux and gradients have been suggested to participate in the resetting of differential auxin transport and gravitational root bending. From Konstantinova et al. (2021).

2. Molecular genetics of root development and architecture

The growth angle of roots, called gravitropic set-point angle, is genetically determined and is the result of two competing mechanisms: gravitropism and anti-gravitropic offset (Roychoudhry et al., 2013). Some genes and QTLs have been demonstrated to regulate gravitropism. *DRO1* was first cloned in rice (Uga et al., 2013), where it causes a steeper root angle leading to deeper rooting; it is conserved in plants and it causes steeper lateral root angle in *Arabidopsis*, steeper and deeper rooting in *Prunus domestica* (Guseman et al., 2017), barley and wheat (Ashraf et al., 2019). It is advantageous to improve yield in drought conditions (Uga et al., 2013). Its homolog, *qSOR1*, is involved in gravity response and its loss of function improves yield in saline paddy fields (Kitomi et al., 2020). *RMD* controls root growth angle in rice by linking actin filaments and statoliths, and it is upregulated in response to low external phosphate causing shallower root systems (Huang et al., 2018). The *LAZY1* family of genes controls gravity signalling through lateral auxin transport, and its loss-of-function has prostrate shoots and shallower roots in several plant species (Furutani & Morita, 2021). A mutation in *ZmCIPK15* causes steeper crown root angle in maize (Schneider et al., 2022).

No gene has been correlated to the anti-gravitropic offset so far.

Plant roots move through the soil by elongation, which is determined by cell division and cell expansion. Like root angle, root elongation varies with environmental signals, for example it is inhibited in *Arabidopsis* in low phosphate condition (Balzergue et al., 2017) or promoted in rice under nitrogen deficiency (Wang et al., 2020).

Many mutants for root length are available and genetically characterized in *Arabidopsis* (Lucas et al., 2010; Petricka et al., 2012), rice (Meng et al., 2019), maize (Bray & Topp, 2018; Hochholdinger et al., 2018). In rice, about twenty genes have been found to affect root elongation with different mechanisms and pathways (Meng et al., 2019). Among these, the *OsGLU3* gene was characterized thanks to the identification of a recessive mutant that caused shorter roots, reduced crystalline cellulose in the root cell wall, slightly reduced root meristem size; the gene codes for an endoglucanase and it is essential for root elongation as it

loosens the cell wall by regulating its cellulose content (Inukai et al., 2012; Zhang et al., 2012), (Figure 4).

No gene influencing root length has been cloned in barley so far.

A few genes have been reported to affect root hair formation and elongation, using mutants or overexpression lines in rice, reviewed in Meng et al. (2019), maize, reviewed in Hochholdinger et al. (2018) and barley (Gajek et al., 2021; Gajewska et al., 2018).

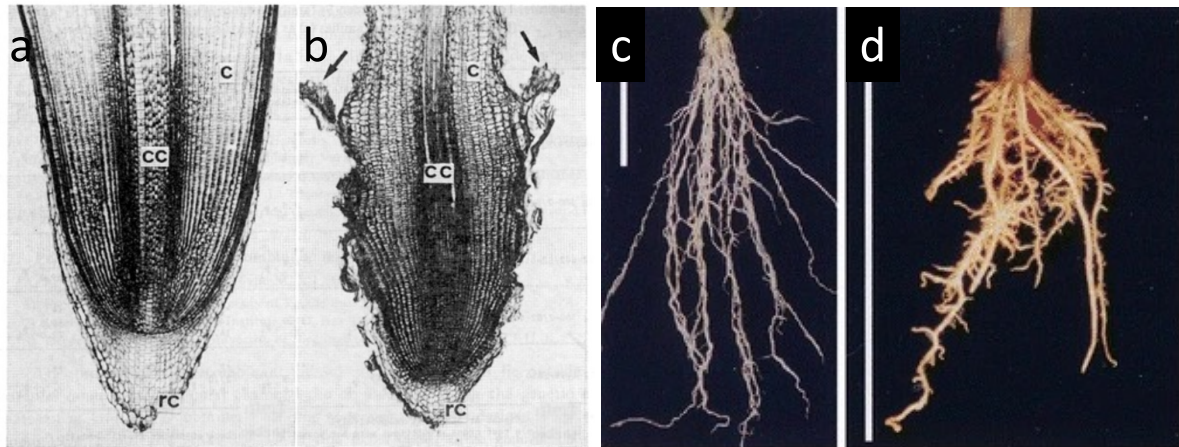


Figure 4. *OsGLU3* short root mutant in rice. (a) Longitudinal sections of a crown root in wild type Fukei 71 and in the mutant (b) the two black rows indicate stripping epidermis. From Oryzabase (Kurata & Yamazaki, 2006) at shigen.nig.ac.jp/rice/oryzabase/asset/rgn/vol3/v3VIII42.html.

REFERENCES

- Anten, N. P., & Chen, B. J. (2021). Detect thy family: mechanisms, ecology and agricultural aspects of kin recognition in plants. *Plant, Cell & Environment*, *44*(4), 1059-1071.
- Ashraf, A., Rehman, O. U., Muzammil, S., Léon, J., Naz, A. A., Rasool, F., . . . Khan, M. R. (2019). Evolution of Deeper Rooting 1-like homoeologs in wheat entails the C-terminus mutations as well as gain and loss of auxin response elements. *PLoS One*, *14*(4), e0214145.
- Balzerque, C., Darteville, T., Godon, C., Laugier, E., Meisrimler, C., Teulon, J.-M., . . . Desnos, T. (2017). Low phosphate activates STOP1-ALMT1 to rapidly inhibit root cell elongation. *Nature Communications*, *8*(1), 15300. <https://doi.org/10.1038/ncomms15300>
- Bray, A. L., & Topp, C. N. (2018). The Quantitative Genetic Control of Root Architecture in Maize. *Plant and Cell Physiology*, *59*(10), 1919-1930. <https://doi.org/10.1093/pcp/pcy141>
- Chimungu, J. G., Maliro, M. F. A., Nalivata, P. C., Kanyama-Phiri, G., Brown, K. M., & Lynch, J. P. (2015). Utility of root cortical aerenchyma under water limited conditions in tropical maize (*Zea mays* L.). *Field Crops Research*, *171*, 86-98. <https://doi.org/https://doi.org/10.1016/j.fcr.2014.10.009>
- Furutani, M., & Morita, M. T. (2021). LAZY1-LIKE-mediated gravity signaling pathway in root gravitropic set-point angle control. *Plant Physiology*, *187*(3), 1087-1095. <https://doi.org/10.1093/plphys/kiab219>
- Fusi, R., Rosignoli, S., Lou, H., Sangiorgi, G., Bovina, R., Patterm, J. K., . . . Milner, S. G. (2022). Root angle is controlled by EGT1 in cereal crops employing an antigravitropic mechanism. *Proceedings of the National Academy of Sciences*, *119*(31), e2201350119.
- Gajek, K., Janiak, A., Korotko, U., Chmielewska, B., Marzec, M., & Szarejko, I. (2021). Whole Exome Sequencing-Based Identification of a Novel Gene Involved in Root Hair Development in Barley (*Hordeum vulgare* L.). *International Journal of Molecular Sciences*, *22*(24), 13411.
- Gajewska, P., Janiak, A., Kwasniewski, M., Kędzierski, P., & Szarejko, I. (2018). Forward genetics approach reveals a mutation in bHLH transcription factor-encoding gene as the best candidate for the root hairless phenotype in barley. *Frontiers in plant science*, *9*, 1229.
- Galindo-Castañeda, T., Brown, K. M., Kuldau, G. A., Roth, G. W., Wenner, N. G., Ray, S., . . . Lynch, J. P. (2019). Root cortical anatomy is associated with differential pathogenic and symbiotic fungal colonization in maize. *Plant, Cell & Environment*, *42*(11), 2999-3014. <https://doi.org/https://doi.org/10.1111/pce.13615>
- Galindo-Castañeda, T., Brown, K. M., & Lynch, J. P. (2018). Reduced root cortical burden improves growth and grain yield under low phosphorus availability in maize. *Plant, Cell & Environment*, *41*(7), 1579-1592. <https://doi.org/https://doi.org/10.1111/pce.13197>
- Galvan-Ampudia, Carlos S., Julkowska, Magdalena M., Darwish, E., Gandullo, J., Korver, Ruud A., Brunoud, G., . . . Testerink, C. (2013). Halotropism Is a Response of Plant Roots to Avoid a Saline Environment. *Current Biology*, *23*(20), 2044-2050. <https://doi.org/https://doi.org/10.1016/j.cub.2013.08.042>
- Guseman, J. M., Webb, K., Srinivasan, C., & Dardick, C. (2017). DRO1 influences root system architecture in Arabidopsis and Prunus species. *The Plant Journal*, *89*(6), 1093-1105. <https://doi.org/https://doi.org/10.1111/tpj.13470>
- Hochholdinger, F., Yu, P., & Marcon, C. (2018). Genetic control of root system development in maize. *Trends in Plant Science*, *23*(1), 79-88.
- Huang, G., Liang, W., Sturrock, C. J., Pandey, B. K., Giri, J., Mairhofer, S., . . . Zhang, D. (2018). Rice actin binding protein RMD controls crown root angle in response to external phosphate. *Nature Communications*, *9*(1), 2346. <https://doi.org/10.1038/s41467-018-04710-x>
- Huang, G., & Zhang, D. (2020). The plasticity of root systems in response to external phosphate. *International Journal of Molecular Sciences*, *21*(17), 5955.
- Inukai, Y., Sakamoto, T., Morinaka, Y., Miwa, M., Kojima, M., Tanimoto, E., . . . Kitano, H. (2012). ROOT GROWTH INHIBITING, a Rice Endo-1,4-β-d-Glucanase, Regulates Cell Wall Loosening and is Essential for Root Elongation. *Journal of Plant Growth Regulation*, *31*(3), 373-381. <https://doi.org/10.1007/s00344-011-9247-3>

- Kawa, D., & Brady, S. M. (2022). Root cell types as an interface for biotic interactions. *Trends in Plant Science*, 27(11), 1173-1186.
<https://doi.org/https://doi.org/10.1016/j.tplants.2022.06.003>
- Kirschner, G. K., Stahl, Y., Von Korff, M., & Simon, R. (2017). Unique and conserved features of the barley root meristem. *Frontiers in plant science*, 8, 1240.
- Kitomi, Y., Hanzawa, E., Kuya, N., Inoue, H., Hara, N., Kawai, S., . . . Uga, Y. (2020). Root angle modifications by the <i>DRO1</i> homolog improve rice yields in saline paddy fields. *Proceedings of the National Academy of Sciences*, 117(35), 21242-21250.
<https://doi.org/doi:10.1073/pnas.2005911117>
- Knipfer, T., & Fricke, W. (2010). Water uptake by seminal and adventitious roots in relation to whole-plant water flow in barley (*Hordeum vulgare* L.). *Journal of Experimental Botany*, 62(2), 717-733. <https://doi.org/10.1093/jxb/erq312>
- Konstantinova, N., Korbei, B., & Luschnig, C. (2021). Auxin and root gravitropism: addressing basic cellular processes by exploiting a defined growth response. *International Journal of Molecular Sciences*, 22(5), 2749.
- Kreszies, T., Eggels, S., Kreszies, V., Osthoff, A., Shellakkutti, N., Baldauf, J. A., . . . Schreiber, L. (2020). Seminal roots of wild and cultivated barley differentially respond to osmotic stress in gene expression, suberization, and hydraulic conductivity. *Plant, Cell & Environment*, 43(2), 344-357. <https://doi.org/https://doi.org/10.1111/pce.13675>
- Kurata, N., & Yamazaki, Y. (2006). Oryzabase. An Integrated Biological and Genome Information Database for Rice. *Plant Physiology*, 140(1), 12-17. <https://doi.org/10.1104/pp.105.063008>
- Lee, D.-K., Jung, H., Jang, G., Jeong, J. S., Kim, Y. S., Ha, S.-H., . . . Kim, J.-K. (2016). Overexpression of the OsERF71 Transcription Factor Alters Rice Root Structure and Drought Resistance. *Plant Physiology*, 172(1), 575-588. <https://doi.org/10.1104/pp.16.00379>
- Lucas, M., Swarup, R., Paponov, I. A., Swarup, K., Casimiro, I., Lake, D., . . . Bennett, M. J. (2010). SHORT-ROOT Regulates Primary, Lateral, and Adventitious Root Development in Arabidopsis. *Plant Physiology*, 155(1), 384-398. <https://doi.org/10.1104/pp.110.165126>
- Lynch, J. P. (2019). Root phenotypes for improved nutrient capture: an underexploited opportunity for global agriculture. *New phytologist*, 223(2), 548-564.
- Lynch, J. P. (2022). Harnessing root architecture to address global challenges. *The Plant Journal*, 109(2), 415-431. <https://doi.org/https://doi.org/10.1111/tpj.15560>
- Lynch, J. P., Strock, C. F., Schneider, H. M., Sidhu, J. S., Ajmera, I., Galindo-Castañeda, T., . . . Hanlon, M. T. (2021). Root anatomy and soil resource capture. *Plant and Soil*, 466(1), 21-63.
- Maqbool, S., Hassan, M. A., Xia, X., York, L. M., Rasheed, A., & He, Z. (2022). Root system architecture in cereals: progress, challenges and perspective. *The Plant Journal*, 110(1), 23-42.
- Marin, M., Feeney, D., Brown, L., Naveed, M., Ruiz, S., Koebernick, N., . . . Puértolas, J. (2021). Significance of root hairs for plant performance under contrasting field conditions and water deficit. *Annals of Botany*, 128(1), 1-16.
- Meng, F., Xiang, D., Zhu, J., Li, Y., & Mao, C. (2019). Molecular Mechanisms of Root Development in Rice. *Rice*, 12(1), 1. <https://doi.org/10.1186/s12284-018-0262-x>
- Molina, A., Miedes, E., Bacete, L., Rodríguez, T., Mérida, H., Denancé, N., . . . Freydier, A. (2021). Arabidopsis cell wall composition determines disease resistance specificity and fitness. *Proceedings of the National Academy of Sciences*, 118(5), e2010243118.
- Morris, E. C., Griffiths, M., Golebiowska, A., Mairhofer, S., Burr-Hersey, J., Goh, T., . . . Bennett, M. J. (2017). Shaping 3D Root System Architecture. *Current Biology*, 27(17), R919-R930.
<https://doi.org/https://doi.org/10.1016/j.cub.2017.06.043>
- Oyiga, B. C., Palczak, J., Wojciechowski, T., Lynch, J. P., Naz, A. A., Léon, J., & Ballvora, A. (2020). Genetic components of root architecture and anatomy adjustments to water-deficit stress in spring barley. *Plant, Cell & Environment*, 43(3), 692-711.
<https://doi.org/https://doi.org/10.1111/pce.13683>
- Pandey, B. K., Huang, G., Bhosale, R., Hartman, S., Sturrock, C. J., Jose, L., . . . Ljung, K. (2021). Plant roots sense soil compaction through restricted ethylene diffusion. *Science*, 371(6526), 276-280.

- Petricka, J. J., Winter, C. M., & Benfey, P. N. (2012). Control of Arabidopsis root development. *Annual review of plant biology*, 63, 563.
- Rossini, L., Muehlbauer, G. J., Okagaki, R., Salvi, S., & Korff, M. v. (2018). Genetics of whole plant morphology and architecture. In *The Barley Genome* (pp. 209-231). Springer.
- Roychoudhry, S., Del Bianco, M., Kieffer, M., & Kepinski, S. (2013). Auxin Controls Gravitropic Setpoint Angle in Higher Plant Lateral Branches. *Current Biology*, 23(15), 1497-1504. <https://doi.org/https://doi.org/10.1016/j.cub.2013.06.034>
- Roychoudhry, S., & Kepinski, S. (2015). Shoot and root branch growth angle control—the wonderfulness of lateralness. *Current Opinion in Plant Biology*, 23, 124-131. <https://doi.org/https://doi.org/10.1016/j.pbi.2014.12.004>
- Sack, F. D. (1991). Plant Gravity Sensing. In K. W. Jeon & M. Friedlander (Eds.), *International Review of Cytology* (Vol. 127, pp. 193-252). Academic Press. [https://doi.org/https://doi.org/10.1016/S0074-7696\(08\)60695-6](https://doi.org/https://doi.org/10.1016/S0074-7696(08)60695-6)
- Sato, E. M., Hijazi, H., Bennett, M. J., Vissenberg, K., & Swarup, R. (2014). New insights into root gravitropic signalling. *Journal of Experimental Botany*, 66(8), 2155-2165. <https://doi.org/10.1093/jxb/eru515>
- Schneider, H. M., Lor, V. S. N., Hanlon, M. T., Perkins, A., Kaeppler, S. M., Borkar, A. N., . . . Lynch, J. P. (2022). Root angle in maize influences nitrogen capture and is regulated by calcineurin B-like protein (CBL)-interacting serine/threonine-protein kinase 15 (ZmCIPK15). *Plant, Cell & Environment*, 45(3), 837-853. <https://doi.org/https://doi.org/10.1111/pce.14135>
- Shah, A. N., Tanveer, M., Anjum, S. A., Iqbal, J., & Ahmad, R. (2017). Lodging stress in cereal—effects and management: an overview. *Environmental Science and Pollution Research*, 24(6), 5222-5237.
- Silva-Navas, J., Moreno-Risueno, M. A., Manzano, C., Téllez-Robledo, B., Navarro-Neila, S., Carrasco, V., . . . del Pozo, J. C. (2016). Flavonols Mediate Root Phototropism and Growth through Regulation of Proliferation-to-Differentiation Transition. *The Plant Cell*, 28(6), 1372-1387. <https://doi.org/10.1105/tpc.15.00857>
- Stubbs, C. J., Cook, D. D., & Niklas, K. J. (2019). A general review of the biomechanics of root anchorage. *Journal of Experimental Botany*, 70(14), 3439-3451.
- Swarup, R., & Bennett, M. J. (2009). Root gravitropism. *Annual Plant Reviews*, 37, 157-174.
- Uga, Y., Sugimoto, K., Ogawa, S., Rane, J., Ishitani, M., Hara, N., . . . Yano, M. (2013). Control of root system architecture by DEEPER ROOTING 1 increases rice yield under drought conditions. *Nat Genet*, 45(9), 1097-1102. <https://doi.org/10.1038/ng.2725>
- Van Zelm, E., Zhang, Y., & Testerink, C. (2020). Salt tolerance mechanisms of plants. *Annual review of plant biology*, 71, 403-433.
- Vives-Peris, V., de Ollas, C., Gómez-Cadenas, A., & Pérez-Clemente, R. M. (2020). Root exudates: from plant to rhizosphere and beyond. *Plant cell reports*, 39(1), 3-17.
- von Wangenheim, D., Banda, J., Schmitz, A., Boland, J., Bishopp, A., Maizel, A., . . . Bennett, M. (2020). Early developmental plasticity of lateral roots in response to asymmetric water availability. *Nature Plants*, 6(2), 73-77.
- Wang, Q., Zhu, Y., Zou, X., Li, F., Zhang, J., Kang, Z., . . . Lin, Y. (2020). Nitrogen Deficiency-Induced Decrease in Cytokinins Content Promotes Rice Seminal Root Growth by Promoting Root Meristem Cell Proliferation and Cell Elongation. *Cells*, 9(4), 916.
- Wang, Z., & Song, Y. (2022). Toward understanding the genetic bases underlying plant-mediated “cry for help” to the microbiota. *iMeta*, 1(1), e8.
- Zhang, J.-W., Xu, L., Wu, Y.-R., Chen, X.-A., Liu, Y., Zhu, S.-H., . . . Yi, K.-K. (2012). OsGLU3, a Putative Membrane-Bound Endo-1,4-Beta-Glucanase, Is Required for Root Cell Elongation and Division in Rice (*Oryza sativa* L.). *Molecular Plant*, 5(1), 176-186. <https://doi.org/https://doi.org/10.1093/mp/ssr084>
- Zhang, Y., Xiao, G., Wang, X., Zhang, X., & Friml, J. (2019). Evolution of fast root gravitropism in seed plants. *Nature communications*, 10(1), 1-10.

CHAPTER 3. Mapping and cloning the short and rigid root mutant TM390

1. OBJECTIVES

Root mutants are important to understand root development and adaptation to abiotic and biotic stress and they are a possible source of alleles for crop improvement.

In this work, our objectives were to map and clone the short and rigid root mutant TM390, which was originally identified within the barley TILLMore collection.

2. MATERIALS AND METHODS

2.1 Plant material and growth conditions

The barley short and rigid root mutant TM390 belongs to the TILLMore collection of mutants obtained with sodium azide mutagenesis on the cultivar Morex (Talamè et al., 2008). TM390 was first identified in a screening of the collection using the paper roll method (Hetz et al., 1996). For seed bulking the line was grown in the greenhouse, in a peat and vermiculite growing medium (Vigorplant Irish and Baltic peat-based professional mix) in 15 × 15 × 30 cm polyethylene pots with a day temperature of 22°C (16 h) and a night temperature of 18°C (8 h). Greenhouse lighting was a mix of natural light supplemented with artificial light by 400 watt high-pressure sodium lamps (Sylvania SHP-TS 400W Grolux).

2.2 Phenotyping

For root phenotyping, seeds were washed in 10% sodium hypochlorite for 10 minutes then rinsed with deionized water and pregerminated for 24 hours in the dark at 28°C on wet filter paper. Germinated seeds were grown for six days in a growth chamber at 25°C, with 16 hours of light, with the germination paper method, see Osthoff et al. (2019).

2.3 Mapping TM390 with MutMap+

As traditional Bulk Segregant Analysis was not possible due to difficulties in outcrossing the mutant, whose flowers were small and stunted, we applied the MutMap+ method (Fekih et al., 2013) which does not require crossing and it is based on the comparison of SNP-index plots of two bulked DNA obtained from a segregating progeny. 59 M₈ seeds produced by 4 M₇ plants showing intermediate root phenotype were screened with the flat screen method. 6

days after germination (DAG) plants were collected and scored into a mutant, a wild type and an intermediate bulk. Leaf DNA of plants in the first two bulks was individually extracted with the Macherey-Nagel Nucleospin Plant II kit and was subsequently added to two bulks in the same quantity for each single plant, reaching a final concentration of 50 ng/ μ l for both bulks.

The whole genomic DNA was sequenced with Illumina NovaSeq PE150, 30 \times of coverage, by Novogene Ltd., Cambridge (UK), producing 1,875,484,604 reads for the mutant bulk and 1,018,342,092 reads for the wild type, with an average depth after quality filtering of 53 \times and 29 \times , respectively. Raw reads were aligned to the reference Morex v.3 (Mascher et al., 2021) using the `bwa mem` command of the Burrows-Wheeler Aligner v.0.7.17 (Li & Durbin, 2009). Variant calling was done with `bcftools` v.1.10.2 (Danecek et al., 2021) filtering for a minimum mapping quality of 30 and a minimum base quality of 20. The effect of the called variants was predicted with `SNPEff` v.5.0c (Cingolani et al., 2012). We discarded multiallelic variants and formatted data with a customised shell script.

After the variant calling, data were analyzed with the Δ SNPIndex method (Takagi et al., 2013), where the index of each SNP is calculated as the ratio between the number of alternate reads at the position and the total number of reads. The Δ SNPIndex is the difference between the indexes of the mutant bulk and the index of the wild type bulk. The greater this difference, the more likely it is that this SNP is associated with the trait of interest. This method was implemented with a customised R 4.2.0 script using RStudio 2022.02.2 Build 485 (Team, 2020). We first discarded indels and filtered for a minimum coverage of 50 \times for the mutant bulk and 30 \times for the wild type and minimum PHRED quality of 40 for both. We calculated SNPIndex for the two bulks and their difference and plotted it on the chromosomes using the R `ggplot2` package (Wickham, 2016).

2.4 Whole Genome Sequencing (WGS)

Whole genome sequencing was applied on TM390 with Illumina HiSeq PE150 using an external sequencing provider, obtaining an average coverage of 19 \times . The variant calling was performed as described in 1.3 for the two bulks. Further filtering was carried out with an R script, we set a minimum coverage of 10 \times , a minimum PHRED quality of 40, and a high or moderate predicted variant effect obtaining only functional SNPs.

To restrict the list of candidate genes, we compared the SNPs of TM390 with those of the two bulks with an R script, using the package `data.table` v.1.14.2 (Dowle & Srinivasan,

2021). We first filtered the SNPs of the mutant bulk for SNPIndex > 0.8. For the comparison we considered the SNPs of TM390 keeping only those that are also present in the mutant bulk and absent from the wild type bulk or, if present, called as reference. In this last step, the minimum depth for the wild type bulk was set at 10×.

2.5 Functional validation of candidate genes

To find the causal gene of TM390, we decided to amplify and Sanger sequence the candidate genes to verify their co-segregation with the phenotype in a mapping population. We grew 100 M₈ seeds from M₇ TM390 plants showing intermediate phenotype with the paper roll method. We extracted DNA from the leaf of each of the 69 plants that germinated using a short chloroform-isopropanol method. We designed PCR primers (Table 1) with Primer3 (Untergasser et al., 2012), Benchling (www.benchling.com) and the IPK Galaxy Blast Suite. We performed PCR with the following settings: initial denaturation for 2' at 98 °C; 34 cycles of denaturation for 20" at 98 °C, annealing for 20" at 60 °C, elongation for 30" at 72 °C; final elongation for 5' at 72 °C. We purified the PCR products with the DNA Clean and Concentration kit by Zymo Research. We verified the results with Nanodrop and 1% agarose gel electrophoresis. Sanger sequencing was done by Microsynth AG, Switzerland.

Table 1. PCR primers used in the validation of mutant alleles of *ssr*.

ID	SEQUENCE
F1	CTGGAGAGGAAGTGGAGTG
R1	AACGATGACACGATGGACAG

3. RESULTS

3.1 Barley mutant TM390 has short and semi-rigid roots

TM390 seedlings show a reduced length of root when compared to the Morex wild type (Figure 1). In our M₆ seed stock, this trait is still segregating. In the most extreme phenotype group, seminal roots are extremely short, curled, irregular on the surface, thicker in diameter, more rigid to the touch, and their color is yellowish to beige instead of white. The shoot length and vigour varies, and length can be from extremely short to comparable with wild type. Most of mutant plants dies in a week after the transplant, a few survive but do not produce seeds.

In the intermediate phenotype group, root length varies greatly from short to comparable to the wild type, their color is white with sometimes a hint of yellow only in a restricted area, there is no apparent stiffness. Shoots varies from short to wild type. Plants that are transplanted in pots usually survive and complete their cycle, but they are shorter, with fewer tillers, smaller spikes and grains, and more sterility compared to the wild type. This could in part be explained by the many additional mutations, in fact this line has 1,668 functional SNPs (Paragraph 2.3).

Measures of root and shoot length of 128 plants at six days after germination, in relation to their phenotype group, are reported in Figure 2 and Figure 3. Roots varied between the phenotypes with a wild type average of 19.6 ± 2.5 cm ($n = 47$), an intermediate average of 12.4 ± 2.2 cm ($n = 31$) and a mutant average of 1.3 ± 0.5 cm ($n = 50$). Shoot length differed between wild type (12.4 ± 2.1 cm) and mutant (7.0 ± 2.8 cm) but not between intermediate (8.0 ± 2.2 cm) and mutant (Anova, $p < 2.2 \times 10^{16}$).

As it was not possible to outcross TM390 due to stunted growth of plants and flowers, we tested the segregation of the 128 M₈ TM390 plants derived from M₇ plants with intermediate phenotype, to check if it adhered to the Mendelian monogenic, incomplete dominance, F₂ 1:2:1 ratio. With 47 wild type, 31 intermediate and 50 mutants, the population did not segregate as expected ($\chi^2 = 3.42$, $p = 3.8 \times 10^{-8}$). If we consider as mutant both the intermediate and the extreme phenotype, with 81 mutant and 47 wild type, the population did not segregate with the expected 1:3 wild type to mutant ratio for $\alpha = 0.05$, which is expected if the mutation is dominant ($\chi^2 = 9.38$, $p = 0.0022$). Seminal root number did not differ between the phenotypes for $\alpha = 0.001$ (5.6 ± 0.8 , 5.4 ± 0.8 , 5.0 ± 1.1 , $p = 0.00751$).



Figure 1. Phenotype of TM390 compared to Morex. (a) Representative image of TM390 in its extreme phenotype (left), in its intermediate phenotype (middle) and Morex (right). (b) Close up of TM390 in its extreme phenotype. The root surface is irregular and yellowish in colour. Picture were taken six days after germination. The white scale bar is 5 cm in length.

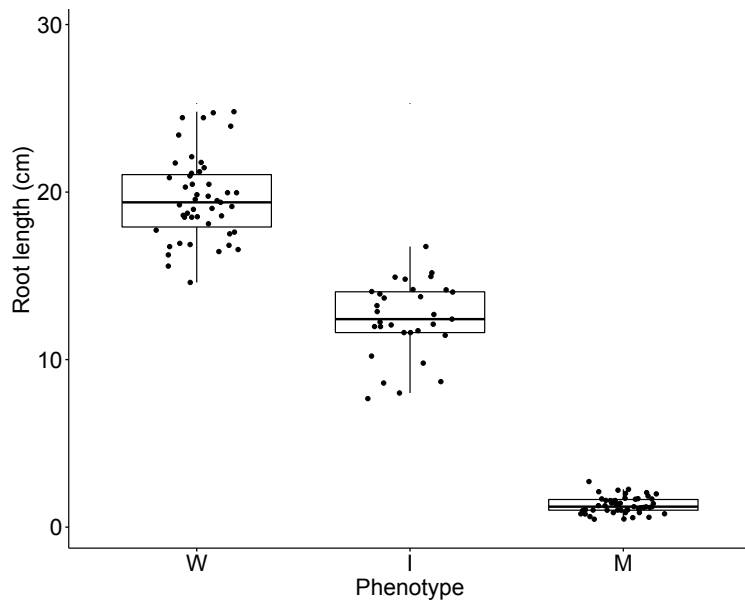


Figure 2. Root length comparison between different phenotypes. Data from 128 plants, six days after germination in paper rolls, visually classified as W= wild type, I= intermediate or M= mutant.

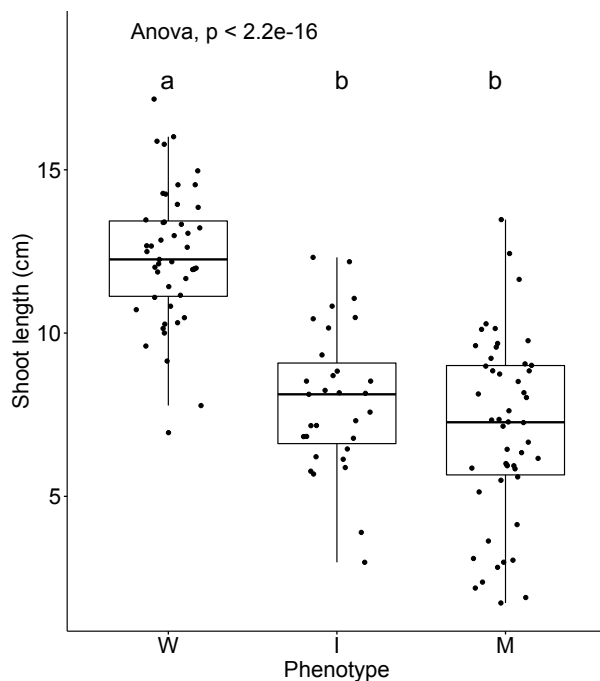


Figure 3. Shoot length comparison between different phenotypes. Data from 128 plants, six days after germination in paper rolls, visually classified as W= wild type, I= intermediate or M= mutant. Shoot lengths were different between wild type and mutant/intermediate, but did not differ between intermediate and mutant, Anova and Fisher's LSD tests were applied.

3.2 TM390 maps on chromosome 2H

We mapped the causal gene of TM390 with MutMap+ applied to 59 M₈ plants derived from self-pollination of heterozygous plants, as described in 1.3. 19 plants were selected for the wild type bulk and 26 for the mutant, showing extreme root phenotype (Figure 4).

After WGS of the two bulks, Δ SNPIndex was calculated for each unfiltered variant (meaning they were filtered only for monoallelic SNP and PHRED quality > 40) as the difference of the ratio between the two bulks and the 140,298 values were plotted against the chromosomal position (Figure 5). Chromosome 2H had a broad interval of 535 Mb between 75 Mb and 610 Mb where Δ SNPIndex is > 0.5. No peak region was found in other chromosomes, where the value of 0.5 was never reached. Δ SNPIndex did not peak around a value of 1, but it had a maximum of 0.71 in the region of the 2H peak. This happened because heterozygous plants were probably included in the wild type bulk, in fact the difference between wild type and intermediate phenotype was not always apparent.

We can affirm that the causal gene of TM390 maps on chromosome 2H between 75 Mb and 610 Mb.

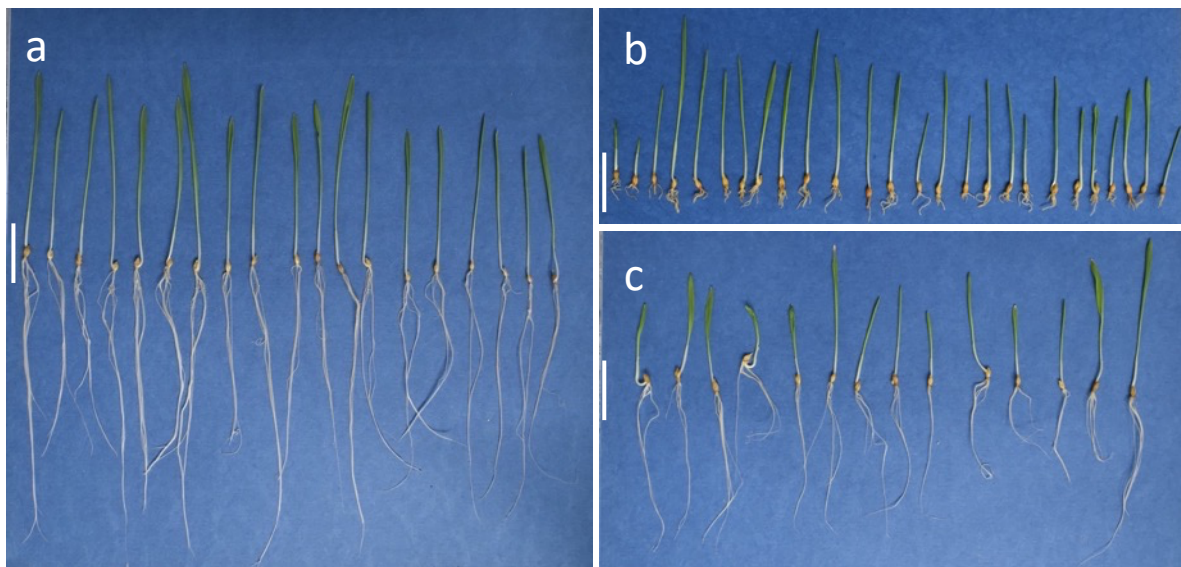


Figure 4. Segregation of 59 M₈ seedlings from 4 M₇ intermediate plants of TM390, six days after germination. The white scale bar is 5 cm. Plants were used for MutMap+: (a) 19 plants were selected for the wild type bulk (b) 26 plants were selected for the mutant bulk (c) 14 plants were considered intermediate and were discarded.

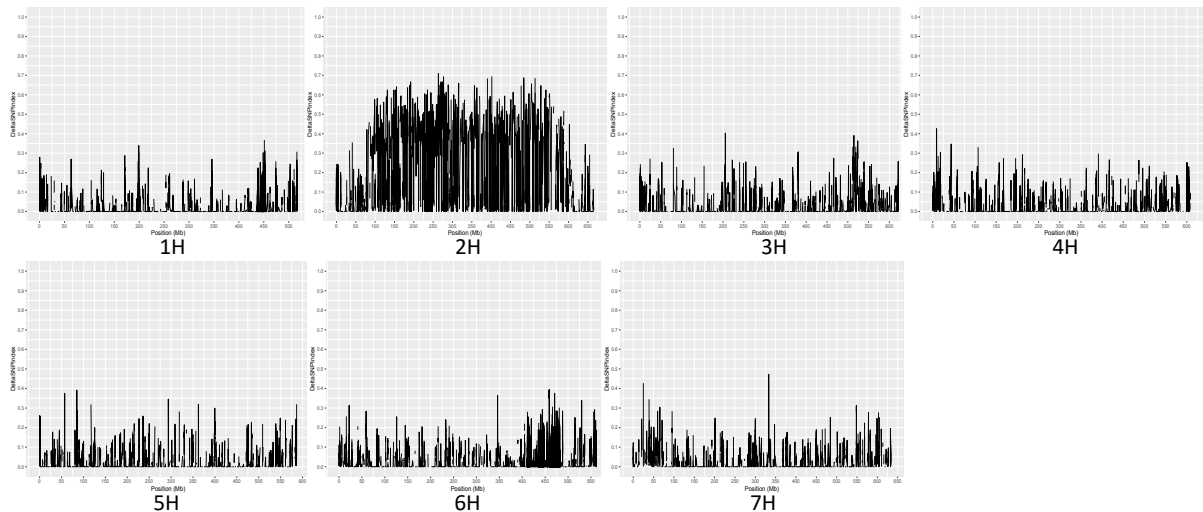


Figure 5. Results of MutMap+. The chart shows the value of Δ SNPIndex as a function of chromosomal position. Δ SNPIndex is calculated as the difference between the SNPIndex of the mutant bulk and that of the wild type bulk. SNPIndex is the ratio between the number of variant reads and read depth at a position. Chromosome 2H has a strong signal in the interval between 75 and 610 Mb.

3.3 WGS of the two bulks compared to TM390 finds 8 candidate genes

Variant calling of the TM390 mutant produced a total of 328,518 SNPs with coverage greater than 10 and SNPIndex greater than 0.8, 1,668 of which were functional SNPs, that is, they affected the protein (1,500 with a predicted moderate effect on the protein and 167 with a high effect, according to SNPEff).

Variant calling of the mutant bulk found 205,389 SNPs with coverage greater than 50 and SNPIndex greater than 0.8, 1,085 of which were functional and 1,054 (97%) were shared with TM390. Variant calling of the wild type bulk produced 144,682 SNPs with coverage greater than 30 and SNPIndex greater than 0.8, of which 779 were functional. Filtering the TM390 SNPs with the results of variant calling on the two bulks, as described in paragraph 1.3, we found only 8 candidate genes, all of them in chromosome 2H, in accordance with the interval produced by MutMap+ (Table 2). Among those genes,

HORVU.MOREX.r3.2HG0178520 is the ortholog of *OsGLU3 = Os04g0497250* in rice, which codes for a putative membrane-bound endo-1,4-beta-glucanase.

The rice *Osglu3-1* mutant has shorter roots with damages in the epidermis, it has a reduced content of crystalline cellulose in the root cell wall, shorter root cells, and less root meristem tissue (Figure 4 of Introduction)(Inukai et al., 2012; Zhang et al., 2012). *OsGLU3* is widely

expressed in various tissues, and especially in the roots, and it regulates root elongation by modulating the cell wall cellulose content (Inukai et al., 2012; Zhang et al., 2012).

Table 2. Eight candidate genes on chr2H for TM390. These genes resulted from the variant calling for TM390 filtered for the SNPs present in the mutant bulk and absent or called as wild type in the wild type bulk. No constraint was put on genomic region, nevertheless all the genes are on 2H, the same chromosome found by MutMap+.

TM390											MUT bulk		WT bulk	
CHR	POS	REF	ALT	DP	ADV	VARIANT	MAGNITUDE	GENE	NT VAR	AA VAR	DP	ADV	DP	AD2
2H	147,730,406	G	A	24	24	missense	MODERATE	HORVU.MOREX.r3.2HG0132300	c.74G>A	p.Arg25His	59	59	41	23
2H	175,120,308	G	A	20	20	missense	MODERATE	HORVU.MOREX.r3.2HG0136000	c.73C>T	p.Pro25Ser	61	61	33	15
2H	230,254,736	G	T	28	28	splice_donor	HIGH	HORVU.MOREX.r3.2HG0142850	c.19+1G>T		63	63	40	24
2H	481,969,052	C	T	18	18	missense	MODERATE	HORVU.MOREX.r3.2HG0169250	c.791G>A	p.Gly264Asp	67	67	29	21
2H	544,529,063	C	T	21	21	missense	MODERATE	HORVU.MOREX.r3.2HG0178520	c.533G>A	p.Ser178Asn	56	56	41	19
2H	548,284,962	C	T	16	16	missense	MODERATE	HORVU.MOREX.r3.2HG0179420	c.44C>T	p.Ser15Phe	54	54	20	9
2H	568,765,571	G	A	21	21	missense	MODERATE	HORVU.MOREX.r3.2HG0184210	c.142C>T	p.Pro48Ser	57	51	36	20
2H	596,904,960	G	A	15	15	missense	MODERATE	HORVU.MOREX.r3.2HG0189840	c.749G>A	p.Gly250Asp	70	58	22	4

(REF) Reference base(s).

(ALT) Alternative base(s).

(DP) Read depth at this position.

(ADV) Allelic depths for the alternative alleles.

(VARIANT) Protein-coding gene transcript effect predictions according to SNPEff: missense_variant = change of one or more bases, resulting in a different amino acid sequence, transcript length is preserved. stop_gain = at least one base of a codon is changed, resulting in a premature stop codon, leading to a shortened transcript. splice_donor = occurs at the boundary of an exon and an intron. It can disrupt RNA splicing with the loss of exons or the inclusion of introns.

(MAGNITUDE) Putative variant impact according to SNPEff (see Materials and Methods).

(NT VAR) Relative position inside the gene and sequence of the mutation.

(AA VAR) Position and sequence of the mutation on the protein.

3.4 Functional validation of candidate genes

Functional validation of candidate genes listed in Table 2 started from the gene with the highest predicted impact on the final protein, and was not complete at the moment of writing, due only to time constraints.

HORVU.MOREX.r3.2HG0142850 codes for an organic solute transporter-like and the SNP in TM390 has a predicted high effect, splice-donor-variant and intron-variant SNP, with the substitution of a guanine with a thymine in position 230,254,736, right at the beginning of the first of four introns.

The gene expression profile from Barlex (Colmsee et al., 2015) shows that the gene is expressed in all tissues, except in young developing inflorescences, and is mostly expressed in four days embryos (> 90 FPKM), inflorescence rachis (> 100 FPKM) and roots (> 130 FPKM).

In Table 3 are the phenotypic and genotypic results for the 69 survived M₈ seedlings coming from four M₇ intermediate plants. The sequencing was successful for 64 out of 69 plants. For six plants (9.4%), genotype and phenotype did not correspond. Five of them carried the mutant allele T, and their phenotype was intermediate in four plants and wild type in one plant. The sixth plant was one in 21 plants (4.8%) with extreme mutant phenotype but with heterozygous genotype. Only one plant out of 64 carried the reference allele at the homozygous state.

From these results, we could conclude that *HORVU.MOREX.r3.2HG0142850* is the causal gene for TM390, hence we plan to apply the sequencing for the other seven candidate genes on the same DNA samples.

Table 3. Resequencing of *HORVU.MOREX.r3.2HG0142850* in 69 plants coming from the first generation of intermediate plants. Six plants out of 64 sequenced plants (9.4%) carry alleles that do not correspond with their phenotype.

Plant ID	Genotype	Phenotype
1.1	T/G	W
1.2	T/G	W
1.3	T/G	W
1.4	T/G	W
1.5	T/G	W
1.6	T/G	W
1.7	T/G	W
1.8	T/G	W
1.9	T/G	W
1.10	T/G	I
1.11	T/G	I
1.12	T/G	I
1.13	T/G	I
1.14	T	M
1.15	T	M
1.16	T	M
1.17	T	M
1.18	T	M
3.1	T/G	W
3.2	T/G	W
3.3	T/G	W
3.4	T/G	W
3.5	T/G	W
3.6	T/G	W
3.7	T/G	W
3.8	T/G	W
3.9	T/G	W
3.10	T	W
3.11	T/G	I
3.12	T/G	I
3.13	T	I
3.14	T	I
3.15	T	M
3.16	failed	M
3.17	T	M
3.18	failed	M
3.19	T	M
3.20	T	M
3.21	T	M
3.22	T	M
3.23	T	M
4.1	T/G	W
4.2	T/G	W
4.3	T/G	W
4.4	failed	I
4.5	T/G	I
4.6	T/G	I
4.7	T	I
4.8	T/G	I
4.9	T/G	I
4.10	T	M
5.1	T/G	W
5.2	T/G	W
5.3	T/G	W
5.4	G	W
5.5	T/G	W
5.6	T/G	W
5.7	T/G	I
5.8	failed	I
5.9	T	I
5.10	T/G	M
5.11	T	M
5.12	T	M
5.13	T	M
5.14	T	M
5.15	faied	M
5.16	T	M
5.17	T	M
5.18	T	M

4. DISCUSSION AND CONCLUSIONS

In this study we carried out the mapping of the causal gene of TM390, a barley mutant originally identified from the TILLMore collection and characterized by short and semi-rigid roots. With the MutMap+ approach we restricted the interval to \approx 530 Mb on chromosome 2H where we found eight candidate genes.

HORVU.MOREX.r3.2HG0142850, that codes for an organic solute transporter-like, had the only SNP among the eight genes with a high magnitude predicted effect on the protein.

However, the genotypic segregation in the population derived from intermediate plants did not correspond to their phenotypic classification. *HORVU.MOREX.r3.2HG0178520*, on the other hand, is the most plausible candidate, as it codes for an endoglucanase. Moreover, it is the ortholog of *OsGLU3 = Os04g0497250* in rice, which codes for a putative membrane-bound endo-1,4-beta-glucanase and whose mutant *Osglu3-1* has the same phenotype with short root caused by a severe defect in cell elongation at the root-elongating zone with additional collapse of epidermal and cortex cells at the root tip caused by the defect in the smooth exfoliation of root cap cells (Inukai et al., 2012; Zhang et al., 2012).

HORVU.MOREX.r3.2HG0178520 is likely the causal gene of TM390, and its function is conserved in barley and rice.

OsGLU3 hydrolyzes the noncrystalline amorphous cellulose fibres of cellulose microfibrils to loosen the hemicellulose and cellulose interaction in cell walls, at the root elongation zone and at the root tips, and it is necessary for cell elongation and for root cap exfoliation from the epidermal cell layer, respectively. Zhang et al. (2012) also found that phosphate starvation induces root elongation by altering cell wall cellulose content through *OsGLU3*. Moreover, the mutant was rescued by the application of exogenous glucose, the substrate of cellulose synthesis. Further validation will likely confirm the candidate gene. We will also perform microscopical characterization of root tips of TM390 in comparison to its wild type Morex and we will test the response of Morex to phosphate starvation and the response of our mutant to exogenous glucose.

Root mutants with altered cell walls are important to unravel wall-associated immune responses. Plant cell walls are components of both pre-existing and inducible plant defence mechanisms against pathogen infection, in fact, they are a mechanical barrier that shields the plant from pathogens but they are also a reservoir of antimicrobial compounds and a source of carbohydrate moieties that are released during degradation and could act as damage-associated molecular patterns (DAMPs) triggering plant immune responses upon their

perception by plant pattern recognition receptors (PRRs) (Molina et al., 2021). β -1,4-endoglucanases are also one of the enzymes secreted by plant-parasitic cyst nematodes to accelerate the migratory movement inside the host (Smant et al., 1998). Moreover, host endoglucanase genes are upregulated after infection with root-knot or cyst nematodes, and they appear to have a role in syncytium formation and giant cell development (Williamson & Gleason, 2003).

It would be interesting to test the resistance of our mutant to pathogens with different parasitic styles compared to its wild type. However, plants that are defective in cellulose biosynthesis usually have a reduced fitness coming from developmental defects like reduced size, biomass, or fertility, and this is the case of our mutant, particularly at the homozygous state.

5. REFERENCES

- Cingolani, P., Platts, A., Wang, I. L., Coon, M., Nguyen, T., Wang, L., . . . Ruden, D. M. (2012). A program for annotating and predicting the effects of single nucleotide polymorphisms, SnpEff: SNPs in the genome of *Drosophila melanogaster* strain w1118; iso-2; iso-3. *Fly (Austin)*, 6(2), 80-92. <https://doi.org/10.4161/fly.19695>
- Colmsee, C., Beier, S., Himmelbach, A., Schmutzer, T., Stein, N., Scholz, U., & Mascher, M. (2015). BARLEX—the barley draft genome explorer. *Molecular Plant*, 8(6), 964-966.
- Danecek, P., Bonfield, J. K., Liddle, J., Marshall, J., Ohan, V., Pollard, M. O., . . . Davies, R. M. (2021). Twelve years of SAMtools and BCFtools. *Gigascience*, 10(2), giab008.
- Dowle, M., & Srinivasan, A. (2021). Data. table: Extension of 'data.frame'[Manual]. In.
- Fekih, R., Takagi, H., Tamiru, M., Abe, A., Natsume, S., Yaegashi, H., . . . Matsumura, H. (2013). MutMap+: genetic mapping and mutant identification without crossing in rice. *PLoS one*, 8(7), e68529.
- Hetz, W., Hochholdinger, F., Schwall, M., & Feix, G. (1996). Isolation and characterization of *rtcs*, a maize mutant deficient in the formation of nodal roots. *The Plant Journal*, 10(5), 845-857.
- Inukai, Y., Sakamoto, T., Morinaka, Y., Miwa, M., Kojima, M., Tanimoto, E., . . . Kitano, H. (2012). ROOT GROWTH INHIBITING, a Rice Endo-1,4- β -d-Glucanase, Regulates Cell Wall Loosening and is Essential for Root Elongation. *Journal of Plant Growth Regulation*, 31(3), 373-381. <https://doi.org/10.1007/s00344-011-9247-3>
- Li, H., & Durbin, R. (2009). Fast and accurate short read alignment with Burrows-Wheeler transform. *Bioinformatics*, 25(14), 1754-1760. <https://doi.org/10.1093/bioinformatics/btp324>
- Mascher, M., Wicker, T., Jenkins, J., Plott, C., Lux, T., Koh, C. S., . . . Stein, N. (2021). Long-read sequence assembly: a technical evaluation in barley. *The Plant Cell*. <https://doi.org/10.1093/plcell/koab077>
- Molina, A., Miedes, E., Bacete, L., Rodríguez, T., Mélida, H., Denancé, N., . . . Freydier, A. (2021). Arabidopsis cell wall composition determines disease resistance specificity and fitness. *Proceedings of the National Academy of Sciences*, 118(5), e2010243118.
- Osthoff, A., Donà dalle Rose, P., Baldauf, J. A., Piepho, H.-P., & Hochholdinger, F. (2019). Transcriptomic reprogramming of barley seminal roots by combined water deficit and salt stress. *BMC genomics*, 20(1), 1-14.
- Smant, G., Stokkermans, J. P., Yan, Y., De Boer, J. M., Baum, T. J., Wang, X., . . . Davis, E. L. (1998). Endogenous cellulases in animals: isolation of β -1, 4-endoglucanase genes from two species of plant-parasitic cyst nematodes. *Proceedings of the National Academy of Sciences*, 95(9), 4906-4911.
- Takagi, H., Abe, A., Yoshida, K., Kosugi, S., Natsume, S., Mitsuoka, C., . . . Takuno, S. (2013). QTL-seq: rapid mapping of quantitative trait loci in rice by whole genome resequencing of DNA from two bulked populations. *The Plant Journal*, 74(1), 174-183.
- Talamè, V., Bovina, R., Sanguineti, M. C., Tuberosa, R., Lundqvist, U., & Salvi, S. (2008). TILLMore, a resource for the discovery of chemically induced mutants in barley. *Plant Biotechnol J*, 6(5), 477-485. <https://doi.org/10.1111/j.1467-7652.2008.00341.x>
- Team, R. (2020). *RStudio: Integrated Development for R*. RStudio, PBC, URL <http://www.rstudio.com/>. In PBC. <http://www.rstudio.com/>
- Untergasser, A., Cutcutache, I., Koressaar, T., Ye, J., Faircloth, B. C., Remm, M., & Rozen, S. G. (2012). Primer3--new capabilities and interfaces. *Nucleic Acids Res*, 40(15), e115. <https://doi.org/10.1093/nar/gks596>
- Wickham, H. (2016). Data analysis. In *ggplot2* (pp. 189-201). Springer.
- Williamson, V. M., & Gleason, C. A. (2003). Plant–nematode interactions. *Current Opinion in Plant Biology*, 6(4), 327-333. [https://doi.org/https://doi.org/10.1016/S1369-5266\(03\)00059-1](https://doi.org/https://doi.org/10.1016/S1369-5266(03)00059-1)
- Zhang, J.-W., Xu, L., Wu, Y.-R., Chen, X.-A., Liu, Y., Zhu, S.-H., . . . Yi, K.-K. (2012). OsGLU3, a Putative Membrane-Bound Endo-1,4-Beta-Glucanase, Is Required for Root Cell Elongation and Division in Rice (*Oryza sativa* L.). *Molecular Plant*, 5(1), 176-186. <https://doi.org/https://doi.org/10.1093/mp/ssr084>

CHAPTER 4. Cloning the barley hypergravitropic root mutants *egt1* and *egt2*

The results of this work are part of two publications:

- Fusi, R., Rosignoli, S., Lou, H., Sangiorgi, G., Bovina, R., Pattem, J.K., Borkar, A.N., Lombardi, M., Forestan, C., Milner, S.G. and Davis, J.L., 2022. Root angle is controlled by *EGT1* in cereal crops employing an antigravitropic mechanism. *Proceedings of the National Academy of Sciences*, 119(31), p.e2201350119.
- Kirschner, G.K., Rosignoli, S., Guo, L., Vardanega, I., Imani, J., Altmüller, J., Milner, S.G., Balzano, R., Nagel, K.A., Pflugfelder, D. and Forestan, C., 2021. *ENHANCED GRAVITROPISM 2* encodes a *STERILE ALPHA MOTIF*-containing protein that controls root growth angle in barley and wheat. *Proceedings of the National Academy of Sciences*, 118(35), p.e2101526118.

1. OBJECTIVES

egt1 and *egt2* are two distinct hypergravitropic root mutants from the TILLMore collection.

Our objectives are:

- to clone *egt1* and *egt2*;
- to verify their natural variation;
- to verify if their functions are conserved in wheat.

2. MATERIALS AND METHODS

2.1 Plant material, growth conditions, and phenotyping

The hypergravitropic root mutants, *egt1* and *egt2*, belong to the TILLMore collection of mutants obtained with sodium azide mutagenesis on the cultivar Morex (Talamè et al., 2008). TM194, TM3580 and TM2835 were identified screening the collection with the semi-hydroponic 2D screens. TM194 and TM3580 are mutated in two different alleles of the same gene, as confirmed by complementation test. Prior to root phenotyping, seeds were washed in 10% sodium hypochlorite for 10 minutes then rinsed with deionized water and pregerminated for 24 hours in the dark at 28°C on wet filter paper.

Each **2D screen** is composed by a black polycarbonate panel measuring 38,5 x 42,5 cm and approximately 0.5 cm thick and by two 50 x 50 cm sheets of germination paper (Carta filtro Labor, Gruppo Cordenons SpA). The sheets are soaked with deionized water and arranged flat, one on top of the other, over the panel. Five pregerminated seeds are placed in line between the two sheets, near the top edge of the panel. Up to 30 panels are placed vertically in a black plastic box 50 cm wide, containing 10 litres of deionized water or enough water to reach a level of 10 cm from the bottom. Plants were grown for 6 days after germination in a

growth room with 16/8 h photoperiod and temperature of 22°C/18°C, and pictures were taken with a Nikon D5600 digital camera. Further phenotyping was carried in soil filled rhizotrons for 2D imaging, in soil filled cylinders with X-ray microCT and X-ray CT 3D image acquisition and in soil filled pots with MRI. For two-dimensional soil experiments, barley *egt1* and *egt2* mutants and their wild type Morex were grown up to 20 days in the **GrowScreen-Rhizo** rhizotrons automated platform in Jülich Plant Phenotyping Center (JPPC), Institute of Bio- and Geosciences – Plant Sciences, Jülich, Germany, and they were analyzed as previously described (Nagel et al., 2012).

X-ray microCT and X-ray CT were carried out at the University of Nottingham, Sutton Bonington Campus, United Kingdom.

For **X-ray microCT**, seeds were pregerminated in Petri dishes for 1 d at 21°C in dark. Successful seedlings with equally germinated roots were grown in PVC columns (8-cm diameter and ~ 15-cm height) filled with sandy loam soil from the University of Nottingham experimental farm field, sieved at <2 mm and maintained at notional field capacity moisture until 9 DAG. Each column was scanned using a Phoenix vjto mejx M 240-kV X-ray microCT scanner (Waygate Technologies) at the Hounsfield Facility at Sutton Bonington Campus. The voltage and current were set at 180 kV and 180 µA, respectively. A voxel resolution of 55 µm was used in all scans. During the scan, the specimen stage rotated through 360° at a rotation step increment of 0.166° collecting a total of 2,160 projection images. Each image was the integration of four frames with a detector exposure time of 250 ms, resulting in a 75-min scan time. A 0.1-mm copper filter was applied to the front of the exit window of the X-ray tube during the scan to reduce beam hardening artifacts.

For the **X-ray CT**, well-watered plants were grown in larger PVC soil columns (20-cm diameter, 100-cm height) until full maturation stage. Each column was then scanned using a Phoenix vjto mejx L Custom 320-kV X-ray CT system (Waygate Technologies) at the Hounsfield Facility (University of Nottingham, Sutton Bonington Campus, United Kingdom). The voltage and current were set at 290 kV and 6,200 µA, respectively. A voxel resolution of 150 µm was used in all scans. During the scan, the specimen stage rotated through 360° at a rotation step increment of 0.15° collecting a total of 2,400 projection images. To reduce image noise, each projection image was an integration of 12 frames with a detector exposure time of 131 ms. Each scan took ~240 min. A 1-mm copper filter was applied to the exit window of the X-ray tube and a further 0.5-mm Cu filter applied over the detector panel to reduce beam hardening artifacts. For all CT images, the scans were reconstructed using DatosRec software (Waygate Technologies, Baker Hughes Digital

Solutions). Radiographs were visually assessed for sample movement before being reconstructed in 16-bit depth volumes with a beam hardening correction of 8. An inline median filter was applied to reduce noise in the image of the CT X-ray data. Reconstructed volumes were then postprocessed in VGStudioMAX (v2.2.0; Volume Graphics). Root system architecture was first segmented from the reconstructed volumes using the polyline tool within VGStudioMAX and then quantified using an in-house software tool called PAM (Polyline Angle Measurement). PAM extracts the 3D coordinate points (2 to 5 XY slices apart) for each polyline and translates these into a 3D model. The angle of each polyline (root) is calculated from the difference of a vertical vector from the position of the uppermost coordinate point of the polyline (e.g., the soil surface). Therefore, steeply growing roots have a low angle value and shallow roots have a large angle value. Measurement of root angle was terminated once the root has touched or interacted with the pot wall to avoid any physical interference on undisturbed root angle.

MRI imaging was carried out at the University of Bonn, Germany. Seeds were sown in field soil, 18 seeds were planted in one pot ($\text{\O} = 12.5$ cm, 12 cm height) in a hexagonal grid with 2.5 cm seed spacing. Seedlings were imaged after 3 days in the growth chamber. For a longer experiment, single seeds were planted into larger pots ($\text{\O} = 9$ cm, 30 cm height) and were grown for one week before imaging. MRI images were acquired on a 4.7 T vertical magnet equipped with a Varian console (van Dusschoten et al., 2016). A multislice spin echo sequence was used. Sequence parameters were adapted to the different pot sizes. For the 9 cm pots, we used a birdcage RF coil with a 10 cm diameter and the following sequence parameters: 0.5 mm resolution, 1-mm slice thickness, 9.6 cm field of view, TE = 9 ms, TR = 2.85 s, Bandwidth = 156 kHz, two averages. For the 12.5 cm pots, the following parameters were changed: birdcage RF coil with 140 mm diameter, 14 cm field of view, and 0.55 mm resolution.

For the **rotation test**, TM194 and Morex were grown for 4 days in 1% agar plates containing Hoagland's No. 2 Basal salt (Sigma, H2395) in a growth room with a 16/8 h photoperiod and a temperature of 22°C/18°C; then they were rotated by 30°, 60° or 90° and their root growth angle was measured after 0.5, 1, 2 and 24 hours. 38 TM2835 plants and 38 Morex plants were grown for 5 days in a 2D screen using blue cardboard instead of the polycarbonate panel and then they were rotated by 90° and their root growth angle was measured after 3, 6, 9, 12, 24, 48 and 72 hours.

For seed bulking and **shoot phenotyping** *egt1*, *egt2* and Morex were grown in the greenhouse, in a peat and vermiculite growing medium (Vigorplant Irish and Baltic peat-

based professional mix) in 15 × 15 × 30 cm polyethylene pots with a day temperature of 22°C (16 h) and a night temperature of 18°C (8 h). Greenhouse lighting was a mix of natural light supplemented with artificial light by 400 watt high-pressure sodium lamps (Sylvania SHP-TS 400W Grolux). Shoot growth angle was measured between the main culm and the gravity vector, leaf insertion angle was measured as in Shaaf et al. (2019) for the three leaves from the top of the main culm.

2.2 Bulk Segregant Analysis (BSA)

SNP-based BSA was carried out on the two F₂ populations derived from the cross TM194 × Barke and TM2835 × Barke, which were phenotyped with 2D screens (see previous paragraph). Fifteen plants for each wild type bulk and fifteen for each mutant bulk were selected for single plant DNA extraction. Leaves were lyophilized and foliar samples of ~2 cm² were homogenized for 3 minutes in a TissueLyser. DNA was extracted with the Macherey-Nagel Nucleospin Plant II kit and quantified with NanoDrop. Two DNA bulks, steeper and wild type root angle phenotype were prepared for each F₂ mixing equal amounts of each plant and bringing to a final concentration of 50 ng/μL, in addition to single plant DNA from 10 plants for each *egt* line showing steeper angle and all sample were genotyped with the 9k Illumina Infinium iSelect barley SNP array by TraitGenetics GmbH, Gatersleben, Germany. The results were analyzed with GenomeStudio (Illumina), and Δ/θ values used as index of allele proportion at each SNP marker. Δ/θ Values were calculated as the squared difference between the theta value of wild-type and steeper angle phenotype bulk.

2.3 Whole Genome Sequencing

Genomic DNA for WGS of the three mutants *TM194*, *TM3580* and *TM2835* was prepared as described above and sequenced with Illumina HiSeq PE150 by Novogene, China, obtaining 727,190,417 paired-end reads for an average coverage of ~24× after mapping for *TM194*, 792,713,857 paired-end reads for an average coverage of ~26× for *TM3580* and 699,353,963 paired-end reads for an average coverage of ~23× for *TM2835*. Reads were aligned to the Morex v1 reference sequence (Mascher et al., 2017) with BWA v7.12 (Li & Durbin, 2009) and variants in the genomic space were called with SAMtools v1.3 (Danecek et al., 2021; Li et al., 2009), filtering for a minimum read depth of 5×, PHRED quality > 40. To discard background mutations due to the differences between the Morex reference sequence and the Morex parental seeds that had previously been used in the mutagenesis, the SNP calling for *TM194* and *TM2835* considered additional WGS data from seven TILLMore mutant that

were available at that moment, filtering with a custom AWK script for a minimum ratio DV/DP of 0.8 for the mutants and a maximum ratio of 0.2 in every other mutant, where DP is the coverage depth at the SNP position and DV is number of nonreference bases at the same position. SNP effects were predicted with SNPEff v3.0.7 (Cingolani et al., 2012).

2.4 CRISPR/CAS9 generation of a second allele of *egt2*

The knock-out allele of *egt2* used for gene validation was created with CRISPR/CAS9 by the group of Crop Functional Genomics, at the University of Bonn, Germany. For CRISPR target sequences, they chose 20 base pair sequences with the protospacer adjacent motif PAM sequence NGG in the first exon of *EGT2* (*HORVU5Hr1G027890*) that was checked at <http://crispr.dbcls.jp/> for off-targets in the barley. They used sites with only one predicted target for a 20mer and only up to 3 predicted targets for the 12mer target sequence upstream of the PAM. The CRISPR guide sequences are marked in Figure 14. The sgRNA shuttle vectors pMGE625 and 627 were used to generate the binary vector pMGE599 as described in (N. Kumar et al., 2018). Transformation was carried out with the spring barley cv. Golden Promise grown in a climate chamber at 18 °C/14 °C (light/dark) with 65% relative humidity, a 16 h photoperiod and a photon flux density of 240 $\mu\text{mol} \cdot \text{m}^{-2} \cdot \text{s}^{-1}$. The binary vector pMGE599 was introduced into *Agrobacterium tumefaciens* AGL-1 strain (Lazo et al., 1991) through electroporation (*E. coli* Pulser; Bio-Rad). The scutella tissue of barley caryopsis was used for *Agrobacterium*-mediated transformation as described previously (Imani et al., 2011). The insert integration in the barley genome was confirmed by detection of hygromycin gene sequences via PCR in generated T₀ lines and were analyzed for mutations in *EGT2* by PCR and Sanger sequencing and the seeds for T₁ generation were used for experiments.

2.5 Haplotype Analysis of *HvEGT1* in the WHEALBI Barley Collection

A haplotype analysis of SNP data from the barley diversity panel WHEALBI (Bustos-Korts et al., 2019), consisting of 459 barley accessions, of which 199 are cultivars, 202 landraces, and 4 wild, was conducted in the coding region of *EGT1*. Files were imported into R Studio and package pegas (Paradis, 2010) v0.14 was used to detect haplotypes. Six haplotypes were found. The MUSCLE multialignment was produced with Mega X v10.2.4 (S. Kumar et al., 2018) and exported to the NEXUS format (Maddison et al., 1997). The haplotype TCS network (Clement et al., 2002) was produced with PopART (popart.otago.ac.nz).

2.6 *egt1* and *egt2* durum wheat mutants

To further validate the function of the *EGT1* and *EGT2* genes, we identified mutant lines carrying premature stop codons from a sequenced mutant population of tetraploid wheat (Krasileva et al., 2017). With proper crossing, we combined mutations in the durum wheat *EGT2* orthologs (homologs on A and B genomes) to generate complete *egt1* and *egt2* knockout lines and we phenotyped them, together with their wild type Kronos, using 2D screens (see above).

3. RESULTS

3.1 TM194 and TM3580 are allelic and distinct from TM2835

To clarify the genotypic differences between the three hypergravitropic lines, we performed a complementation test crossing TM194 with TM3580 and TM194 with TM2835. F₁ seedlings from TM194 × TM3580 have hypergravitropic roots (Figure 1), hence the trait is caused by the same gene. On the contrary, F₁ plants from TM2835 × TM194 and from TM194 × TM2835 showed a wild type phenotype (Figure 2), hence they have different causal genes.

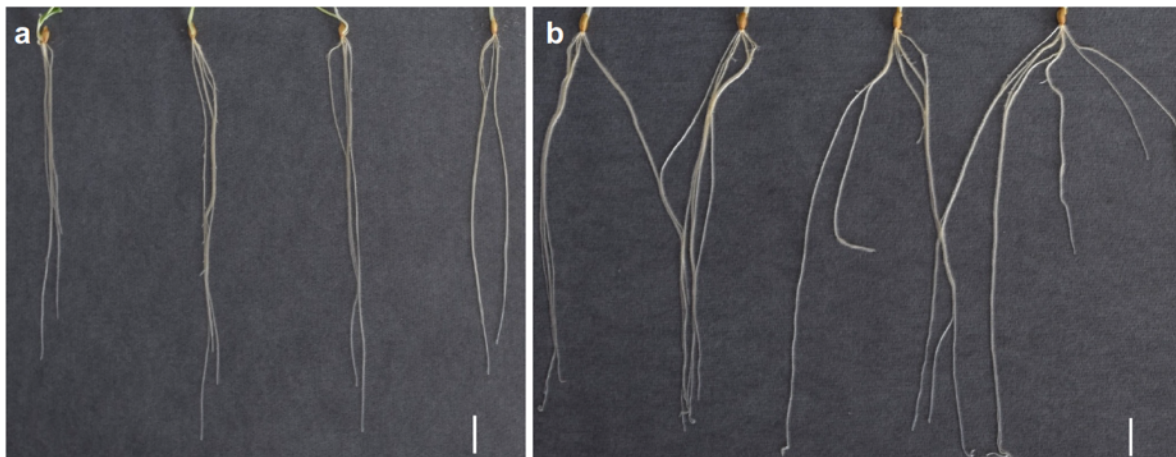


Figure 1. Complementation test between TM194 and TM3580. The two lines were crossed and the result of their F₁ showed hypergravitropic phenotype of seminal roots in 2D screens, 7 DAG (a), compared to the wild type Morex (b) The two lines did not complement, hence they are caused by the same gene. Scale bar 2 cm.

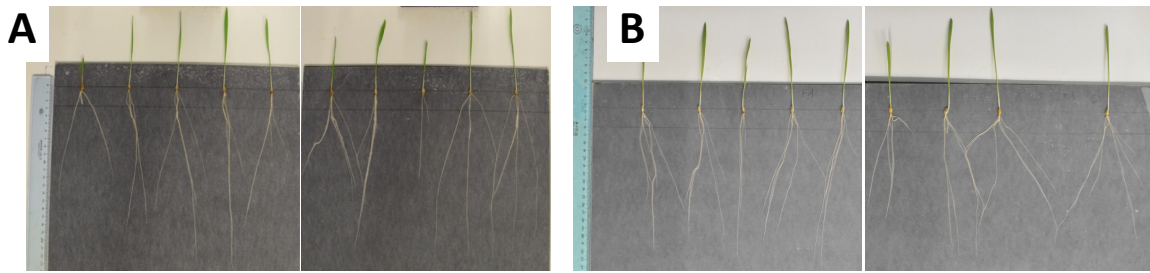


Figure 2. Complementation test between TM194 and TM2835. (a) F₁ from TM2835 × TM194, 7 DAG; (b) F₁ from TM194 × TM2835, 6DAG, in 2D screens. The two lines complement in both crosses, showing wild type phenotype, hence they are caused by different genes.

3.2 *egt1* and *egt2* have hypergravitropic roots of all classes

TM194, exhibiting a striking steeper seminal and lateral root phenotype (Figure 3) was initially identified using the semi-hydroponic 2D screening system. Three-dimensional (3D) root architecture phenotyping of 10-days-old TM194 roots using X-ray microcomputed tomography (microCT) revealed the steeper seminal root angle phenotype directly in soil (Figure 4A). Phenotyping TM194 roots 20 d after germination (DAG, using soil-filled rhizotrons) and at grain maturation stage (using X-ray CT) revealed lateral and crown root angles are also significantly steeper compared to wild-type Morex (Figure 4B–D). Hence, the TM194 mutant exhibited steeper root growth angle in every root class examined, in both semi-hydroponic and soil conditions.

TM2835 root was characterized with 2D screens (Figure 6A), showing hypergravitropic root growth angle compared to the wild type Morex. This phenotype was consistent in plants grown in soil-filled rhizotrons (Figure 6B) and pots (Figure 6C, 8E), the latter visualized by MRI. Furthermore, the lateral roots growing from the seminal roots also displayed a steeper root growth angle (Figure 6B and 8A). Apart from the root growth angle, we did not detect any other aberrant root phenotypes, neither a changed number of seminal roots nor a difference in root length (Figure 8B-C).

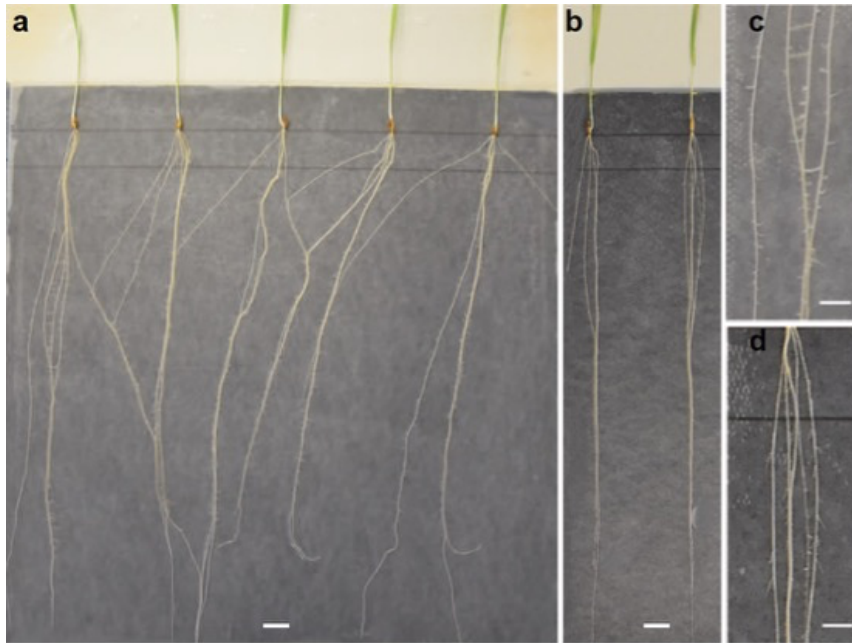


Figure 3. 2D screens were used to identify TM194 as a hypergravitropic root mutant. (a) 2D root architecture phenotype of 10 DAG seedlings of barley cv. Morex, and (b) TM194 in semi-hydroponic conditions. Scale bar 1cm. Magnified image of (c) Morex and (d) TM194 seminal roots highlighting phenotypic difference in lateral root insertion angles. Scale bar 1 cm.

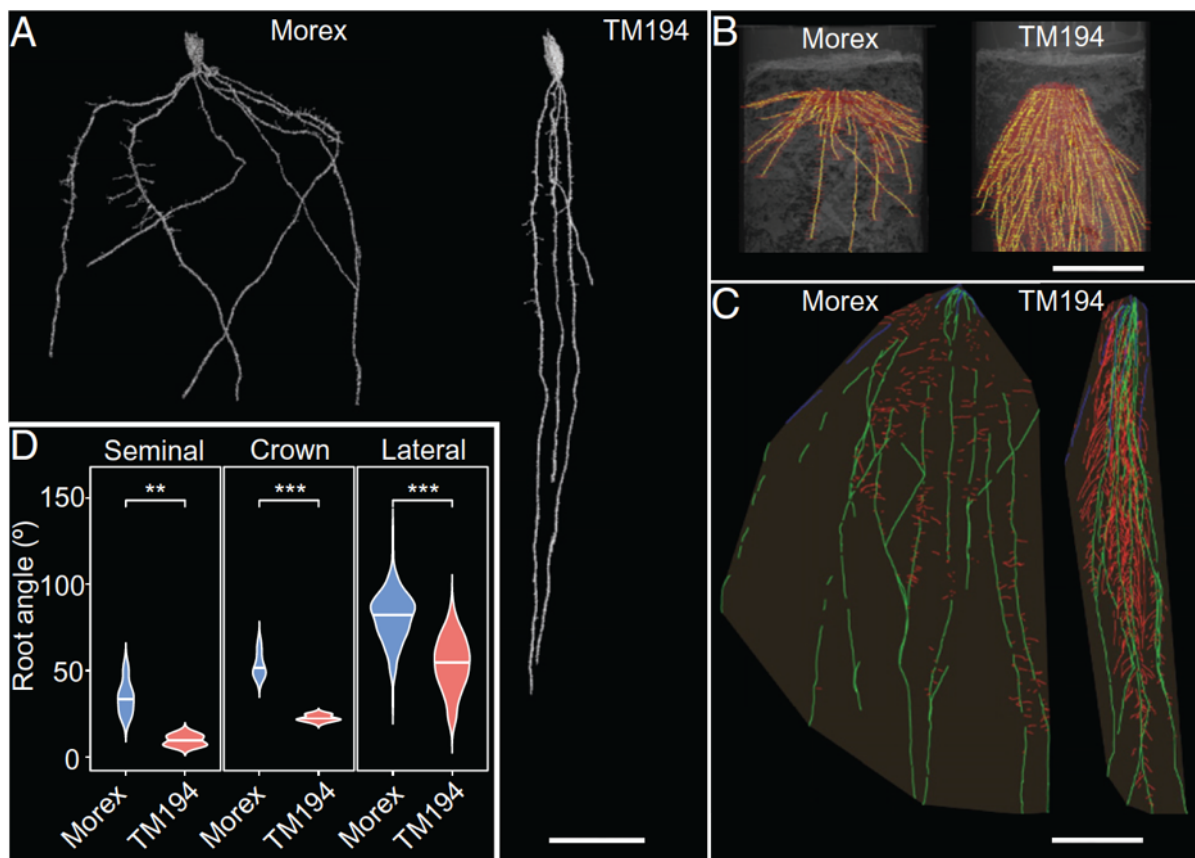


Figure 4. TM194 mutant shows hypergravitropic root angle in every root class in soil conditions. (A) Representative X-ray microCT scan image of 10 DAG wild type (Morex) and *TM194* roots (Scale bar 2 cm) (B) Representative X-ray CT scan image of plants at grain maturation stage revealing major difference in crown root growth angle between Morex and *TM194* (Scale bar 10 cm) (C) Representative image of 20 DAG Morex and *TM194* revealing difference in lateral root growth angles (red) (Scale bar 10 cm) (D) Root growth angle from seminal roots, crown roots, and lateral roots. Welch's t test, *** $p < 0.001$ and ** $p < 0.001$ in $n > 4$ independent replicates.

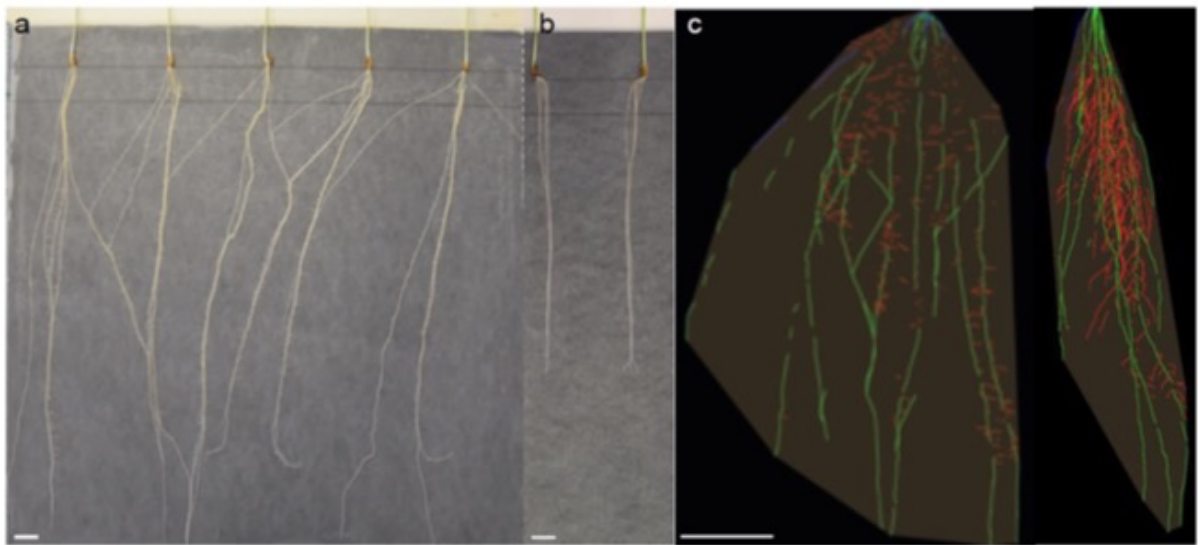


Figure 5. TM3580 root phenotype in semi-hydroponic conditions and in soil. The mutant shows steeper seminal and lateral root angle phenotype in semi-hydroponic conditions, 10 DAG (b) compared to Morex (a), scale bar 1cm. (c) 20 DAG Morex and TM3580 in soil filled rhizotrons reveals difference in crown root angle (green) and lateral root insertion angles (red). Scale bar 10 cm.

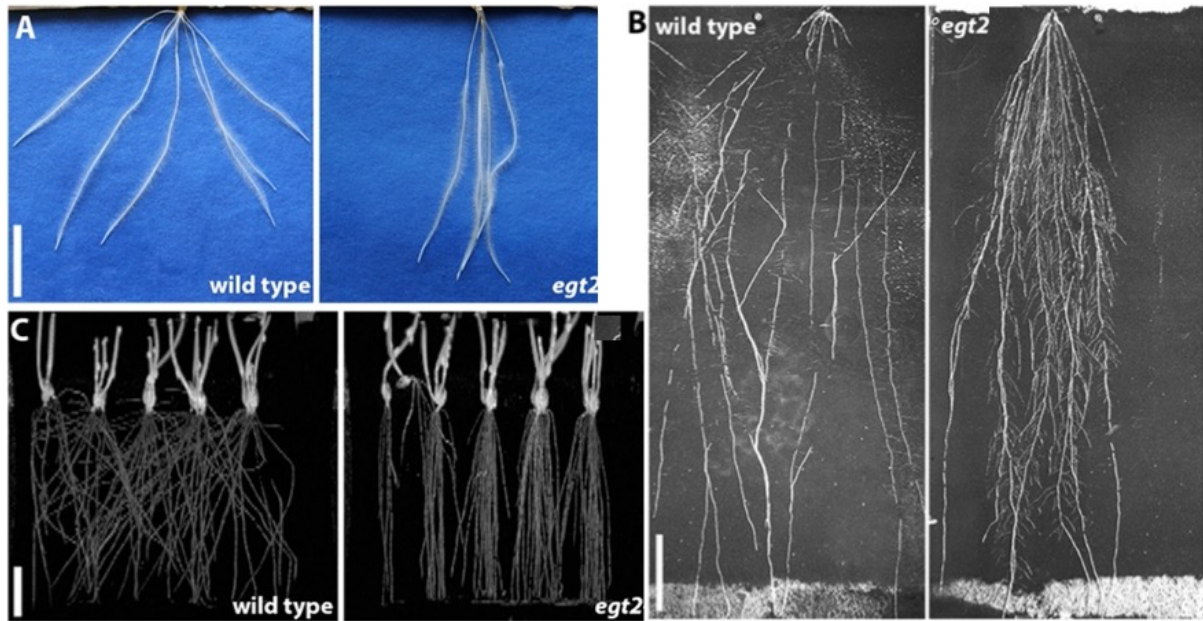


Figure 6. Root phenotype of *egt2*. (A) Wild type and *egt2* roots grown on germination paper, 7 DAG (Scale bar 2 cm) (B) Wild type and *egt2* roots grown in rhizotrons 26 DAG (Scale bar 10 cm) (C) MRI pictures of wild type and *egt2* plants grown in soil 7 DAG (Scale bar 4 cm).

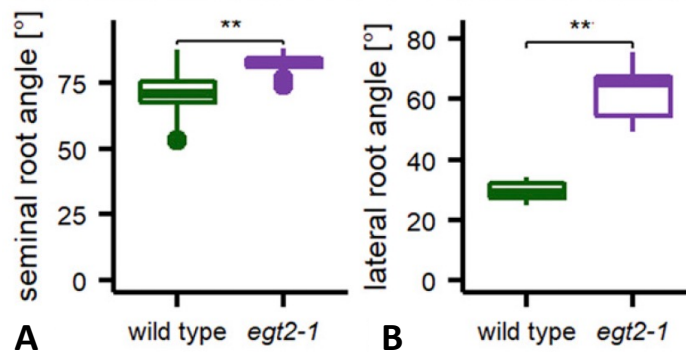


Figure 7. Difference in root angle between *egt2* and Morex. (A) Root angle of seminal roots 7 DAG; n = 40 per genotype in one experiment; two-tailed t test, ** $p < 0.01$. (B) Lateral root angle 14 DAG; n = 8 to 9 per genotype in two independent experiments; two-tailed t test, ** $p < 0.01$.

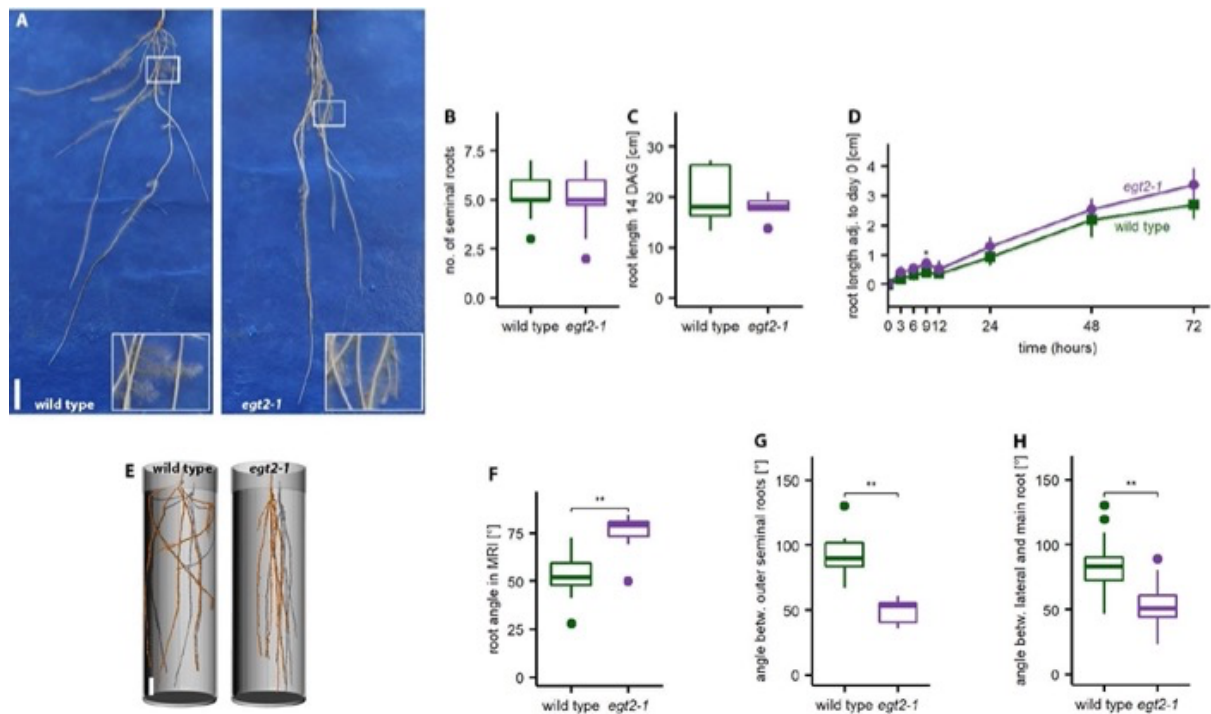


Figure 8. Root phenotype of *egt2*. (A) Wild type and *egt2* roots grown on 2D screens, 14 DAG. Scale bar 2 cm. (B) Number of seminal roots 7 DAG; $n = 40$ per genotype in one experiment. (C) Root length 14 DAG; $n = 8-9$ per genotype in two independent experiments. (D) Root length after rotation; $n = 32$ in three independent experiments; standard deviation is depicted; two-tailed t-test did not show any significant differences between the genotypes at respective time points; all measurements were normalized to the starting length of the roots at time point 0. (E) Magnetic resonance imaging (MRI) pictures of wild type and *egt2-1* roots grown in soil for 7 DAG. Scale bar 2 cm. (F) Root angle of roots grown in soil for 3 DAG and captured by MRI (see D); $n = 17-18$ per genotype; two-tailed t-test, $** p < 0.01$. (G) Root angle of seminal roots of plants grown in rhizotrons, measured by angle between the outermost seminal roots; 26 DAG; $n = 10-11$ per genotype; two-tailed t-test, $** p < 0.01$. (H) Root angle of lateral roots of plants grown in rhizotrons, angle measured between main roots and lateral roots; 26 DAG; $n = 5$ (30 lateral roots per plant) per genotype; two-tailed t-test, $** p < 0.01$.

3.3 *egt1* and *egt2* have a root-specific angle defect

At visual observation, both TM194 and TM2835 appear similar to the wild type in their shoot, in terms of angle of stems and tillers and angle of insertion of leaves and no other defect is present, except a slightly diminished growth that is however expected and observed in most of the mutant of the collection, likely correlated to their mutation load.

Following a greenhouse phenotyping, no significant difference in shoot growth angle (the angle between the main culm and the gravity vector) ($p = 0.4819$) at seedling stage (Figure 9A) or leaf growth angle (that is, leaf insertion angle of the three leaves from the top of the main culm) ($p = 0.566$) at the flowering stage (Figure 9B) was observed in the TM194 mutant compared to wild type. Hence, the TM194 mutation causes a root-specific angle defect.

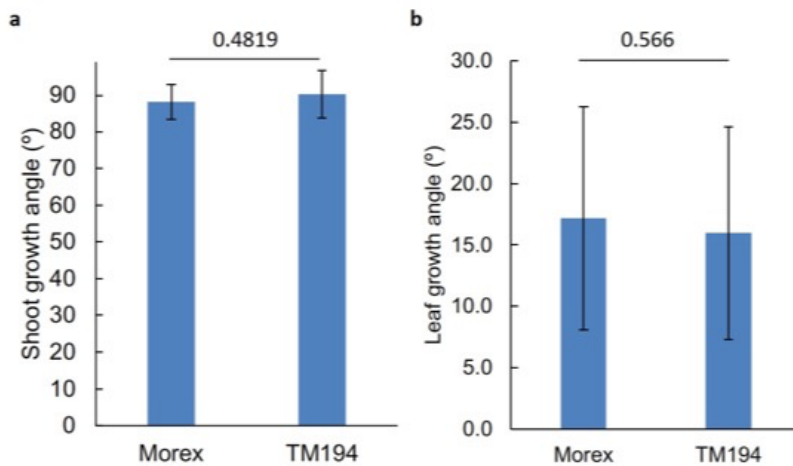


Figure 9. TM194 mutant do not show significant difference in shoot growth angle at seedling stage and leaf insertion angle at flowering stage. (a) Bar plot showing mean +/- standard deviation of coleoptile growth angle in 8 individual seedlings of mutant and Morex during seedling stage (7 days) grown vertically in a growth pouch system. No statistical difference (Student's T-test, $p = 0.4819$) in shoot growth angle was observed for mutant vs Morex. (b) Leaf growth angle in three young leaves in TM194 mutant and Morex at flowering time. Three leaves each were measured from > 13 individual plants grown in pots (TM194, n=39 leaves and Morex, n=42 leaves). Welch's test (Not significant, $p = 0.566$). Both Morex and TM194 mutant showed similar flowering time.

3.4 Root growth angle of *egt1* and *egt2* depends on gravity

To assess if *egt1* and *egt2* roots sense gravity, we performed a rotation test on seedlings. For *egt1*, roots exhibited a significantly higher bending angle and faster gravitropic response than Morex even after 0.5 h at a 30° rotation and this difference increased even more with rotation angle (Figure 10). Roots of the *egt2* mutant bent much faster and stronger than wild-type roots, approaching 90° after 3 d compared to just 30° in wild-type roots (Figure 11). Root growth rate, however, was not altered (Figure 8D).

Both mutants can sense gravity in their root and it appears that their response to gravitropism is stronger than *Morex*.

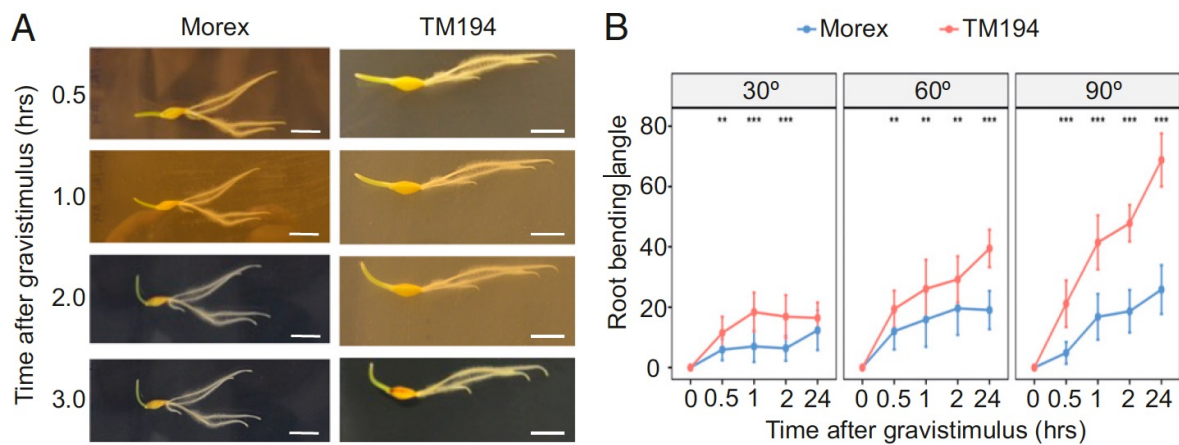


Figure 10. Rotation test on TM194. (A) Representative images of root bending response of 4-d-old seminal roots in *Morex* and TM194 at 0.5, 1, 2, and 3 h after 90° rotation. Scale bar 1 cm. (B) Measurement of change in root tip bending angle with different rotation (30°, 60° and 90°) in the two genotypes, n=5 plants per genotype per treatment.

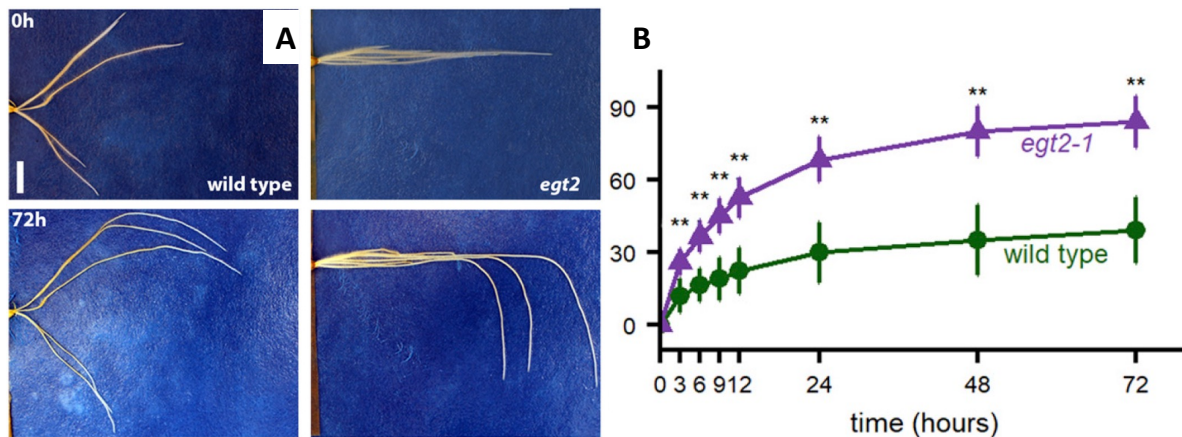


Figure 11. Rotation test on TM2835. (A) Root tip angle after rotation; plants at 5 DAG were rotated by 90° (time 0), and the root tip angle was measured over time; n = 38 per genotype in three independent experiments. Scale bar 1 cm. (B) Root tip angle of the two genotypes were compared between each other at the respective time points, by a two-tailed t test, ** $p < 0.01$. SD is depicted; to account for the different starting angles of the roots, all measurements were normalized to the starting angle of the roots at time 0.

3.5 *egt1* and *egt2* segregates like a Mendelian recessive trait

All F₁ plants derived from both TM194 × Barke and TM2835 × Barke exhibited a wild-type phenotype. F₂ plants of TM194 (n = 75) segregated in a Mendelian pattern, with 59 wild type plants and 16 hypergravitropic plants, χ^2 3:1, n.s., hence the TM194 root growth angle phenotype segregates as a single recessive allele. F₂ plants of TM2835 (n = 106) segregated in a Mendelian pattern as well, with 88 wild type and 18 mutants, χ^2 3:1, n.s.

3.6 *EGT1* encodes a Tubby-like F-box protein

Using the F₂ population from the cross TM194 × Barke, BSA revealed that the causal mutated locus mapped to chromosome 6H (Figure 12A) in a large pericentromeric region spanning ~130 Mb between markers BOPA2_12_30144 and BOPA1_4109-90. To pinpoint the root angle mutation, whole genome sequencing was performed on TM194. This revealed missense mutations in four genes within the region highlighted by BSA (Figure 12B and). To find the causal gene, we whole genome sequenced TM3580 as well, the independent root angle mutant allele (Figure 5). TM3580 contains six mutations in the same chromosome region, where only one mutated gene is shared with TM194: *HORVU6Hr1G068970* (encoding Tubby-like F-box protein). Specifically, TM194 contains substitution in the fourth exons leading to a missense mutation and TM3580 contains a mutation in the first intron of *HORVU6Hr1G068970*, predicted to cause a splice acceptor variant.

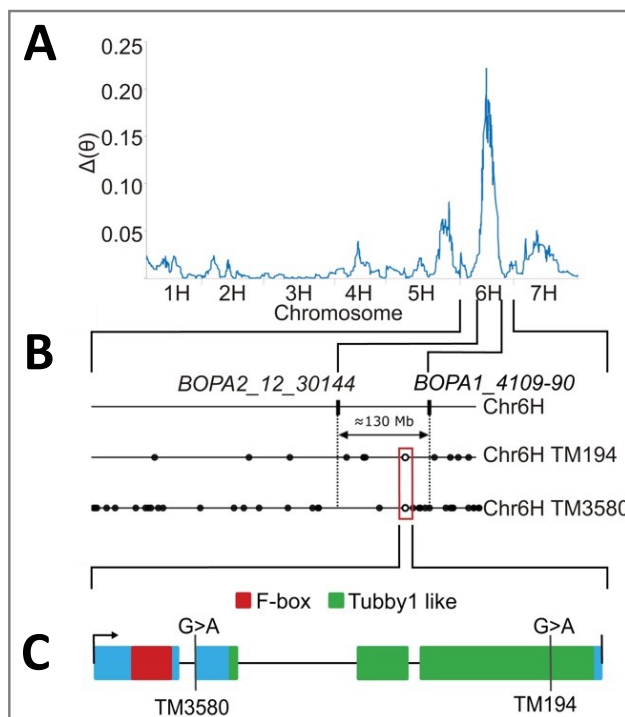


Figure 12. Mapping and cloning of *egt1*. (A) SNP-based BSA from F₂ plants from TM194 × cv. Barke. The $\Delta\theta$ parameter represents the difference in allele frequency for each tested SNP. (B) Schematic representing a region spanning ~130 Mb on chromosome 6H between markers BOPA2_12_30144 and BOPA1_4109-90. Filled circles indicate all SNPs within genes present in this region while empty circles (in red rectangle) indicate SNPs within pinpointed *HORVU6Hr1G068970* gene, in the two allelic lines TM194 and TM3580. (C) Mutational landscape of *EGT1* in relation to the F-box domain (red) and the Tubby-like protein domains (green).

3.7 *EGT2* encodes a SAM Domain–Containing Protein

BSA on the F₂ population from TM2835 × Barke mapped a 312 Mbp interval on the short arm of chromosome 5H (Figure 13A) between markers SCRI_RS_222345 and SCRI_RS_13395. Subsequently, TM2835 was subject to whole genome sequencing, which led to the identification of seven genes within the previous interval and which carried missense, splice site, or stop-codon gain mutations when compared with wild-type Morex sequence. Among these, was a gene encoding for a 252 amino acid SAM domain–containing protein *HORVU5Hr1G027890* or *HORVU.MOREX.r2.5HG0370880.1* with a mutation (G447A) leading to a premature stop codon at the beginning of the functional domain (W149*) (Figure 13B and 14B).

To validate *HORVU.MOREX.r2.5HG0370880.1* as *EGT2*, we used CRISPR/Cas9 to create an additional mutant allele (*egt2-2*) in the barley cv. Golden Promise. We targeted two sites in the 5' untranslated region (5' UTR) and exon 1, separated by 196 bp, and recovered a 215 bp deletion including the start codon, leading to the translation of a truncated protein (Figure 13B and 14A). We analyzed the root phenotype of the homozygous T₁ line and determined a significantly higher root angle of both seminal and lateral roots in the mutant in comparison to the wild type (Figure 13C-E). Hence, we confirmed that the altered root angle phenotype of *egt2-2* is caused by a truncation of *HORVU.MOREX.r2.5HG0370880.1*. Like in the *egt2-1* mutant in Morex background, the root length of *egt2-2* was similar to the wild type (Figure 15A). The reaction of the *egt2-2* roots after rotation was faster than in the wild type but not statistically significant (Figure 15C). It is notable that Golden Promise and Morex differ in seminal root angle growth although they both carry a wild-type *EGT2* allele (compare Figures 6A and 7A with 13C-D). Additionally, the reorientation of the roots after rotation occurs much faster in wild-type Golden Promise than in Morex (compare Figures 11B and 15C). Thus, other genetic factors influence the root growth angle in addition to *EGT2*.

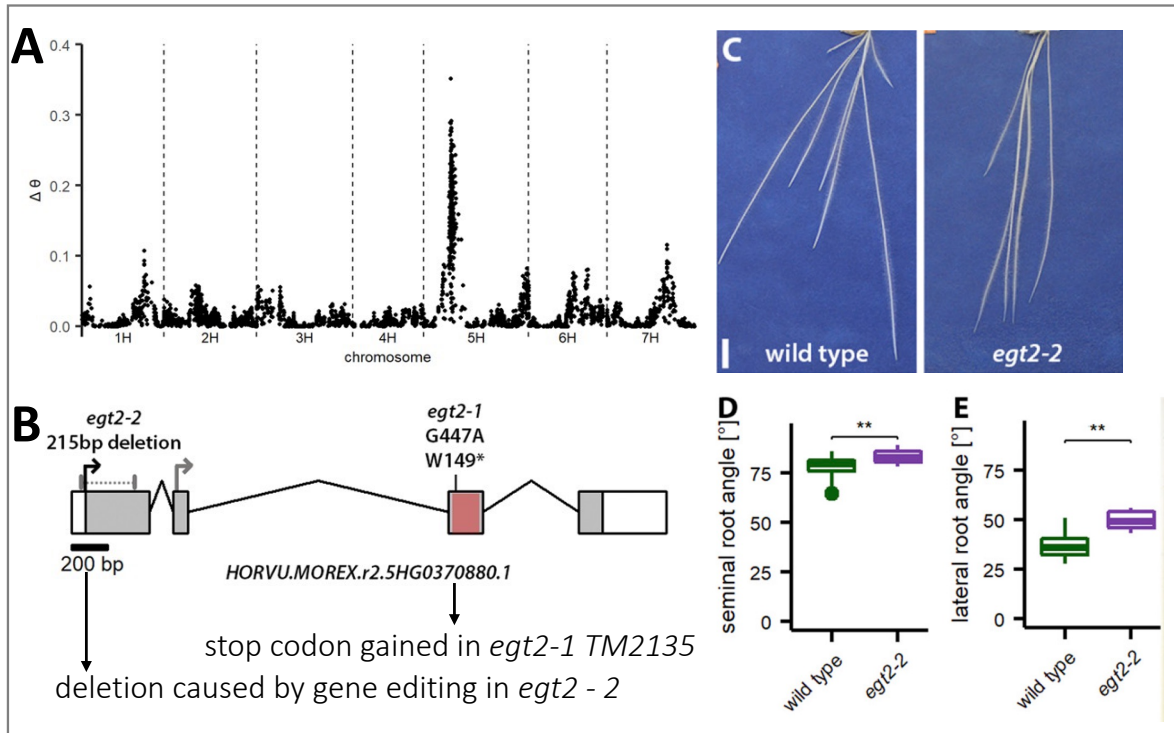


Figure 13. Mapping and cloning of *egt2*. (A) SNP-based BSA from F₂ plants from TM2835 cv. Barke. The $\Delta\theta$ parameter represents the difference in allele frequency for each tested SNP (B) Gene structure of *EGT2* (*HORVU.MOREX.r2.5HG0370880.1*) with mutations in *egt2* (*egt2-1*: G to A transition and *egt2-2*: deletion); translational start site in wild type is shown as a black arrow and start site in the *egt2-2* mutant as a gray arrow; exons are depicted as a gray box, introns as lines, and UTRs as white boxes. The red box indicates the sequence encoding for the SAM domain (C) Exemplary pictures of wild type (cv. Golden Promise) and mutant *egt2-2* roots 7 DAG (Scale bar: 2 cm) (D) Seminal root angle of wild-type (cv. Golden Promise) and mutant *egt2-2* 7 DAG; n = 15 to 17 in two independent experiments. (E) Root angle of lateral roots 14 DAG; n = 16 to 18 in two independent experiments; t-test, * $p < 0.05$, ** < 0.01 .

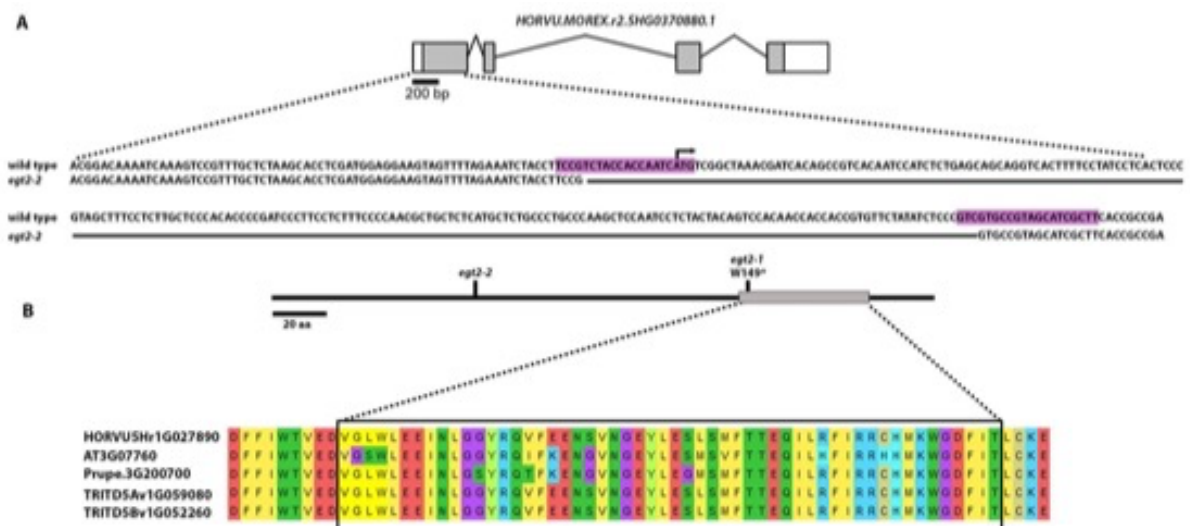


Figure 14. CRISPR/Cas9 induced mutation in *EGT2* and conserved function in wheat (A) Gene model of *EGT2* and partial DNA sequence; arrow marks translation start site; purple boxes mark the CRISPR target sites; in the *egt2-2* mutant line, CRISPR/Cas induced a deletion between the target sites as depicted. (B) Protein structure of *EGT2* with the SAM domain from amino acid 172 - 225; protein alignment of *EGT2*, *AtSAM5* (*At3g07760*) and peach *WEEP* (*Prupe. 3G200700*) in the SAM region.

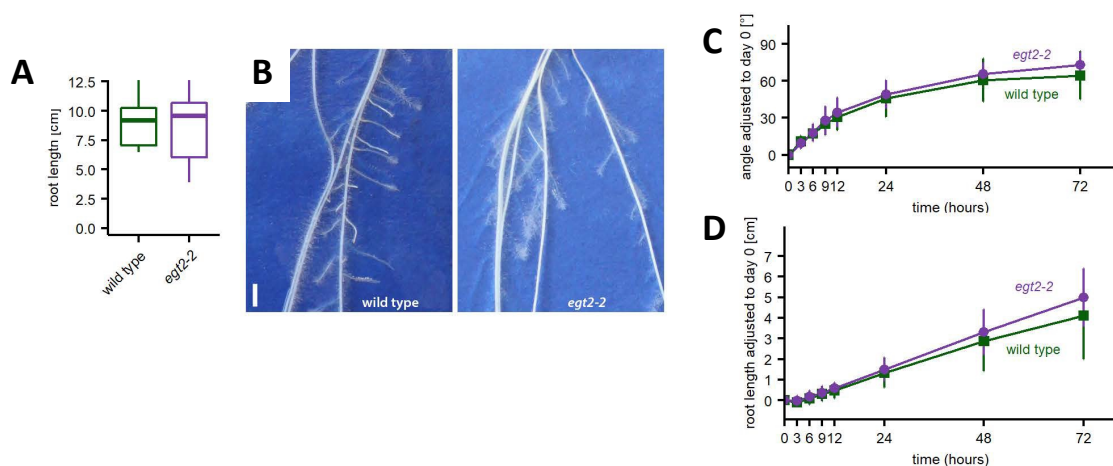


Figure 15. CRISPR/Cas9 *egt2-2* root characterization. (A) Root length 7 DAG, two-tailed t-test does not show a significant difference ($p < 0.05$); $n = 15-17$ in two independent experiments. (B) Wild type GP and *egt2-2* lateral roots 14 DAG. Scale bar 1 cm. (C) Root tip angle after rotation: plants at 5 DAG were rotated by 90° (time 0) and the root tip angle was measured over time; $n = 20$ per genotype in two independent experiments; the two genotypes were compared between each other at the respective time points by a two-tailed t-test and no significant difference was detected; standard deviation is depicted; to account for the

different starting angles of the roots, all measurements were normalized to the starting angle of the roots at time 0. (D) Root length after rotation as described in (C); $n = 20$ per genotype in two independent experiments.

3.8 *egt1* is involved in the adaptation of root growth angle to the environment

To know whether nucleotide polymorphisms within *EGT1* or *EGT2* could provide a source of natural variation in root growth angle in barley diversity panels, we exploited the barley exome sequences of WHEALBI, a large germplasm collection (Bustos-Korts et al., 2019). With haplotype network analysis of nucleotide sequence variation within the *EGT1* coding sequence, we identified two haplotypes (II and IV) carrying missense substitutions and four other haplotypes carrying synonymous substitutions (I, III, V, and VI) (Figure 16A). Based on this result, we phenotyped barley accessions carrying haplotypes II ($n = 86$) and IV ($n = 25$) using the 2D screens. Accessions carrying haplotype II exhibited significantly steeper seminal root angle distribution than accessions carrying haplotype IV (50.9 ± 14.8 vs. 64.3 ± 17.6 , median \pm SD degree angle, respectively; $P < 0.001$) (Figure 16B). For *EGT2*, on the contrary, we did not find any variant in WHEALBI.

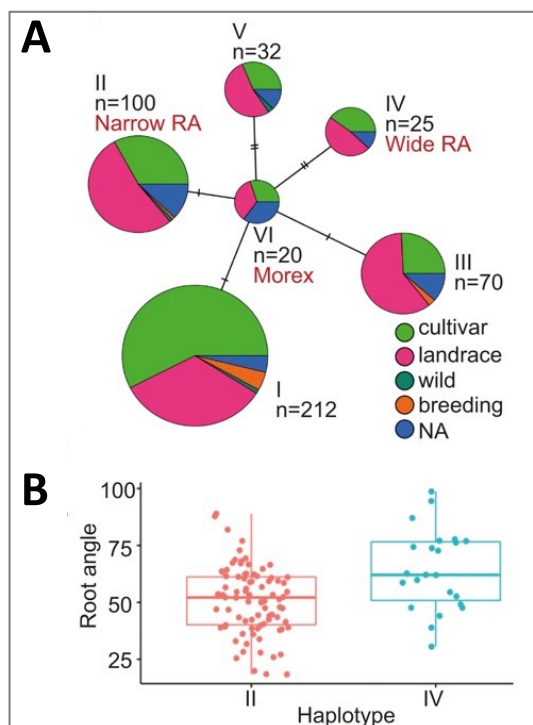


Figure 16. Haplotype network analysis of *EGT1* in the WHEALBI barley germplasm collection. (A) Six haplotypes are found, II and IV carry missense substitutions, while the remaining four haplotypes carry synonymous substitutions. n indicates number of genotypes

within each class. (B) Root growth angle distribution of WHEALBI barley lines in haplotype II (86 lines) and IV (25 lines), their average root growth angle is different (t-test, $p < 0.001$).

3.9 *EGT1* and *EGT2* functions are conserved in durum wheat

To address *EGT1* and *EGT2* functions in wheat, we screened in silico a TILLING population of tetraploid (AA BB) wheat cv. Kronos (Krasileva et al., 2017). Kronos2551 and Kronos3926 lines encoded premature termination codons in *TRITD6Bv1G159700* (*HvEGT1* homeologous gene on wheat B genome) and the Kronos2708 line carrying a splice donor mutation in *TRITD6Av1G172130* (*HvEGT1* homeologous gene on wheat A genome).

Kronos2551 × Kronos2708 and Kronos3926 × Kronos2708 were crossed, then F₁ plants were self-pollinated to obtain F₂ plants. Progenies of selected wild-type and homozygous double mutants from two independent crosses were grown for 7 days in rhizoboxes for root growth angle analysis. Both the double mutants exhibited steeper seminal and lateral root growth angle compared with the progenies carrying wild-type alleles in both homeologs as well as homozygous mutations in just one homeolog (Figure 17). Hence, our results revealed that *TdEGT1* loci also controls root growth angle in wheat.

Tdegt2 mutants were identified in the same population. Two selected lines (Kronos2138 and Kronos3589) carrying premature termination codons in the two *EGT2* homeologous coding sequences (*TraesCS5A01G102000* and *TraesCS5B02G164200LC*) were crossed, F₁ plants self-pollinated and progenies of selected wild-type and double mutant F₂ individuals derived from two independent initial crosses were grown in rhizoboxes. These double mutants showed narrower seminal root growth angle in rhizoboxes compared with the sibling lines carrying wild-type alleles in both homeologs (Figure 18). Like barley, the number and length of seminal roots was unaffected in 7-d-old seedlings.

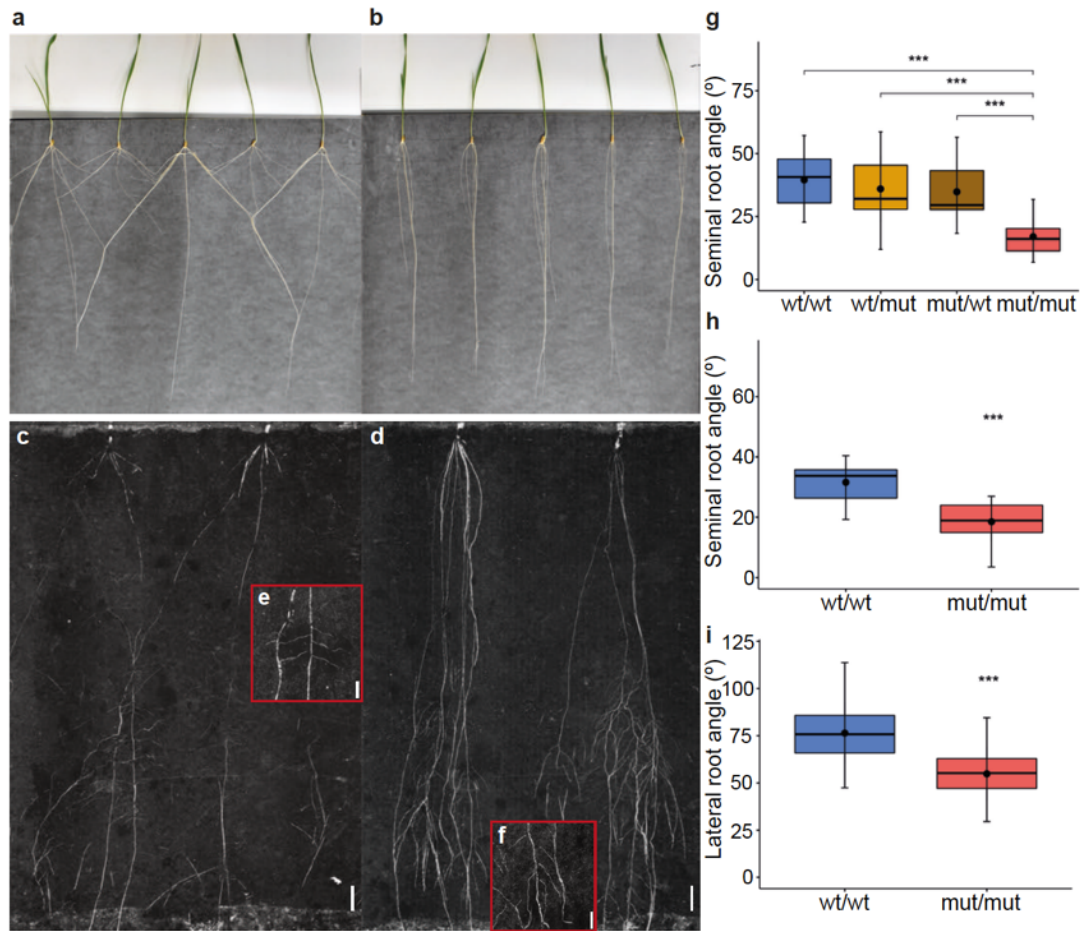


Figure 17. *Tdegt1* roots are hypergravitropic, the gene is conserved in wheat. Representative images showing root growth angle, 8 DAG (a) wildtype *TdEGT1* (wtA/wtB) and (b) homozygous cross of *Tdegt1* mutant (*mutA/mutB*) grown in 2D screens. Scale bar = 2 cm. Representative images of 20-days old (c) wtA/wtB and (d) *mutA/mutB* mutant grown in soil rhizotrons. Scale bar = 2 cm. (e, f) Magnified images of lateral roots from (c) and (d). Scale bar = 1 cm. Quantification of seminal root angle from 8 DAG (g) wtA/wtB, wtA/mutB, mutA/wtB and mutA/mutB, and of 12 DAG (h) and 20 DAG (i) double homozygous. Welch's t-test, $p < 0.001$.

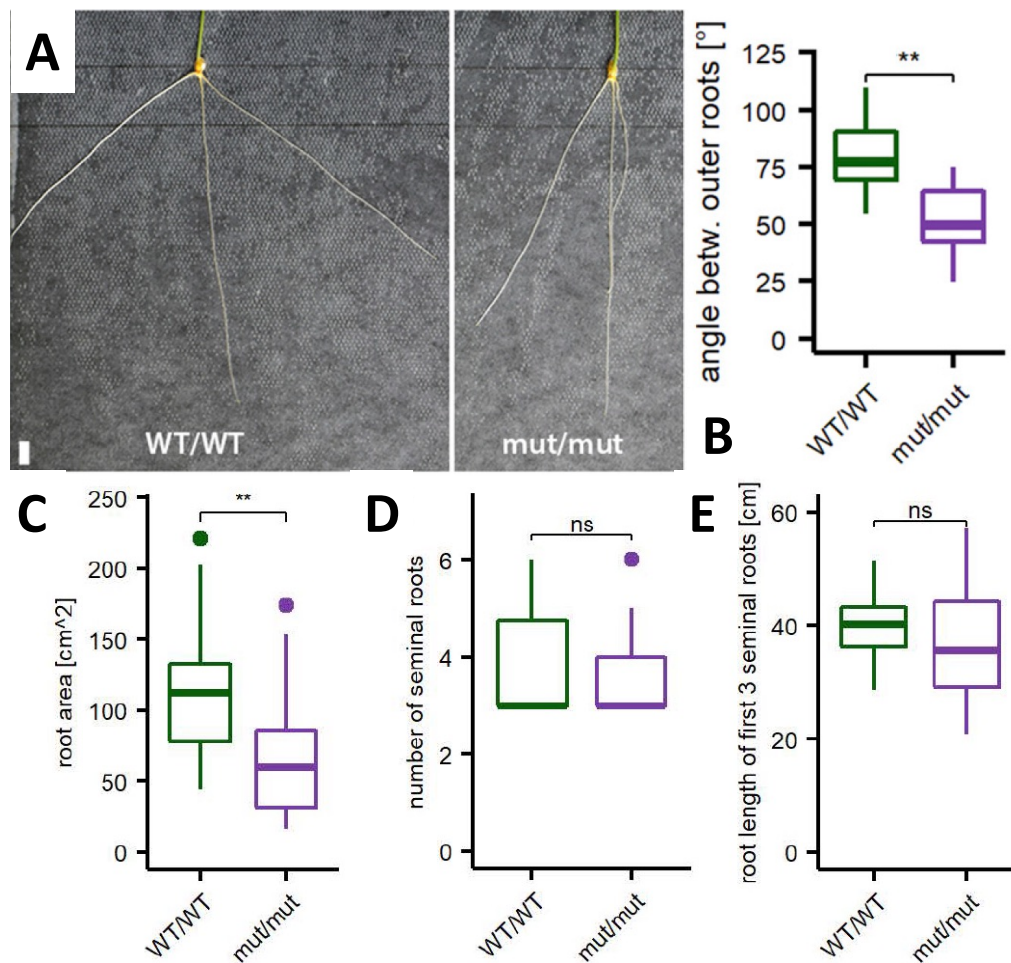


Figure 18. *Tdegt2* roots are hypergravitropic, the gene is conserved in wheat. (A) Representative images of wheat wild-type (WT/WT) and *egt2* (mut/mut) roots, 7 DAG. (Scale bar 1 cm) (B) Root angle between second and third seminal root of wild-type (WT/WT) and *egt2* (mut/mut) wheat seedling at 7 DAG; n = 18 and 39 for wild type and mutant, respectively (C) Area enclosed by the first three seminal root of wild type (WT/WT) and *egt2* (mut/mut) wheat seedling at 7 DAG; n = 16 and 35 for wild type and mutant (D) Number of seminal roots of wild type (WT/WT) and *egt2* (mut/mut) wheat seedling at 7 DAG; n = 18 and 39 for wild type and mutant (E) Length of the first three seminal root in wild type (WT/WT) and *egt2* (mut/mut) wheat seedling at 7DAG; n = 16 and 35 for wild type and mutant. Wheat plants in C, D and E were derived from two independent segregating populations; the two genotypes were compared by a two-tailed t-test (* $p < 0.05$, ns = no significant difference).

4. DISCUSSION

Root angle is a key trait in crops to ensure efficient capture of soil resources. Variation of root growth angle can affect the way roots anchor to and explore different soil layers and capture nutrients and water and thus can influence drought tolerance, as shown for *DRO1* in rice (Uga et al., 2013). Specifically modelling and experimental evidence showed that steeper root angle growth can increase root system depth, thus helping plants in foraging for water and mobile nutrients, such as nitrogen (Lynch, 2019; Uga et al., 2013; Voss-Fels et al., 2018; Wasson et al., 2012). Possible trade-offs are inefficient acquisition of less mobile, superficial nutrients such as phosphate or increased susceptibility to waterlogging and salinity (Kitomi et al., 2020; Lynch, 2019). Steeper root system is also expected to reduce the total volume of soil explored, alter intra- and interplant root competition, and contribute to root lodging, although these effects are strongly interconnected with crop management factors such as seeding rate (Dreccer et al., 2020; Rubio et al., 2001; Uga et al., 2013).

Although recent studies have identified major quantitative trait loci associated with seminal root angle by genome-wide association studies based on phenotyping of different barley genomic populations (Jia et al., 2019; Robinson et al., 2016), knowledge about the underlying genes controlling root angle in barley remains limited. A small number of root angle regulatory genes have been identified in other cereals, including *DRO1* (Uga et al., 2013), *VLN2* (Wu et al., 2015), *PIN2* (Wang et al., 2018), *RMD* (Huang et al., 2018), and *CIPK15* (Schneider et al., 2022).

To address this knowledge gap, we screened TILLMore, a chemically mutagenized population of the cv. Morex (Talamè et al., 2008) for a steeper seminal root phenotype, and we identified the TM194, TM3580 and TM2835 mutants that exhibited steeper growth angle for seminal roots and also for lateral and crown roots. Genetic and genomic approaches revealed that a mutation in the *EGT1* (for TM194 and TM3580) or in the *EGT2* (for TM2835) gene are independently responsible for the steeper root angle phenotype. *EGT1* encodes a Tubby-like protein (TLP) that contains conserved C-terminal Tubby and N-terminal F-box domains (Gagne et al., 2002; Lai et al., 2004). Tubby domain-containing proteins are proposed to act as bipartite transcription regulator (Boggon et al., 1999; Santagata et al., 2001), whereas F-box proteins facilitate protein ubiquitination by acting as bridges between specific substrates and the components of the SCF-type (Skp1-Cullin-F-box) or ECS-type (ElonginC-Cullin-SOCS-box) E3 ubiquitin ligase complexes (Gagne et al.,

2002; Kile et al., 2002). Previous mutant studies in *A. thaliana* have identified that TLPs *AtTLP3* and *AtTLP2* could play roles in regulation of ROS signaling and cell wall related genes, respectively (Reitz et al., 2012; Wang et al., 2019).

EGT2 encodes a Sterile Alpha Motive protein. In animals, SAM domain-containing proteins function as transcription factors, receptors, kinases, or ER proteins (Denay et al., 2017). In plants, the best known protein containing a SAM domain is the transcription factor LEAFY (LFY), which is involved in flower and meristem identity formation. Modeling of *Arabidopsis* SAM proteins based on structure predictions and LFY characterization suggests that the majority of these proteins are able to form head-to-tail homo- or hetero-oligomers/polymers (Denay et al., 2017). The close phylogenetic relationship of *EGT2* with *AtSAM5* (*At3g07760*) indicates a similar potential of oligomerization for *EGT2*. *EGT2* is also closely related to *WEEP*, a SAM domain containing protein that was discovered because of the prominent shoot phenotype in peach tree mutants (Hollender et al., 2018). Peach trees with deletions in *WEEP* show a weeping shoot growth phenotype; thus, the branches grow in a wider angle, and after gravistimulation by rotation by 90°, the branches do not orient their growth upward again (Hollender et al., 2018). Therefore, *EGT2* and *WEEP* are likely involved in a similar pathway that regulates gravitropism, but in different plant organs. Bud grafting experiments in peach implied that *WEEP* encodes an autonomous determinant of shoot orientation for each branch and that no mobile signals from other parts of the plants (like phytohormones) are necessary (Hollender et al., 2018). Furthermore, no difference of auxin or abscisic acid concentration was detected in growing shoots between peach wild-type and *WEEP* mutants, nor were genes associated with auxin biosynthesis or perception differentially expressed (Hollender et al., 2018).

Both *EGT1* and *EGT2* are conserved in durum wheat.

Could new crop varieties with altered root angle be selected using *EGT1* or *EGT2*? Loss of function *egt* alleles exhibit very steep angles for all root classes, likely causing them to inefficiently compete for resource capture. However, results from haplotype analysis appear more promising since nucleotide polymorphisms within the *HvEGT1* sequence were observed to determine natural variation in root growth angle in a barley diversity panel. For *EGT2*, on the contrary, we did not find natural variation, suggesting it could belong to an evolutionary conserved mechanism of seminal and lateral root growth angle in barley and wheat.

Selecting or engineering *EGT1* and *EGT2* alleles to adapt cultivars for specific environmental conditions, such as different soil types or variable water table depth, would appear possible.

Further studies are planned to introgress *egt1* and *egt2* into elite barley and wheat varieties and to test their performance in the field, under different water and nutrients conditions.

5. REFERENCES

- Alqudah, A. M., & Schnurbusch, T. (2015). Barley leaf area and leaf growth rates are maximized during the pre-anthesis phase. *Agronomy*, 5(2), 107-129.
- Alqudah, A. M., Youssef, H. M., Graner, A., & Schnurbusch, T. (2018). Natural variation and genetic make-up of leaf blade area in spring barley. *Theoretical and Applied Genetics*, 131(4), 873-886. <https://doi.org/10.1007/s00122-018-3053-2>
- Anten, N. P., & Chen, B. J. (2021). Detect thy family: mechanisms, ecology and agricultural aspects of kin recognition in plants. *Plant, Cell & Environment*, 44(4), 1059-1071.
- Ashraf, A., Rehman, O. U., Muzammil, S., Léon, J., Naz, A. A., Rasool, F., . . . Khan, M. R. (2019). Evolution of Deeper Rooting 1-like homoeologs in wheat entails the C-terminus mutations as well as gain and loss of auxin response elements. *PLoS One*, 14(4), e0214145.
- Balzerque, C., Darteville, T., Godon, C., Laugier, E., Meisrimler, C., Teulon, J.-M., . . . Desnos, T. (2017). Low phosphate activates STOP1-ALMT1 to rapidly inhibit root cell elongation. *Nature Communications*, 8(1), 15300. <https://doi.org/10.1038/ncomms15300>
- Berdahl, J. D., Rasmusson, D. C., & Moss, D. N. (1972). Effects of Leaf Area on Photosynthetic Rate, Light Penetration, and Grain Yield in Barley1. *Crop Science*, 12(2), crops1972.0011183X001200020006x. <https://doi.org/https://doi.org/10.2135/crops1972.0011183X001200020006x>
- Blum, A. (2005). Drought resistance, water-use efficiency, and yield potential—are they compatible, dissonant, or mutually exclusive? *Australian Journal of Agricultural Research*, 56(11), 1159-1168.
- Boggon, T. J., Shan, W.-S., Santagata, S., Myers, S. C., & Shapiro, L. (1999). Implication of tubby proteins as transcription factors by structure-based functional analysis. *Science*, 286(5447), 2119-2125.
- Bray, A. L., & Topp, C. N. (2018). The Quantitative Genetic Control of Root Architecture in Maize. *Plant and Cell Physiology*, 59(10), 1919-1930. <https://doi.org/10.1093/pcp/pcy141>
- Bustos-Korts, D., Dawson, I. K., Russell, J., Tondelli, A., Guerra, D., Ferrandi, C., . . . van Eeuwijk, F. A. (2019). Exome sequences and multi-environment field trials elucidate the genetic basis of adaptation in barley. *The Plant Journal*, 99(6), 1172-1191. <https://doi.org/https://doi.org/10.1111/tpj.14414>
- Caine, R. S., Yin, X., Sloan, J., Harrison, E. L., Mohammed, U., Fulton, T., . . . Coe, R. A. (2019). Rice with reduced stomatal density conserves water and has improved drought tolerance under future climate conditions. *New Phytologist*, 221(1), 371-384.
- Chimungu, J. G., Maliro, M. F. A., Nalivata, P. C., Kanyama-Phiri, G., Brown, K. M., & Lynch, J. P. (2015). Utility of root cortical aerenchyma under water limited conditions in tropical maize (*Zea mays* L.). *Field Crops Research*, 171, 86-98. <https://doi.org/https://doi.org/10.1016/j.fcr.2014.10.009>
- Cingolani, P., Platts, A., Wang, I. L., Coon, M., Nguyen, T., Wang, L., . . . Ruden, D. M. (2012). A program for annotating and predicting the effects of single nucleotide polymorphisms, SnpEff: SNPs in the genome of *Drosophila melanogaster* strain w1118; iso-2; iso-3. *Fly (Austin)*, 6(2), 80-92. <https://doi.org/10.4161/fly.19695>
- Clement, M., Snell, Q., Walker, P., Posada, D., & Crandall, K. (2002). TCS: Estimating gene genealogies. *Parallel and Distributed Processing Symposium, International Proceedings*, 2, 184.

- Colmsee, C., Beier, S., Himmelbach, A., Schmutzer, T., Stein, N., Scholz, U., & Mascher, M. (2015). BARLEX—the barley draft genome explorer. *Molecular Plant*, *8*(6), 964-966.
- Danecek, P., Bonfield, J. K., Liddle, J., Marshall, J., Ohan, V., Pollard, M. O., . . . Davies, R. M. (2021). Twelve years of SAMtools and BCFtools. *Gigascience*, *10*(2), giab008.
- Denay, G., Vachon, G., Dumas, R., Zubieta, C., & Parcy, F. (2017). Plant SAM-domain proteins start to reveal their roles. *Trends in Plant Science*, *22*(8), 718-725.
- Digel, B., Tavakol, E., Verderio, G., Tondelli, A., Xu, X., Cattivelli, L., . . . von Korff, M. (2016). Photoperiod-H1 (Ppd-H1) Controls Leaf Size. *Plant Physiology*, *172*(1), 405-415. <https://doi.org/10.1104/pp.16.00977>
- Dowle, M., & Srinivasan, A. (2021). Data. table: Extension of ‘data. frame’[Manual]. In.
- Dreccer, M. F., Condon, A. G., Macdonald, B., Rebetzke, G. J., Awasi, M.-A., Borgognone, M. G., . . . Jackway, P. (2020). Genotypic variation for lodging tolerance in spring wheat: Wider and deeper root plates, a feature of low lodging, high yielding germplasm. *Field Crops Research*, *258*, 107942.
- Du, B., Liu, L., Wang, Q., Sun, G., Ren, X., Li, C., & Sun, D. (2019). Identification of QTL underlying the leaf length and area of different leaves in barley. *Scientific Reports*, *9*(1), 4431. <https://doi.org/10.1038/s41598-019-40703-6>
- Fekih, R., Takagi, H., Tamiru, M., Abe, A., Natsume, S., Yaegashi, H., . . . Matsumura, H. (2013). MutMap+: genetic mapping and mutant identification without crossing in rice. *PLoS one*, *8*(7), e68529.
- Furutani, M., & Morita, M. T. (2021). LAZY1-LIKE-mediated gravity signaling pathway in root gravitropic set-point angle control. *Plant Physiology*, *187*(3), 1087-1095. <https://doi.org/10.1093/plphys/kiab219>
- Fusi, R., Rosignoli, S., Lou, H., Sangiorgi, G., Bovina, R., Pattem, J. K., . . . Milner, S. G. (2022). Root angle is controlled by EGT1 in cereal crops employing an antigravitropic mechanism. *Proceedings of the National Academy of Sciences*, *119*(31), e2201350119.
- Gagne, J. M., Downes, B. P., Shiu, S.-H., Durski, A. M., & Vierstra, R. D. (2002). The F-box subunit of the SCF E3 complex is encoded by a diverse superfamily of genes in Arabidopsis. *Proceedings of the national academy of sciences*, *99*(17), 11519-11524.
- Gajek, K., Janiak, A., Korotko, U., Chmielewska, B., Marzec, M., & Szarejko, I. (2021). Whole Exome Sequencing-Based Identification of a Novel Gene Involved in Root Hair Development in Barley (*Hordeum vulgare* L.). *International Journal of Molecular Sciences*, *22*(24), 13411.
- Gajewska, P., Janiak, A., Kwasniewski, M., Kędziorski, P., & Szarejko, I. (2018). Forward genetics approach reveals a mutation in bHLH transcription factor-encoding gene as the best candidate for the root hairless phenotype in barley. *Frontiers in plant science*, *9*, 1229.
- Galindo-Castañeda, T., Brown, K. M., Kuldau, G. A., Roth, G. W., Wenner, N. G., Ray, S., . . . Lynch, J. P. (2019). Root cortical anatomy is associated with differential pathogenic and symbiotic fungal colonization in maize. *Plant, Cell & Environment*, *42*(11), 2999-3014. <https://doi.org/https://doi.org/10.1111/pce.13615>
- Galindo-Castañeda, T., Brown, K. M., & Lynch, J. P. (2018). Reduced root cortical burden improves growth and grain yield under low phosphorus availability in maize. *Plant, Cell & Environment*, *41*(7), 1579-1592. <https://doi.org/https://doi.org/10.1111/pce.13197>
- Galvan-Ampudia, Carlos S., Julkowska, Magdalena M., Darwish, E., Gandullo, J., Korver, Ruud A., Brunoud, G., . . . Testerink, C. (2013). Halotropism Is a Response of Plant Roots to Avoid a Saline Environment. *Current Biology*, *23*(20), 2044-2050. <https://doi.org/https://doi.org/10.1016/j.cub.2013.08.042>

- George-Jaeggli, B., Mortlock, M. Y., & Borrell, A. K. (2017). Bigger is not always better: Reducing leaf area helps stay-green sorghum use soil water more slowly. *Environmental and Experimental Botany*, *138*, 119-129. <https://doi.org/https://doi.org/10.1016/j.envexpbot.2017.03.002>
- Guseman, J. M., Webb, K., Srinivasan, C., & Dardick, C. (2017). DRO1 influences root system architecture in Arabidopsis and Prunus species. *The Plant Journal*, *89*(6), 1093-1105. <https://doi.org/https://doi.org/10.1111/tpj.13470>
- Haefele, S. M., Johnson, D. E., M'Bodj, D., Wopereis, M. C. S., & Miezán, K. M. (2004). Field screening of diverse rice genotypes for weed competitiveness in irrigated lowland ecosystems. *Field Crops Research*, *88*(1), 39-56. <https://doi.org/https://doi.org/10.1016/j.fcr.2003.11.010>
- Hetz, W., Hochholdinger, F., Schwall, M., & Feix, G. (1996). Isolation and characterization of rctcs, a maize mutant deficient in the formation of nodal roots. *The Plant Journal*, *10*(5), 845-857.
- Hibara, K.-i., Miya, M., Benvenuto, S. A., Hibara-Matsuo, N., Mimura, M., Yoshikawa, T., . . . Itoh, J.-i. (2021). Regulation of the plastochron by three many-noded dwarf genes in barley. *PLoS genetics*, *17*(5), e1009292.
- Hochholdinger, F., Yu, P., & Marcon, C. (2018). Genetic Control of Root System Development in Maize. *Trends in Plant Science*, *23*(1), 79-88. <https://doi.org/https://doi.org/10.1016/j.tplants.2017.10.004>
- Hollender, C. A., Pascal, T., Tabb, A., Hadiarto, T., Srinivasan, C., Wang, W., . . . Dardick, C. (2018). Loss of a highly conserved sterile alpha motif domain gene (WEEP) results in pendulous branch growth in peach trees. *Proceedings of the National Academy of Sciences*, *115*(20), E4690-E4699.
- Hu, J., Wang, X., Zhang, G., Jiang, P., Chen, W., Hao, Y., . . . Wang, H. (2020). QTL mapping for yield-related traits in wheat based on four RIL populations. *Theoretical and Applied Genetics*, *133*(3), 917-933. <https://doi.org/10.1007/s00122-019-03515-w>
- Huang, G., Liang, W., Sturrock, C. J., Pandey, B. K., Giri, J., Mairhofer, S., . . . Zhang, D. (2018). Rice actin binding protein RMD controls crown root angle in response to external phosphate. *Nature Communications*, *9*(1), 2346. <https://doi.org/10.1038/s41467-018-04710-x>
- Huang, G., & Zhang, D. (2020). The plasticity of root systems in response to external phosphate. *International Journal of Molecular Sciences*, *21*(17), 5955.
- Hughes, J., Hepworth, C., Dutton, C., Dunn, J. A., Hunt, L., Stephens, J., . . . Gray, J. E. (2017). Reducing Stomatal Density in Barley Improves Drought Tolerance without Impacting on Yield. *Plant Physiology*, *174*(2), 776-787. <https://doi.org/10.1104/pp.16.01844>
- Hunter, R. (1980). Increased Leaf Area (Source) and Yield of Maize in Short-season Areas 1. *Crop science*, *20*(5), 571-574.
- Imani, J., Li, L., Schaefer, P., & Kogel, K. H. (2011). STARTS—A stable root transformation system for rapid functional analyses of proteins of the monocot model plant barley. *The Plant Journal*, *67*(4), 726-735.
- Inukai, Y., Sakamoto, T., Morinaka, Y., Miwa, M., Kojima, M., Tanimoto, E., . . . Kitano, H. (2012). ROOT GROWTH INHIBITING, a Rice Endo-1,4-β-d-Glucanase, Regulates Cell Wall Loosening and is Essential for Root Elongation. *Journal of Plant Growth Regulation*, *31*(3), 373-381. <https://doi.org/10.1007/s00344-011-9247-3>
- Jia, Z., Liu, Y., Gruber, B. D., Neumann, K., Kilian, B., Graner, A., & von Wirén, N. (2019). Genetic Dissection of Root System Architectural Traits in Spring Barley. *Front Plant Sci*, *10*, 400. <https://doi.org/10.3389/fpls.2019.00400>

- Jöst, M., Hensel, G., Kappel, C., Druka, A., Sicard, A., Hohmann, U., . . . Lenhard, M. (2016). The INDETERMINATE DOMAIN Protein BROAD LEAF1 Limits Barley Leaf Width by Restricting Lateral Proliferation. *Curr Biol*, 26(7), 903-909. <https://doi.org/10.1016/j.cub.2016.01.047>
- Kawa, D., & Brady, S. M. (2022). Root cell types as an interface for biotic interactions. *Trends in Plant Science*, 27(11), 1173-1186. <https://doi.org/https://doi.org/10.1016/j.tplants.2022.06.003>
- Kile, B. T., Schulman, B. A., Alexander, W. S., Nicola, N. A., Martin, H. M., & Hilton, D. J. (2002). The SOCS box: a tale of destruction and degradation. *Trends in biochemical sciences*, 27(5), 235-241.
- Kirschner, G. K., Stahl, Y., Von Korff, M., & Simon, R. (2017). Unique and conserved features of the barley root meristem. *Frontiers in plant science*, 8, 1240.
- Kitomi, Y., Hanzawa, E., Kuya, N., Inoue, H., Hara, N., Kawai, S., . . . Uga, Y. (2020). Root angle modifications by the *DRO1* homolog improve rice yields in saline paddy fields. *Proceedings of the National Academy of Sciences*, 117(35), 21242-21250. <https://doi.org/doi:10.1073/pnas.2005911117>
- Klein, H., Xiao, Y., Conklin, P. A., Govindarajulu, R., Kelly, J. A., Scanlon, M. J., . . . Bartlett, M. (2018). Bulk-Segregant Analysis Coupled to Whole Genome Sequencing (BSA-Seq) for Rapid Gene Cloning in Maize. *G3 (Bethesda)*, 8(11), 3583-3592. <https://doi.org/10.1534/g3.118.200499>
- Knipfer, T., & Fricke, W. (2010). Water uptake by seminal and adventitious roots in relation to whole-plant water flow in barley (*Hordeum vulgare* L.). *Journal of Experimental Botany*, 62(2), 717-733. <https://doi.org/10.1093/jxb/erq312>
- Konstantinova, N., Korbei, B., & Luschnig, C. (2021). Auxin and root gravitropism: addressing basic cellular processes by exploiting a defined growth response. *International Journal of Molecular Sciences*, 22(5), 2749.
- Krasileva, K. V., Vasquez-Gross, H. A., Howell, T., Bailey, P., Paraiso, F., Clissold, L., . . . Dubcovsky, J. (2017). Uncovering hidden variation in polyploid wheat. *Proc Natl Acad Sci U S A*, 114(6), E913-E921. <https://doi.org/10.1073/pnas.1619268114>
- Kreszies, T., Eggels, S., Kreszies, V., Osthoff, A., Shellakkutti, N., Baldauf, J. A., . . . Schreiber, L. (2020). Seminal roots of wild and cultivated barley differentially respond to osmotic stress in gene expression, suberization, and hydraulic conductivity. *Plant, Cell & Environment*, 43(2), 344-357. <https://doi.org/https://doi.org/10.1111/pce.13675>
- Kumar, N., Galli, M., Ordon, J., Stuttmann, J., Kogel, K. H., & Imani, J. (2018). Further analysis of barley MORC 1 using a highly efficient RNA-guided Cas9 gene-editing system. *Plant biotechnology journal*, 16(11), 1892-1903.
- Kumar, S., Stecher, G., Li, M., Knyaz, C., & Tamura, K. (2018). MEGA X: molecular evolutionary genetics analysis across computing platforms. *Molecular biology and evolution*, 35(6), 1547-1549.
- Kurata, N., Miyoshi, K., Nonomura, K.-I., Yamazaki, Y., & Ito, Y. (2005). Rice mutants and genes related to organ development, morphogenesis and physiological traits. *Plant and cell physiology*, 46(1), 48-62.
- Kurata, N., & Yamazaki, Y. (2006). Oryzabase. An Integrated Biological and Genome Information Database for Rice. *Plant Physiology*, 140(1), 12-17. <https://doi.org/10.1104/pp.105.063008>
- Lai, C.-P., Lee, C.-L., Chen, P.-H., Wu, S.-H., Yang, C.-C., & Shaw, J.-F. (2004). Molecular analyses of the Arabidopsis TUBBY-like protein gene family. *Plant Physiology*, 134(4), 1586-1597.

- Lazo, G. R., Stein, P. A., & Ludwig, R. A. (1991). A DNA transformation-competent Arabidopsis genomic library in Agrobacterium. *Bio/technology*, 9(10), 963-967.
- Lee, D.-K., Jung, H., Jang, G., Jeong, J. S., Kim, Y. S., Ha, S.-H., . . . Kim, J.-K. (2016). Overexpression of the OsERF71 Transcription Factor Alters Rice Root Structure and Drought Resistance. *Plant Physiology*, 172(1), 575-588. <https://doi.org/10.1104/pp.16.00379>
- Li, H., & Durbin, R. (2009). Fast and accurate short read alignment with Burrows-Wheeler transform. *Bioinformatics*, 25(14), 1754-1760. <https://doi.org/10.1093/bioinformatics/btp324>
- Li, H., Handsaker, B., Wysoker, A., Fennell, T., Ruan, J., Homer, N., . . . Subgroup, G. P. D. P. (2009). The Sequence Alignment/Map format and SAMtools. *Bioinformatics*, 25(16), 2078-2079. <https://doi.org/10.1093/bioinformatics/btp352>
- Li, S., Zhao, Q., Zhu, D., & Yu, J. (2018). A DREB-like transcription factor from maize (*Zea mays*), ZmDREB4. 1, plays a negative role in plant growth and development. *Frontiers in plant science*, 9, 395.
- Li, W., Yang, Z., Yao, J., Li, J., Song, W., & Yang, X. (2018). Cellulose synthase-like D1 controls organ size in maize. *BMC Plant Biology*, 18(1), 239. <https://doi.org/10.1186/s12870-018-1453-8>
- Liu, J., Zhang, F., Zhou, J., Chen, F., Wang, B., & Xie, X. (2012). Phytochrome B control of total leaf area and stomatal density affects drought tolerance in rice. *Plant Molecular Biology*, 78(3), 289-300. <https://doi.org/10.1007/s11103-011-9860-3>
- Liu, K., Xu, H., Liu, G., Guan, P., Zhou, X., Peng, H., . . . Du, J. (2018). QTL mapping of flag leaf-related traits in wheat (*Triticum aestivum* L.). *Theoretical and Applied Genetics*, 131(4), 839-849. <https://doi.org/10.1007/s00122-017-3040-z>
- Liu, L., Sun, G., Ren, X., Li, C., & Sun, D. (2015). Identification of QTL underlying physiological and morphological traits of flag leaf in barley. *BMC Genetics*, 16(1), 29. <https://doi.org/10.1186/s12863-015-0187-y>
- Lucas, M., Swarup, R., Paponov, I. A., Swarup, K., Casimiro, I., Lake, D., . . . Bennett, M. J. (2010). SHORT-ROOT Regulates Primary, Lateral, and Adventitious Root Development in Arabidopsis. *Plant Physiology*, 155(1), 384-398. <https://doi.org/10.1104/pp.110.165126>
- Lynch, J. P. (2019). Root phenotypes for improved nutrient capture: an underexploited opportunity for global agriculture. *New phytologist*, 223(2), 548-564.
- Lynch, J. P. (2022). Harnessing root architecture to address global challenges. *The Plant Journal*, 109(2), 415-431. <https://doi.org/https://doi.org/10.1111/tpj.15560>
- Lynch, J. P., Strock, C. F., Schneider, H. M., Sidhu, J. S., Ajmera, I., Galindo-Castañeda, T., . . . Hanlon, M. T. (2021). Root anatomy and soil resource capture. *Plant and Soil*, 466(1), 21-63.
- Ma, J., Tu, Y., Zhu, J., Luo, W., Liu, H., Li, C., . . . Lan, X. (2020). Flag leaf size and posture of bread wheat: genetic dissection, QTL validation and their relationships with yield-related traits. *Theoretical and Applied Genetics*, 133(1), 297-315. <https://doi.org/10.1007/s00122-019-03458-2>
- Maddison, D. R., Swofford, D. L., & Maddison, W. P. (1997). NEXUS: an extensible file format for systematic information. *Systematic biology*, 46(4), 590-621.
- Makhtoum, S., Sabouri, H., Gholizadeh, A., Ahangar, L., Katouzi, M., & Mastinu, A. (2022). Mapping of QTLs controlling barley agronomic traits (*Hordeum vulgare* L.) under normal conditions and drought and salinity stress at reproductive stage. *Plant Gene*, 31, 100375. <https://doi.org/https://doi.org/10.1016/j.plgene.2022.100375>

- Maqbool, S., Hassan, M. A., Xia, X., York, L. M., Rasheed, A., & He, Z. (2022). Root system architecture in cereals: progress, challenges and perspective. *The Plant Journal*, *110*(1), 23-42.
- Marin, M., Feeney, D., Brown, L., Naveed, M., Ruiz, S., Koebernick, N., . . . Puértolas, J. (2021). Significance of root hairs for plant performance under contrasting field conditions and water deficit. *Annals of Botany*, *128*(1), 1-16.
- Mascher, M., Gundlach, H., Himmelbach, A., Beier, S., Twardziok, S. O., Wicker, T., . . . Stein, N. (2017). A chromosome conformation capture ordered sequence of the barley genome. *Nature*, *544*(7651), 427-433. <https://doi.org/10.1038/nature22043>
- Mascher, M., Wicker, T., Jenkins, J., Plott, C., Lux, T., Koh, C. S., . . . Stein, N. (2021). Long-read sequence assembly: a technical evaluation in barley. *The Plant Cell*. <https://doi.org/10.1093/plcell/koab077>
- Meng, F., Xiang, D., Zhu, J., Li, Y., & Mao, C. (2019). Molecular Mechanisms of Root Development in Rice. *Rice*, *12*(1), 1. <https://doi.org/10.1186/s12284-018-0262-x>
- Molina, A., Miedes, E., Bacete, L., Rodríguez, T., Mérida, H., Denancé, N., . . . Freydier, A. (2021). Arabidopsis cell wall composition determines disease resistance specificity and fitness. *Proceedings of the National Academy of Sciences*, *118*(5), e2010243118.
- Monat, C., Padmarasu, S., Lux, T., Wicker, T., Gundlach, H., Himmelbach, A., . . . Mascher, M. (2019). TRITEX: chromosome-scale sequence assembly of Triticeae genomes with open-source tools. *Genome Biol*, *20*(1), 284. <https://doi.org/10.1186/s13059-019-1899-5>
- Morris, E. C., Griffiths, M., Golebiowska, A., Mairhofer, S., Burr-Hersey, J., Goh, T., . . . Bennett, M. J. (2017). Shaping 3D Root System Architecture. *Current Biology*, *27*(17), R919-R930. <https://doi.org/https://doi.org/10.1016/j.cub.2017.06.043>
- Nagel, K., Putz, A., Gilmer, F., Heinz, K., Fischbach, A., Pfeifer, J., . . . Schurr, U. (2012). GROWSCREEN-Rhizo is a novel phenotyping robot enabling simultaneous measurements of root and shoot growth for plants grown in soil-filled rhizotrons [Article]. *Functional Plant Biology*, *39*(10-11), 891-904. <https://doi.org/10.1071/FP12023>
- Nelissen, H., Gonzalez, N., & Inzé, D. (2016). Leaf growth in dicots and monocots: so different yet so alike. *Current Opinion in Plant Biology*, *33*, 72-76. <https://doi.org/https://doi.org/10.1016/j.pbi.2016.06.009>
- Neuffer, M. G., Coe, E. H., & Wessler, S. R. (1997). *Mutants of maize*. Cold Spring Harbor Laboratory Press.
- Osthoff, A., Donà dalle Rose, P., Baldauf, J. A., Piepho, H.-P., & Hochholdinger, F. (2019). Transcriptomic reprogramming of barley seminal roots by combined water deficit and salt stress. *BMC genomics*, *20*(1), 1-14.
- Oyiga, B. C., Palczak, J., Wojciechowski, T., Lynch, J. P., Naz, A. A., Léon, J., & Ballvora, A. (2020). Genetic components of root architecture and anatomy adjustments to water-deficit stress in spring barley. *Plant, Cell & Environment*, *43*(3), 692-711. <https://doi.org/https://doi.org/10.1111/pce.13683>
- Pandey, B. K., Huang, G., Bhosale, R., Hartman, S., Sturrock, C. J., Jose, L., . . . Ljung, K. (2021). Plant roots sense soil compaction through restricted ethylene diffusion. *Science*, *371*(6526), 276-280.
- Paradis, E. (2010). pegas: an R package for population genetics with an integrated-modular approach. *Bioinformatics*, *26*(3), 419-420.
- Petricka, J. J., Winter, C. M., & Benfey, P. N. (2012). Control of Arabidopsis root development. *Annual review of plant biology*, *63*, 563.

- Qi, J., Qian, Q., Bu, Q., Li, S., Chen, Q., Sun, J., . . . Li, X. (2008). Mutation of the rice Narrow leaf1 gene, which encodes a novel protein, affects vein patterning and polar auxin transport. *Plant Physiology*, *147*(4), 1947-1959.
- Reitz, M. U., Bissue, J. K., Zocher, K., Attard, A., Hückelhoven, R., Becker, K., . . . Schäfer, P. (2012). The subcellular localization of Tubby-like proteins and participation in stress signaling and root colonization by the mutualist *Piriformospora indica*. *Plant physiology*, *160*(1), 349-364.
- Robinson, H., Hickey, L., Richard, C., Mace, E., Kelly, A., Borrell, A., . . . Fox, G. (2016). Genomic regions influencing seminal root traits in barley. *The plant genome*, *9*(1), plantgenome2015.2003.0012.
- Rossini, L., Muehlbauer, G. J., Okagaki, R., Salvi, S., & Korff, M. v. (2018). Genetics of whole plant morphology and architecture. In *The Barley Genome* (pp. 209-231). Springer.
- Rostoks, N., Schmierer, D., Mudie, S., Drader, T., Brueggeman, R., Caldwell, D. G., . . . Kleinhofs, A. (2006). Barley necrotic locus nec1 encodes the cyclic nucleotide-gated ion channel 4 homologous to the Arabidopsis HLM1. *Mol Genet Genomics*, *275*(2), 159-168. <https://doi.org/10.1007/s00438-005-0073-9>
- Roychoudhry, S., Del Bianco, M., Kieffer, M., & Kepinski, S. (2013). Auxin Controls Gravitropic Setpoint Angle in Higher Plant Lateral Branches. *Current Biology*, *23*(15), 1497-1504. <https://doi.org/https://doi.org/10.1016/j.cub.2013.06.034>
- Roychoudhry, S., & Kepinski, S. (2015). Shoot and root branch growth angle control—the wonderfulness of lateralness. *Current Opinion in Plant Biology*, *23*, 124-131. <https://doi.org/https://doi.org/10.1016/j.pbi.2014.12.004>
- Rubio, G., Walk, T., Ge, Z., Yan, X., Liao, H., & Lynch, J. P. (2001). Root gravitropism and below-ground competition among neighbouring plants: a modelling approach. *Annals of Botany*, *88*(5), 929-940.
- Sack, F. D. (1991). Plant Gravity Sensing. In K. W. Jeon & M. Friedlander (Eds.), *International Review of Cytology* (Vol. 127, pp. 193-252). Academic Press. [https://doi.org/https://doi.org/10.1016/S0074-7696\(08\)60695-6](https://doi.org/https://doi.org/10.1016/S0074-7696(08)60695-6)
- Santagata, S., Boggan, T. J., Baird, C. L., Gomez, C. A., Zhao, J., Shan, W. S., . . . Shapiro, L. (2001). G-protein signaling through tubby proteins. *Science*, *292*(5524), 2041-2050.
- Sato, E. M., Hijazi, H., Bennett, M. J., Vissenberg, K., & Swarup, R. (2014). New insights into root gravitropic signalling. *Journal of Experimental Botany*, *66*(8), 2155-2165. <https://doi.org/10.1093/jxb/eru515>
- Schneider, C. A., Rasband, W. S., & Eliceiri, K. W. (2012). NIH Image to ImageJ: 25 years of image analysis. *Nat Methods*, *9*(7), 671-675. <https://doi.org/10.1038/nmeth.2089>
- Schneider, H. M., Lor, V. S. N., Hanlon, M. T., Perkins, A., Kaeppler, S. M., Borkar, A. N., . . . Lynch, J. P. (2022). Root angle in maize influences nitrogen capture and is regulated by calcineurin B-like protein (CBL)-interacting serine/threonine-protein kinase 15 (ZmCIPK15). *Plant, Cell & Environment*, *45*(3), 837-853. <https://doi.org/https://doi.org/10.1111/pce.14135>
- Shaaf, S., Bretani, G., Biswas, A., Fontana, I. M., & Rossini, L. (2019). Genetics of barley tiller and leaf development. *Journal of Integrative Plant Biology*, *61*(3), 226-256. <https://doi.org/https://doi.org/10.1111/jipb.12757>
- Shah, A. N., Tanveer, M., Anjum, S. A., Iqbal, J., & Ahmad, R. (2017). Lodging stress in cereal—effects and management: an overview. *Environmental Science and Pollution Research*, *24*(6), 5222-5237.
- Silva-Navas, J., Moreno-Risueno, M. A., Manzano, C., Téllez-Robledo, B., Navarro-Neila, S., Carrasco, V., . . . del Pozo, J. C. (2016). Flavonols Mediate Root Phototropism and

- Growth through Regulation of Proliferation-to-Differentiation Transition. *The Plant Cell*, 28(6), 1372-1387. <https://doi.org/10.1105/tpc.15.00857>
- Smant, G., Stokkermans, J. P., Yan, Y., De Boer, J. M., Baum, T. J., Wang, X., . . . Davis, E. L. (1998). Endogenous cellulases in animals: isolation of β -1, 4-endoglucanase genes from two species of plant-parasitic cyst nematodes. *Proceedings of the National Academy of Sciences*, 95(9), 4906-4911.
- Strable, J. (2021). Developmental genetics of maize vegetative shoot architecture. *Molecular Breeding*, 41(3), 19. <https://doi.org/10.1007/s11032-021-01208-1>
- Stubbs, C. J., Cook, D. D., & Niklas, K. J. (2019). A general review of the biomechanics of root anchorage. *Journal of Experimental Botany*, 70(14), 3439-3451.
- Sun, X., Cahill, J., Van Hautegeem, T., Feys, K., Whipple, C., Novák, O., . . . Nelissen, H. (2017). Altered expression of maize PLASTOCHRON1 enhances biomass and seed yield by extending cell division duration. *Nature Communications*, 8(1), 14752. <https://doi.org/10.1038/ncomms14752>
- Swarup, R., & Bennett, M. J. (2009). Root gravitropism. *Annual Plant Reviews*, 37, 157-174.
- Takagi, H., Abe, A., Yoshida, K., Kosugi, S., Natsume, S., Mitsuoka, C., . . . Takuno, S. (2013). QTL-seq: rapid mapping of quantitative trait loci in rice by whole genome resequencing of DNA from two bulked populations. *The Plant Journal*, 74(1), 174-183.
- Talamè, V., Bovina, R., Sanguineti, M. C., Tuberosa, R., Lundqvist, U., & Salvi, S. (2008). TILLMore, a resource for the discovery of chemically induced mutants in barley. *Plant Biotechnol J*, 6(5), 477-485. <https://doi.org/10.1111/j.1467-7652.2008.00341.x>
- Team, R. (2020). *RStudio: Integrated Development for R*. RStudio, PBC, URL <http://www.rstudio.com/>. In PBC. <http://www.rstudio.com/>
- Thirulogachandar, V., Alqudah, A. M., Koppolu, R., Rutten, T., Graner, A., Hensel, G., . . . Kuhlmann, M. (2017). Leaf primordium size specifies leaf width and vein number among row-type classes in barley. *The Plant Journal*, 91(4), 601-612. <https://doi.org/https://doi.org/10.1111/tpj.13590>
- Turner, A., Beales, J., Faure, S., Dunford, R. P., & Laurie, D. A. (2005). The pseudo-response regulator Ppd-H1 provides adaptation to photoperiod in barley. *Science*, 310(5750), 1031-1034.
- Uga, Y., Sugimoto, K., Ogawa, S., Rane, J., Ishitani, M., Hara, N., . . . Yano, M. (2013). Control of root system architecture by DEEPER ROOTING 1 increases rice yield under drought conditions. *Nat Genet*, 45(9), 1097-1102. <https://doi.org/10.1038/ng.2725>
- Untergasser, A., Cutcutache, I., Koressaar, T., Ye, J., Faircloth, B. C., Remm, M., & Rozen, S. G. (2012). Primer3--new capabilities and interfaces. *Nucleic Acids Res*, 40(15), e115. <https://doi.org/10.1093/nar/gks596>
- van Dusschoten, D., Metzner, R., Kochs, J., Postma, J. A., Pflugfelder, D., Bühler, J., . . . Jahnke, S. (2016). Quantitative 3D analysis of plant roots growing in soil using magnetic resonance imaging. *Plant physiology*, 170(3), 1176-1188.
- Van Zelm, E., Zhang, Y., & Testerink, C. (2020). Salt tolerance mechanisms of plants. *Annual review of plant biology*, 71, 403-433.
- Vives-Peris, V., de Ollas, C., Gómez-Cadenas, A., & Pérez-Clemente, R. M. (2020). Root exudates: from plant to rhizosphere and beyond. *Plant cell reports*, 39(1), 3-17.
- von Wangenheim, D., Banda, J., Schmitz, A., Boland, J., Bishopp, A., Maizel, A., . . . Bennett, M. (2020). Early developmental plasticity of lateral roots in response to asymmetric water availability. *Nature Plants*, 6(2), 73-77.
- Voss-Fels, K. P., Snowdon, R. J., & Hickey, L. T. (2018). Designer roots for future crops. *Trends in plant science*, 23(11), 957-960.

- Wang, F., Tang, Z., Wang, Y., Fu, J., Yang, W., Wang, S., . . . Yin, H. (2022). Leaf Mutant 7 Encoding Heat Shock Protein OsHSP40 Regulates Leaf Size in Rice. *International journal of molecular sciences*, 23(8), 4446.
- Wang, J., Liu, H., Zhao, C., Tang, H., Mu, Y., Xu, Q., . . . Ma, J. Mapping and validation of major and stable QTL for flag leaf size from tetraploid wheat. *The Plant Genome*, n/a(n/a), e20252. <https://doi.org/https://doi.org/10.1002/tpg2.20252>
- Wang, L., Guo, M., Li, Y., Ruan, W., Mo, X., Wu, Z., . . . Peng, J. (2018). LARGE ROOT ANGLE1, encoding OsPIN2, is involved in root system architecture in rice. *Journal of Experimental Botany*, 69(3), 385-397.
- Wang, M., Xu, Z., Ahmed, R. I., Wang, Y., Hu, R., Zhou, G., & Kong, Y. (2019). Tubby-like protein 2 regulates homogalacturonan biosynthesis in Arabidopsis seed coat mucilage. *Plant molecular biology*, 99(4), 421-436.
- Wang, Q., Zhu, Y., Zou, X., Li, F., Zhang, J., Kang, Z., . . . Lin, Y. (2020). Nitrogen Deficiency-Induced Decrease in Cytokinins Content Promotes Rice Seminal Root Growth by Promoting Root Meristem Cell Proliferation and Cell Elongation. *Cells*, 9(4), 916.
- Wang, Z., & Song, Y. (2022). Toward understanding the genetic bases underlying plant-mediated “cry for help” to the microbiota. *iMeta*, 1(1), e8.
- Wasson, A., Richards, R., Chatrath, R., Misra, S., Prasad, S. S., Rebetzke, G., . . . Watt, M. (2012). Traits and selection strategies to improve root systems and water uptake in water-limited wheat crops. *Journal of experimental botany*, 63(9), 3485-3498.
- Waterhouse, A. M., Procter, J. B., Martin, D. M., Clamp, M., & Barton, G. J. (2009). Jalview Version 2--a multiple sequence alignment editor and analysis workbench. *Bioinformatics*, 25(9), 1189-1191. <https://doi.org/10.1093/bioinformatics/btp033>
- Wickham, H. (2016). Data analysis. In *ggplot2* (pp. 189-201). Springer.
- Williamson, V. M., & Gleason, C. A. (2003). Plant–nematode interactions. *Current Opinion in Plant Biology*, 6(4), 327-333. [https://doi.org/https://doi.org/10.1016/S1369-5266\(03\)00059-1](https://doi.org/https://doi.org/10.1016/S1369-5266(03)00059-1)
- Wu, S., Xie, Y., Zhang, J., Ren, Y., Zhang, X., Wang, J., . . . Wang, J. (2015). VLN2 regulates plant architecture by affecting microfilament dynamics and polar auxin transport in rice. *The Plant Cell*, 27(10), 2829-2845.
- Yan, X., Wang, S., Yang, B., Zhang, W., Cao, Y., Shi, Y., . . . Jing, R. (2020). QTL mapping for flag leaf-related traits and genetic effect of QFLW-6A on flag leaf width using two related introgression line populations in wheat. *Plos one*, 15(3), e0229912.
- Yoshikawa, T., Tanaka, S.-Y., Masumoto, Y., Nobori, N., Ishii, H., Hibara, K.-I., . . . Taketa, S. (2016). Barley NARROW LEAFED DWARF1 encoding a WUSCHEL-RELATED HOMEODOMAIN 3 (WOX3) regulates the marginal development of lateral organs. *Breeding Science*, 16019.
- Zhang, D., Sun, W., Singh, R., Zheng, Y., Cao, Z., Li, M., . . . Zhang, Z. (2018). GRF-interacting factor1 Regulates Shoot Architecture and Meristem Determinacy in Maize. *The Plant Cell*, 30(2), 360-374. <https://doi.org/10.1105/tpc.17.00791>
- Zhang, J.-W., Xu, L., Wu, Y.-R., Chen, X.-A., Liu, Y., Zhu, S.-H., . . . Yi, K.-K. (2012). OsGLU3, a Putative Membrane-Bound Endo-1,4-Beta-Glucanase, Is Required for Root Cell Elongation and Division in Rice (*Oryza sativa* L.). *Molecular Plant*, 5(1), 176-186. <https://doi.org/https://doi.org/10.1093/mp/ssr084>
- Zhang, Y., Xiao, G., Wang, X., Zhang, X., & Friml, J. (2019). Evolution of fast root gravitropism in seed plants. *Nature communications*, 10(1), 1-10.
- Zhao, C., Bao, Y., Wang, X., Yu, H., Ding, A., Guan, C., . . . Cui, F. (2018). QTL for flag leaf size and their influence on yield-related traits in wheat. *Euphytica*, 214(11), 209. <https://doi.org/10.1007/s10681-018-2288-y>

- Zhao, S., Zhao, L., Liu, F., Wu, Y., Zhu, Z., Sun, C., & Tan, L. (2016). NARROW AND ROLLED LEAF 2 regulates leaf shape, male fertility, and seed size in rice. *Journal of integrative plant biology*, 58(12), 983-996.
- Zhao, T., Xue, J., Kao, S.-m., Li, Z., Zwaenepoel, A., Schranz, M. E., & Van de Peer, Y. (2020). Novel phylogeny of angiosperms inferred from whole-genome microsynteny analysis. *bioRxiv*, 2020.2001.2015.908376.
<https://doi.org/10.1101/2020.01.15.908376>
- Zheng, Y., Xu, J., Wang, F., Tang, Y., Wei, Z., Ji, Z., . . . Zhao, K. (2021). Mutation Types of CYP71P1 Cause Different Phenotypes of Mosaic Spot Lesion and Premature Leaf Senescence in Rice. *Frontiers in plant science*, 12, 488.